A HOP, SWITCH, AND JUMP: STOCHASTICITY IN MODELS OF MOTOR-MEDIATED INTRACELLULAR TRANSPORT

by

Christopher Edward Miles

A dissertation submitted to the faculty of
The University of Utah
in partial fulfillment of the requirements for the degree of

Doctor of Philosophy

Department of Mathematics

The University of Utah

May 2018

The University of Utah Graduate School

STATEMENT OF DISSERTATION APPROVAL

The dissertation of **Christopher Edward Miles**
has been approved by the following supervisory committee members:

James P. Keener ,	Chair(s)	**26 Feb 2018** Date Approved
Alla R. Borisyuk ,	Member	**26 Feb 2018** Date Approved
Paul C. Bressloff ,	Member	**26 Feb 2018** Date Approved
Aaron L. Fogelson ,	Member	**26 Feb 2018** Date Approved
Michael D. Vershinin ,	Member	**26 Feb 2018** Date Approved

by **Davar Khoshnevisan** , Chair/Dean of
the Department/College/School of **Mathematics**
and by **David B. Kieda** , Dean of The Graduate School.

ABSTRACT

Active transport of cargoes is critical for cellular function. To accomplish this, networks of cytoskeletal filaments form highways along which small teams of mechanochemical enzymes (molecular motors) take steps to pull associated cargoes. The robustness of this transport system is juxtaposed by the stochasticity that exists at several spatial and temporal scales. For instance, individual motors stochastically step, bind, and unbind while the cargo undergoes nonnegligible thermal fluctuations. Experimental advances have produced rich quantitative measurements of each of these stochastic elements, but the interaction between them remains elusive. In this thesis, we explore the roles of stochasticity in motor-mediated transport with four specific projects at different scales.

We first construct a mean-field model of a cargo transported by two teams of opposing motors. This system is known to display bidirectionality: switching between phases of transport in opposite directions. We hypothesize that thermal fluctuations of the cargo drive the switching. From our model, we predict how cargo size influences the switching time, an experimentally measurable quantity to verify the hypothesis. In the second work, we investigate the force dependence of motor stepping, formulated as a state-dependent jump-diffusion model. We prove general results regarding the computation of the statistics of this process. From this framework, we find that thermal fluctuations may provide a nonmonotonic influence on the stepping rate of motors.

The remaining projects investigate the behavior of nonprocessive motors, which take few steps before detaching. In collaboration with experimentalists, we study seemingly diffusive data of motor-mediated transport. Using a jump-diffusion model, the active and passive portions of the diffusivity are disentangled, and curious higher order statistics are explained as a sampling issue. Lastly, we construct a model of cooperative transport by nonprocessive motors, which we study using reward-renewal theory. The theory provides predictions about measured quantities such as run length, which suggest that geometric effects have a large influence on the transport ability of these motors.

CONTENTS

ABSTRACT . . . . . **iii**

ACKNOWLEDGEMENTS . . . . . **vii**

CHAPTERS

1. INTRODUCTION **1**

1.1 Molecular motors, intracellular transport 2
1.2 Stochastic models 5
1.2.1 Langevin and Fokker–Planck equations 5
1.2.1.1 Ornstein–Uhlenbeck process 6
1.2.2 Jump processes 7
1.3 Contents of dissertation 7
1.4 References 9

2. BIDIRECTIONALITY FROM CARGO THERMAL FLUCTUATIONS **13**

2.1 Introduction 14
2.2 Methods 15
2.2.1 Model formulation 15
2.2.2 Steady-state analysis 17
2.2.3 Forces exerted by motors 17
2.2.3.1 Ornstein–Uhlenbeck approximation 17
2.2.3.2 Force evolution approximation 18
2.2.4 Full model 18
2.2.5 Dimensional reduction 18
2.3 Results 19
2.3.1 Linear motor force-velocity curve 19
2.3.2 Force delay approximation 19
2.3.3 Metastable behavior 21
2.3.4 Mean first passage time analysis 22
2.4 Discussion & conclusion 22
2.5 Appendix A: Ornstein–Uhlenbeck mean evolution 23
2.6 Appendix B: Methods for 1D MFPT problems 23
2.6.1 Shooting method 24
2.6.2 Arrhenius (deep well) approximation 24
2.7 Supplementary material 24
2.8 References 24

3. JUMP LOCATIONS OF JUMP-DIFFUSION PROCESSES WITH STATE-DEPENDENT RATES **26**

3.1 Abstract 27

3.2 Introduction . . . 28
3.3 Formulation . . . 29
3.3.1 Jump-diffusion . . . 29
3.3.2 Diffusion component . . . 29
3.3.3 Jump component . . . 30
3.3.3.1 Jump operator examples . . . 30
3.4 Results . . . 31
3.4.1 Jump distributions . . . 31
3.4.2 Jump location sequential mapping . . . 32
3.4.3 Moments . . . 34
3.5 Examples . . . 35
3.5.1 Neuronal integrate-and-fire . . . 35
3.5.2 Transport by a molecular motor . . . 37
3.5.3 Independence of $\lambda(x)$ . . . 38
3.6 Discussion and conclusion . . . 39
3.7 Appendix A: Higher order interjump time moments . . . 40
3.8 Appendix B: Spectral properties of iterated map . . . 41
3.9 References . . . 42

4. DISENTANGLING ACTIVE AND PASSIVE DIFFUSION IN TRANSPORT DATA . . . 44

4.1 Introduction . . . 44
4.2 Experimental basis . . . 45
4.2.1 Bead assay . . . 45
4.2.2 Lipid droplet data . . . 49
4.2.3 Subdiffusive behavior . . . 49
4.3 Jump–diffusion conceptual model . . . 52
4.3.1 Moments . . . 53
4.3.2 Relation to MSD analysis . . . 54
4.3.3 Comparison to simulations . . . 55
4.4 Conclusion . . . 56
4.5 References . . . 58

5. COOPERATIVE TRANSPORT BY NONPROCESSIVE MOTORS . . . 62

5.1 Introduction . . . 62
5.2 Mathematical model . . . 64
5.2.1 Nondimensionalization and assumptions . . . 66
5.3 Cargo position as a renewal reward process . . . 67
5.4 Mathematical analysis of transport ability . . . 70
5.4.1 Expected run time . . . 71
5.4.2 Decomposing stochasticity . . . 72
5.4.2.1 Conditioning on jump realizations . . . 72
5.4.2.2 Separation of timescales . . . 73
5.4.3 Run length and velocity . . . 75
5.4.3.1 Run length . . . 75
5.4.3.2 Velocity . . . 76
5.4.4 Cases $M = 1$, $M = 2$, and $M = 3$ . . . 78

5.4.5 Numerical simulations 79
5.5 Biological application 80
5.6 Discussion 83
5.7 References 84

6. FUTURE DIRECTIONS 87

6.1 Bidirectional transport with asymmetric populations 87
6.2 Bayesian methods for motor-mediated transport data 89
6.3 Cytoskeletal manipulation by nonprocessive motors 90
6.4 Geometric effects in motor transport 92
6.5 References 93

APPENDICES

A. SUPPLEMENTAL INFORMATION FOR CHAPTER 2 96

B. SUPPLEMENTAL INFORMATION FOR CHAPTER 5 101

ACKNOWLEDGEMENTS

The work described in this thesis has been influenced by many individuals, both directly and indirectly. To all of these people, I would like to extend my long-winded, sincere gratitude.

Foremost, none of this would have been possible without my advisor, James Keener. More importantly than constantly getting me unstuck from the bog of pesky details that appeared to be the demise of these projects, he taught me how be a scientist. His unwavering curiosity and excitement for the unknown has shaped how I approach mathematics and the physical world.

At some point, I have bothered every one of my committee members (Alla Borisyuk, Paul Bressloff, Michael Vershinin, Aaron Fogelson) with a barrage of questions about a topic I knew embarrassingly little about. They have all provided patient insight and have steered the scientific direction of this work.

Utah's mathematical biology group fostered a uniquely friendly and stimulating environment. Between group meetings, seminars, and just chatting at the water fountain, I can't imagine a better supporting cast.

I would like to thank my officemates (Greg, Andy, Daniel) for letting me talk to myself throughout the day, always appropriately knowing when to respond or completely ignore me. Surviving graduate school without the therapeutic presence of friends would be impossible, and for that I would like to acknowledge Ethan, Heather, Leif, and Sam among others. I am genuinely worried about how to spend my time without walking to Two Creek Coffee inappropriately many times in a single day.

Despite bewilderment about what it is I actually do, my family and my girlfriend, Katherine, have provided unrelenting support and understanding for my inability to leave work at the office.

I have a great appreciation for the various academic advocates I have had throughout the years. This journey started with an awkward teenager that was barely passing high

school but was inspired by his teacher's passion for science and knowledge. From there, my own love for mathematics and science blossomed as a reflection of the copious support I continued to received as an undergrad. Without these influences, I would not be here today.

Lastly, I acknowledge the funding from the National Science Foundation (NSF) that supported me throughout a significant portion of my time here. It is my hope to continue doing science that contributes to the greater good of humanity, as this is the same group that allows me to do this work.

CHAPTER 1

INTRODUCTION

For many years, mathematical models of cellular systems were largely deterministic. While this modeling revealed countless insights regarding the function of these systems [28], recent years have brought a new paradigm: stochasticity is unavoidable at the cellular and molecular level. An immediate question arises: how do cells function in the face of randomness? For instance, how do cells manage to signal robustly in heavily fluctuating, noisy environments? Questions such as these illuminate the power of mathematical biology. Experiments with heavily stochastic components can be difficult to perform or assess, so modeling serves as an invaluable probe in understanding stochasticity in these biological systems [4]. Although motivated by biological questions, modeling of these stochastic systems has also led to a volume of novel interesting mathematical questions.

From modeling efforts, a surprising theme has emerged: cells function not only in spite of noise, but *because* of it. That is, cellular function appears from stochasticity, for instance in [40]. Another way of interpreting this statement is that stochasticity cannot be always averaged or neglected into a deterministic model that accurately describes a system. Stochasticity is the cog in the machine that allows these systems to function, and models that do not include it fundamentally fail to describe the essence of the behavior. For this reason, modeling with stochasticity must be embraced to truly understand biology at the cellular and molecular scale.

In this thesis, we study a system with a rich array of stochasticity: intracellular transport by molecular motors. Modeling always involves a decision regarding the scale of interest in which to describe a system. Intracellular transport has the interesting property of involving noise at a variety of scales [5]. One might hope for fundamental relationships between the description of noise at different scales, but a unified theory remains largely unclear. Another interesting facet of the noise in intracellular transport is its variety. Because

this system is fundamentally spatial, modeling often incorporates classical continuous processes (such as Brownian motion) along with jump processes describing the stepping or binding kinetics of individual motors. Transport typically involves a small team of motors, and consequently the behavior of individuals contributes meaningfully to the behavior. Understanding the net behavior of this system therefore requires disentangling an intertwined mix of stochasticity that exists at different spatial and temporal scales. In this thesis, we embark upon exploring how stochasticity in intracellular transport interweaves and how it can be disentangled. In doing so, both biological and mathematical insights are achieved.

1.1 Molecular motors, intracellular transport

Cells are spatially compartmental structures, where different compartments produce and consume particular components for the cell to function. Transactions of cargoes between these compartments (through crowded environments [15]) drive the need for cells to have a mechanism of transport. Small cargoes, such as glucose, can be transported via diffusion, a passive transport mechanism. However, for larger cargoes, such as organelles, diffusion is not sufficiently fast [28] for the timescale of cellular function. Instead, an active transport mechanism is utilized: transport mediated by molecular motors along cytoskeletal filaments.

Molecular motors are, in general, mechanochemical machines that convert energy into mechanical work. The mechanism of stepping varies dramatically from motor to motor [7, 10, 21], for which kinesin-1 provides a canonical example. Each kinesin consists of two heads connected together by a stalk region, ending in a tail region. Kinesin-1 walks along microtubules in a "hand-overhand" matter, where each of the heads alternate between tightly bound to the microtubule and diffusing freely, resulting in 8 nm steps [12, 17]. The mechanism that drives the alternation of these two heads is ATP hydrolysis, which produces a conformational change in the protein. Specifically, ATP binding to the microtubule-bound stiffens the rear linker, causing a "power stroke" motion of the rear linker toward the plus end of the microtubule. This head binds to the microtubule and now is the leading head, and the process cycles producing motion toward the positive direction on the microtubule. An illustration of this process can be found in **Figure 1.1a**.

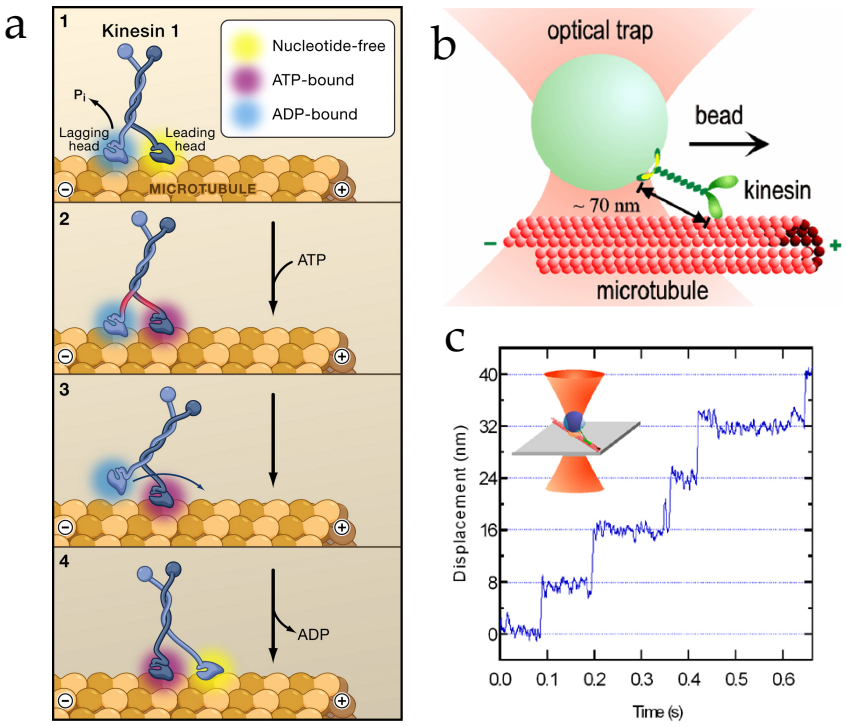

Figure 1.1. Depictions of kinesin stepping behavior and laser tweezers to measure the force generated by this process. **a**: Sequence depicting ATP-dependent kinesin-1 walking, adapted from [11]. **b**: optical trap setup, a force/displacement measurement tool for single molecule systems involving molecular motors, **c**: result of optical tweezer measurements for a single kinesin-1 motor, showing distinct stepping, both adapted from [2].

One classification of motors relevant to this thesis is whether the motor is *processive*, in which the motor takes many (hundreds) steps before detaching, as seen in **Figure 1.1c**, or *nonprocessive*, such as those in the kinesin-14 family, which take 1 to 5 steps before detaching [8, 16]. From a mathematical perspective, modeling processive motors allows for the large number of steps to be averaged into a velocity using a central limit theorem flavored argument. Whether an analogous technique is possible for nonprocessive motors remains unclear. Beyond processivity, motors are categorized into three main superfamilies: kinesin, dynein, and myosin, seen **Figure 1.2a**. The two key differences that distinguish these motors is, aside from chemical structure, the cytoskeletal filaments with which they are associated and the direction they walk [48]. Kinesin and dynein are typically associated with microtubules, but kinesins primarily walk in the anterograde direction, whereas dynein transport in the retrograde. Myosin motors are, however, typically

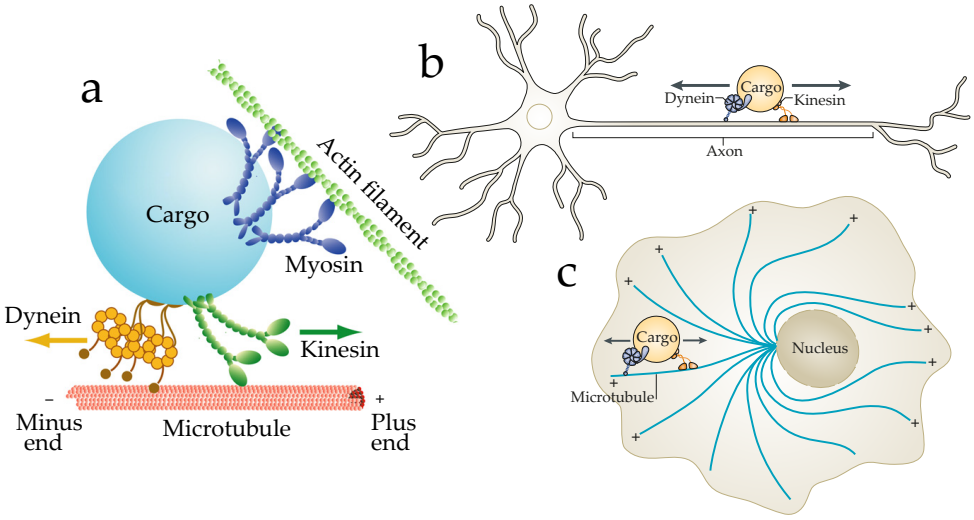

Figure 1.2. Cartoons describing the biological contexts in which different motors are utilized. **a**: Diagram illustrating the different types of molecular motors and the cytoskeletal filaments they are associated with, redrawn from [47]. **b, c**: Two depictions of intracellular transport, either along radial microtubule networks or along axonal filaments, redrawn from [23].

associated with actin filaments.

The cargoes transported by molecular motors reflect the diversity of the motors themselves, including vesicles, organelles, or even other cytoskeletal filaments [48, 23]. Two canonical examples can be seen in **Figures 1.2b, 1.2c**. In the first, vesicles are delivered along long arrays of parallel microtubules, transported by teams of both kinesin and dynein motors. These same motor families also spatially organize organelles throughout the cell along radially microtubule networks stemming from the microtubule organizing center. Because of the wide scope of utility intracellular transport provides for the cell, defects in molecular motors are associated with a number of diseases [44]. Consequently, investigating the function of molecular motors is of natural interest in order to understand how they fail.

In contrast to experimental findings of other systems at the molecular scale, advances in experimental techniques have enabled richly quantitative measurements of molecular motors. Optical tweezers, as seen in **Figures 1.1b, 1.1c** have allowed for measurements of how motors respond to force, including the rate at which they step [7, 10, 21, 49] and unbind [34], and split force among teams [14, 24]. Advances in DNA manipulation have

also allowed experiments to precisely control the number of motors associated with a cargo, as in [1, 13, 19]. This body of quantitative measurements of both individual molecular motors and ensembles makes intracellular transport attractive for modeling studies at a variety of scales. Although not an extensive list, reviews can be found in [5, 50], and specific examples include modeling individual motors [32, 42, 46], teams of motors [25, 29, 30, 31, 33, 36, 39, 43], and macroscale models at the cellular level [6, 9, 22, 26].

1.2 Stochastic models

In this section, we briefly review some of the common mathematical structures used throughout this thesis.

1.2.1 Langevin and Fokker–Planck equations

The systems in this thesis are primarily described by stochastic differential equations, which govern the evolution of $X(t) \in \mathbb{R}$ and take the form

$$\mathrm{d}X(t) = A(X)\,\mathrm{d}t + \sqrt{2B(X)}\,\mathrm{d}W(t), \tag{1.1}$$

where $A(x)$ describes the deterministic drift, $B(x)$ the magnitude of random fluctuations, and $W(t)$ the classical Weiner process with stationary, Gaussian increments [20]. Note that trajectories arising from the description (1.1) have continuous paths.

Throughout the work, we utilize an alternative formulation of (1.1). While $x(t)$ describes the (random-valued) position of a single trajectory, define $p(x,t)$ to be the probability density of this process conditioned on a known starting position x_0. Then, (1.1) is equivalent to the *Fokker–Planck equation*

$$\partial_t p(x,t) = -\partial_x \left\{A(x)p\right\} + \partial_{xx}\left\{B(x)p\right\}, \tag{1.2}$$

where (1.1) is interpreted in the Itô (rather than Stratonovich) sense, which would modify the form of (1.2) slightly.

(1.2) is accompanied with some initial condition $p(x,t_0) = p_0(x)$ and describes the evolution of the process forward in time. Consequently, this relation is also known as the *Kolmogorov forward equation*. In contrast, the *Kolmogorov backward equation*, which describes the backward evolution of $\tilde{p}(x,t)$, accompanied by a terminal condition $\tilde{p}(x,T) = p_T(x)$, takes the form

$$\partial_t \tilde{p} = A(x)\partial_x \tilde{p} + B(x)\partial_{xx}\tilde{p}. \tag{1.3}$$

It is worth noting that if we abbreviate the right-hand side of (1.2) as $\mathbb{L}p$, then the right-hand side of (1.3) is the formal adjoint, $\mathbb{L}^\dagger \tilde{p}$.

1.2.1.1 Ornstein–Uhlenbeck process

The *Ornstein–Uhlenbeck process* [20] is used commonly in this thesis, as experiments support that the force response of motor linkers can be modeled as a Hookean spring [27, 35].

Consider $x(t)$ the displacement (from rest) of a single molecular motor attached to a cargo at time t. Then, $X(t)$ evolves by the relation

$$\gamma \mathrm{d}X(t) = -kX(t)\,\mathrm{d}t + \sqrt{2D}\,\mathrm{d}W(t). \tag{1.4}$$

The SDE relation (1.4) can be thought of as a balance of forces, where γ is the drag coefficient of the cargo, and the lefthand side represents the viscous force. The second term represents the Hookean force, with k as the stiffness of the motor, and finally the random force from thermal fluctuations of the cargo is captured described with diffusivity D scaling Brownian increments. The *fluctuation-dissipation* theorem states that

$$D = k_B T \gamma,$$

where k_B is Boltzmann's factor, T temperature, and γ is again the drag coefficient of the cargo. Furthermore, the *Stokes-Einstein relation* states that, for a spherical cargo (such as a vesicle),

$$\gamma = 6\pi r \eta,$$

with η the viscosity of the cytosol, and r the radius of the sphere.

The Ornstein–Uhlenbeck process (1.4) can be written in Fokker–Planck form

$$\partial_t p(x,t) = \partial_x \left\{(\kappa x)p\right\} + \mathcal{D}\partial_{xx} p.$$

This classical process is often a convenient starting point due to having known Gaussian solutions, with $x(0) = y$,

$$p(x,t) = \sqrt{\frac{\theta}{2\pi\mathcal{D}(1-e^{-2\kappa t})}}\exp\left\{\frac{-\kappa}{2\mathcal{D}}\left[\frac{\left(x-ye^{-\kappa t}\right)^2}{1-e^{-2\kappa t}}\right]\right\}.$$

1.2.2 Jump processes

Molecular motors bind, step due to conformational changes, and then unbind, so their behavior can be partitioned into discrete states. The canonical model for transitions between such states is a Markov jump process. This process differs from those described by SDEs, as it does not necessarily provide continuous trajectories.

Consider a process $X(t)$ that can be in states Ω. The rates of transition between the states are encoded in a matrix $Q = [q_{ij}]$ with $i, j \in \Omega$,

$$\mathbb{P}\left[X(t+h) = j | X(t) = i\right] = \delta_{ij} + q_{ij}h + o(h),$$

which imposes the requirement that $q_{ij} \geq 0$ for $i \neq j$ and $\sum_j q_{ij} = 0$. The corresponding *forward Kolmogorov equation* (analogous to the Fokker–Planck equation) is then

$$P'(t) = P(t)Q,$$

where $P(t)$ is the vector of probability densities of each state at time t.

It is often convenient to transform a continuous time Markov jump process into its *embedded* discrete chain, where only the sequence of states is tracked [41]. The matrix $S = [s_{ij}]$ of transition probabilities from state i to state j can be computed by

$$S = I - (\operatorname{diag} Q)^{-1} Q.$$

Let p_n be the vector of probabilities of each state n, which satisfies

$$p_{n+1} = p_n S.$$

This transformation often provides a convenient way of computing the stationary distribution, π, which satisfies the matrix equation

$$\pi = \pi S.$$

Equivalently, π is the (normalized) eigenvector corresponding to the eigenvalue $\lambda = 1$.

1.3 Contents of dissertation

In **Chapter 2**, we explore a mean-field model of transport by two opposing populations of motors [37]. This study is motivated by the observation that cargoes associated with opposing populations (say, kinesin and dynein) switch directions, or behave *bidirectionally*

[23]. Previous modeling of this system focuses on motor number as the driver of switching [34, 39], but we instead conjecture that cargo thermal fluctuations (diffusion) drive switching. To explore this possibility, we reduce our mean-field model to a system of reduced dimensionality, which is found to be metastable. The metatstable states correspond to positive and negative average velocities, or bidirectional motion. The mean first passage time to switch directions is computed and used to make an experimentally verifiable prediction about how cargo size influences switching time.

In **Chapter 3**, mathematical theory is developed to study jump-diffusion systems with state-dependent jump rates [38]. The stepping of molecular motors is well-known to depend on the force exerted on them [7], but stepping itself modifies the force resulting in a feedback loop, all while thermal fluctuations of the cargo also continuously modify the force. This stepping process can be modeled as a state-dependent jump diffusion process, for which previous tools provide limited insight. We provide an iterated map formulation for the sequence of jump locations (the process evaluated at jump times), and use this formulation to extract physically relevant statistics of the process. We ultimately find that cargo fluctuations may have a nonmonotonic influence on the stepping on individual motors.

Both **Chapters 4 and 5** focus on the study of transport of nonprocessive motors, those that take very few steps before detaching. **Chapter 4** describes the results of a collaboration with experimental scientists to understand the observed motion of particles associated with N340k, a mutant nonprocessive motor that takes steps in both directions. The observed particle motion is observed to be diffusive (with a linear mean-squared displacement). Diffusive motion of motor-associated cargoes has been observed to occur due cytoskeletal complexity [45]. However, in this case, only a single filament is used, so the motors themselves must drive this motion. A jump-diffusion model is constructed to explain the mean-squared displacement observations by decomposing the diffusivity into passive and active components. This model also explains the curious skewed distribution of diffusivities observed in the data as a sampling issue.

Finally, **Chapter 5** focuses on interesting experimental observations made in [19]: Although individual nonprocessive motors are poor at transporting cargoes, teams are able to act cooperatively to transport cargoes long distances. We construct a simple model

where motors can bind, step, and unbind. Using asymptotic analysis and reward-renewal theory, we derive rigorous results allowing for the computation of experimentally observed quantities such as the run time, run length, and velocity. From these quantities, we find that this cooperative transport is only possible when the binding and step kinetics have a complex dependence on the current number of bound motors, which we conjecture stems from observed geometric tethering effects [3, 18].

1.4 References

[1] V. Belyy, M. A. Schlager, H. Foster, A. E. Reimer, A. P. Carter, and A. Yildiz, *The mammalian dynein-dynactin complex is a strong opponent to kinesin in a tug-of-war competition*, Nat. Cell Biol., 18 (2016), pp. 1018–1024.

[2] S. Block, *An introduction to optical tweezers*. `https://blocklab.stanford.edu/`, 2015.

[3] M. Braun, Z. Lansky, A. Szuba, F. W. Schwarz, A. Mitra, M. Gao, A. Lüdecke, P. R. ten Wolde, and S. Diez, *Changes in microtubule overlap length regulate kinesin-14-driven microtubule sliding*, Nat. Chem. Biol., (2017), pp. 1245–1252.

[4] P. C. Bressloff, *Stochastic Processes in Cell Biology*, vol. 41 of Interdisciplinary Applied Mathematics, Springer International Publishing, 2014.

[5] P. C. Bressloff and J. M. Newby, *Stochastic models of intracellular transport*, Rev. Mod. Phys., 85 (2013), pp. 135–196.

[6] H. A. Brooks and P. C. Bressloff, *A mechanism for Turing pattern formation with active and passive transport*, SIAM J. Appl. Dyn. Syst., 15 (2016), pp. 1823–1843.

[7] N. J. Carter and R. A. Cross, *Mechanics of the kinesin step.*, Nature, 435 (2005), pp. 308–12.

[8] R. B. Case, D. W. Pierce, N. Hom-Booher, C. L. Hart, and R. D. Vale, *The directional preference of kinesin motors is specified by an element outside of the motor catalytic domain*, Cell, 90 (1997), pp. 959–966.

[9] M.-V. Ciocanel, J. A. Kreiling, J. A. Gagnon, K. L. Mowry, and B. Sandstede, *Analysis of active transport by fluorescence recovery after photobleaching*, Biophys. J., 112 (2017), pp. 1714–1725.

[10] A. E.-M. Clemen, M. Vilfan, J. Jaud, J. Zhang, M. Bärmann, and M. Rief, *Force-dependent stepping kinetics of myosin-V*, Biophys. J., 88 (2005), pp. 4402–4410.

[11] J. C. Cochran and F. J. Kull, *Kinesin motors: No strain, no gain*, Cell, 134 (2008), pp. 918–919.

[12] D. L. Coy, M. Wagenbach, and J. Howard, *Kinesin takes one 8-nm step for each ATP that it hydrolyzes*, J. Biol. Chem., 274 (1999), pp. 3667–3671.

[13] N. D. Derr, B. S. Goodman, R. Jungmann, A. E. Leschziner, W. M. Shih, and S. L. Reck-Peterson, *Tug-of-war in motor protein ensembles*, Science, 338 (2012), pp. 662–666.

[14] J. W. Driver, D. K. Jamison, K. Uppulury, A. R. Rogers, A. B. Kolomeisky, and M. R. Diehl, *Productive cooperation among processive motors depends inversely on their mechanochemical efficiency*, Biophys. J., 101 (2011), pp. 386–395.

[15] R. J. Ellis, *Macromolecular crowding: Obvious but underappreciated*, Trends Biochem. Sci., 26 (2001), pp. 597–604.

[16] S. A. Endow and H. Higuchi, *A mutant of the motor protein kinesin that moves in both directions on microtubules.*, Nature, 406 (2000), pp. 913–6.

[17] A. N. Fehr, C. L. Asbury, and S. M. Block, *Kinesin steps do not alternate in size*, Biophys. J., 94 (2008), pp. L20–L22.

[18] Q. Feng, K. J. Mickolajczyk, G.-Y. Chen, and W. O. Hancock, *Motor reattachment kinetics play a dominant role in multimotor-driven cargo transport*, Biophys. J., 114 (2017), pp. 1–12.

[19] K. Furuta, A. Furuta, Y. Y. Toyoshima, M. Amino, K. Oiwa, and H. Kojima, *Measuring collective transport by defined numbers of processive and nonprocessive kinesin motors*, Proc. Natl. Acad. Sci., 110 (2013), pp. 501–506.

[20] C. Gardiner, *Stochastic Methods: A Handbook for the Natural and Social Sciences*, vol. 13 of Springer Series in Synergetics, Springer Berlin Heidelberg, 4th ed., 2009.

[21] A. Gennerich, A. P. Carter, S. L. Reck-Peterson, and R. D. Vale, *Force-induced bidirectional stepping of cytoplasmic dynein*, Cell, 131 (2007), pp. 952–965.

[22] J. Gou, L. Edelstein-Keshet, and J. Allard, *Mathematical model with spatially uniform regulation explains long-range bidirectional transport of early endosomes in fungal hyphae*, Mol. Biol. Cell, 25 (2014), pp. 2408–2415.

[23] W. O. Hancock, *Bidirectional cargo transport: Moving beyond tug of war*, Nature Rev. Mol. Cell Biol., 15 (2014), pp. 615–628.

[24] A. G. Hendricks, E. Perlson, J. L. Ross, H. W. Schroeder, M. Tokito, and E. L. F. Holzbaur, *Motor coordination via a tug-of-war mechanism drives bidirectional vesicle transport*, Curr. Biol., 20 (2010), pp. 697–702.

[25] F. Jülicher and J. Prost, *Cooperative molecular motors*, Phys. Rev. Lett., 75 (1995), pp. 2618–2621.

[26] B. R. Karamched and P. C. Bressloff, *Delayed feedback model of axonal length sensing*, Biophys. J., 108 (2015), pp. 2408–2419.

[27] K. Kawaguchi, S. Uemura, and S. Ishiwata, *Equilibrium and transition between single- and double-headed binding of kinesin as revealed by single-molecule mechanics*, Biophys. J., 84 (2003), pp. 1103–1113.

[28] J. P. Keener and J. Sneyd, *Mathematical Physiology*, Springer Science & Business Media, 2008.

[29] S. Klumpp and R. Lipowsky, *Cooperative cargo transport by several molecular motors*, Proc. Natl. Acad. Sci., 102 (2005), pp. 17284–17289.

[30] A. B. Kolomeisky and M. E. Fisher, *Molecular motors: A theorist's perspective*, Annu. Rev. Phys. Chem., 58 (2007), pp. 675–695.

[31] C. B. Korn, S. Klumpp, R. Lipowsky, and U. S. Schwarz, *Stochastic simulations of cargo transport by processive molecular motors*, J. Chem. Phys., 131 (2009), p. 245107.

[32] A. Krishnan and B. I. Epureanu, *Renewal-reward process formulation of motor protein dynamics*, Bull. Math. Biol., 73 (2011), pp. 2452–2482.

[33] A. Kunwar and A. Mogilner, *Robust transport by multiple motors with nonlinear force-velocity relations and stochastic load sharing*, Phys. Biol., 7 (2010), p. 016012.

[34] A. Kunwar, S. K. Tripathy, J. Xu, M. K. Mattson, P. Anand, R. Sigua, M. Vershinin, R. J. McKenney, C. C. Yu, A. Mogilner, and S. P. Gross, *Mechanical stochastic tug-of-war models cannot explain bidirectional lipid-droplet transport*, Proc. Natl. Acad. Sci., 108 (2011), pp. 18960–18965.

[35] C. B. Lindemann and A. J. Hunt, *Does axonemal dynein push, pull, or oscillate?*, Cell Motil. Cytoskel., 56 (2003), pp. 237–244.

[36] S. A. McKinley, A. Athreya, J. Fricks, and P. R. Kramer, *Asymptotic analysis of microtubule-based transport by multiple identical molecular motors*, J. Theor. Biol., 305 (2012), pp. 54–69.

[37] C. E. Miles and J. P. Keener, *Bidirectionality from cargo thermal fluctuations in motor-mediated transport*, J. Theor. Biol., 424 (2017), pp. 37–48.

[38] ——, *Jump locations of jump-diffusion processes with state-dependent rates*, J. Phys. A: Math. Theor., 50 (2017), p. 425003.

[39] M. J. Müller, S. Klumpp, and R. Lipowsky, *Tug-of-war as a cooperative mechanism for bidirectional cargo transport by molecular motors*, Proc. Natl. Acad. Sci., 105 (2008), pp. 4609–4614.

[40] B. Nadrowski, P. Martin, and F. Jülicher, *Active hair-bundle motility harnesses noise to operate near an optimum of mechanosensitivity*, Proc. Natl. Acad. Sci., 101 (2004), pp. 12195–12200.

[41] J. Norris, *Markov Chains*, Statistical & Probabilistic Mathematics, Cambridge University Press, 1998.

[42] C. S. Peskin and T. C. Elston, *The role of protein flexibility in molecular motor function: coupled diffusion in a tilted periodic potential*, SIAM J. Appl. Math., 60 (2000), pp. 842–867.

[43] N. Saito and K. Kaneko, *Embedding dual function into molecular motors through collective motion*, Sci. Rep., 7 (2017), p. 44288.

[44] M. Schliwa and G. Woehlke, *Molecular motors*, Nature, 422 (2003), pp. 759–65.

[45] M. Scholz, S. Burov, K. L. Weirich, B. J. Scholz, S. M. Tabei, M. L. Gardel, and A. R. Dinner, *Cycling state that can lead to glassy dynamics in intracellular transport*, Phys. Rev. X, 6 (2016), pp. 1–9.

[46] B. Shtylla and J. P. Keener, *Mathematical modeling of bacterial track-altering motors: Track cleaving through burnt-bridge ratchets*, Phys. Rev. E, 91 (2015), p. 042711.

[47] G. T. Shubeita and S. P. Gross, *4.15 Intracellular transport: Relating single-molecule properties to in vivo function*, in Comprehensive Biophysics, H. E. Egelman, ed., vol. 4, Elsevier, 2012, pp. 287–297.

[48] R. D. Vale, *The molecular motor toolbox for intracellular transport*, Cell, 112 (2003), pp. 467–480.

[49] K. Visscher, M. J. Schnitzer, and S. M. Block, *Single kinesin molecules studied with a molecular force clamp*, Nature, 400 (1999), pp. 184–9.

[50] H. Wang, *Several issues in modeling molecular motors*, J. Comp. Theor. Neuro., 5 (2008), pp. 2311–2345.

CHAPTER 2

BIDIRECTIONALITY FROM CARGO THERMAL FLUCTUATIONS

The article in this chapter is reprinted with permission from *Journal of Theoretical Biology*, **424** (2017) 37–48.

Journal of Theoretical Biology 424 (2017) 37–48

Contents lists available at ScienceDirect

Journal of Theoretical Biology

journal homepage: www.elsevier.com/locate/jtbi

Bidirectionality from cargo thermal fluctuations in motor-mediated transport

Christopher E. Miles*, James P. Keener

University of Utah, Department of Mathematics, 155 S 1400 E, room 233, Salt Lake City, UT 84112-0090, United States

ARTICLE INFO

Article history:
Received 10 December 2016
Revised 26 April 2017
Accepted 29 April 2017
Available online 1 May 2017

Keywords:
Molecular motors
Intracellular transport
Diffusion
Stochastic processes
Mean first passage times

ABSTRACT

Molecular motor proteins serve as an essential component of intracellular transport by generating forces to haul cargoes along cytoskeletal filaments. Two species of motors that are directed oppositely (e.g. kinesin, dynein) can be attached to the same cargo, which is known to produce bidirectional net motion. Although previous work focuses on the motor number as the driving noise source for switching, we propose an alternative mechanism: cargo diffusion. A mean-field mathematical model of mechanical interactions of two populations of molecular motors with cargo thermal fluctuations (diffusion) is presented to study this phenomenon. The delayed response of a motor to fluctuations in the cargo velocity is quantified, allowing for the reduction of the full model a single "characteristic distance", a proxy for the net force on the cargo. The system is then found to be metastable, with switching exclusively due to cargo diffusion between distinct directional transport states. The time to switch between these states is then investigated using a mean first passage time analysis. The switching time is found to be non-monotonic in the drag of the cargo, providing an experimental test of the theory.

1. Introduction

Active transport is a key component of cellular function due to the compartmental nature of cellular machinery. This transport is achieved through the use of molecular motor proteins, which undergo a series of conformational changes to walk along cytoskeletal filaments and generate forces to haul cargoes (Howard, 2001). The transport of a single cargo can often involve two families of motors that are directed oppositely. For instance, kinesin, which primarily walks in the positive direction of a microtubule, and dynein, primarily in the negative direction, can be attached to the same cargo. Another possibility is that two populations of the same family of kinesin motor can be attached to a cargo but walk along oppositely oriented microtubule tracks (Osunbayo et al., 2015). This phenomenon of opposing motor populations is observed for a wide variety of cargoes: mRNA particles, virus particles, endosomes, and lipid droplets (Hendricks et al., 2010; Kunwar et al., 2008). Although both families of motors are exerting forces on the cargo in opposite directions, the net motion of cargo transport is able to switch. That is, the cargo spends periods of time with a net positive, negative, and zero velocity (denoted a pause state), the overall motion of which is denoted *bidirectional transport* (Hancock, 2014). This intuitively inefficient transport phenomenon is thought to serve a role in pattern formation (Brooks and Bressloff, 2016) or spatially uniform cargo delivery (Bressloff and Levien, 2015). However, this work focuses on the *mechanism* of switching. That is, the distinct switching between directions suggests the existence of a mechanism of *cooperation* between the motor families, which has been explored previously from both experimental and theoretical perspectives.

The role of external influences in the cooperation mechanism remains unclear. A number of studies have identified regulators of kinesin and dynein (Fu and Holzbaur, 2014). For instance, LIS1 and NudE have been found to modulate dynein's force production capabilities (McKenney et al., 2010). In Shojania Feizabadi et al. (2015), the authors found that the microtubule itself can regulate kinesin force production. However, the necessity of these external regulators for motor coordination in bidirectional transport remains unestablished. The alternative hypothesis relies on the notion that the coordination is a product of the mechanical interactions of the motors with the cargo, denoted a *tug-of-war* scenario.

The tug-of-war hypothesis has also been investigated from a theoretical and experimental perspective. The authors in Müller et al. (2008) formulate the most notable mathematical model capable of producing bidirectionality. In the model, the motors share the load equally. This assumption is not always invoked in later mathematical models. For instance, Kunwar et al. (2011) performs stochastic simulations of unequally distributed motors. However,

* Corresponding author.
E-mail address: miles@math.utah.edu (C.E. Miles).

http://dx.doi.org/10.1016/j.jtbi.2017.04.032
0022-5193/

these authors compare the results of the stochastic simulation with experiments and conclude that switching statistics do not match as the number of motors varies. In Soppina et al. (2009), another mathematical model is proposed where the two motor populations are required to be asymmetric. That is, the two opposing motor populations must have different force generating properties to break symmetry. Lipowsky et al. (2010); 2006) also provide noteworthy mathematical models, thinking of motor transport as a "rubber-band"-like process and find rich dynamics. Although not specifically about tug-of-war, motor population models such as the Huxley crossbridge model (Huxley, 1957; Keener and Sneyd, 2008) use force-velocity relationships for the motor populations. However, since this analysis is a steady-state analysis, it is difficult to infer dynamics, which we address in our model. In Bouzat (2016), the authors reexamine the mathematical model of Kunwar et al. (2011) and stress the importance of cargo diffusion for the model to produce the right behavior, specifically pointing out the issue of relating steady-state force-velocity curves to dynamics. An asymptotic analysis of a model bearing many similarities to our proposed model (but still with discrete motor number) can be found in McKinley et al. (2012). The authors include cargo diffusion in a stochastic differentialequation description and note that motor dynamics slow compared to fast fluctuations in the cargo velocity, which ultimately is an important ingredient of our work.

In this work, we present a new tug-of-war model of bidirectional motor-mediated transport. Our proposed model contains fundamentally different essential components than previous work. Broadly, the proposed model is a mean-field model with unequally distributed load. This differs from previous discrete motor, unequal load descriptions and therefore requires a different source of noise to induce switching. By examining the force generation of bound motors, we quantify the delayed response to instantaneous changes in the cargo velocity. We make an approximation (and justify numerically) that this delay structure extends beyond the scope of only bound motors, allowing for the use of a force-velocity relationship to study the full system. This reduction leads to a system of two "characteristic distances", one for each motor population. By symmetry, this two-variable system is collapsed to a single dimension which is found to be metastable, with two states corresponding to positive and negative net velocities, or bidirectional motion. The noise that drives switching between these two states is due to cargo diffusion (thermal fluctuations), an aspect of this process previously noticed but under-emphasized until recently (Bouzat, 2016).

Previous work has indeed illustrated the significance of motor number fluctuations (Nadrowski et al., 2004). However, in this present work, we choose to use a mean-field model to emphasize the lack of necessity of discrete motor number for bidirectionality. Our proposed model still incorporates binding and unbinding dynamics and therefore has the same *mean* behavior as a discrete motor model, but lacks the noise associated with discrete events. The only remaining noise source is then cargo diffusion, which we show to be sufficient for bidirectionality. The difference in magnitudes between the fluctuations due to motor number and cargo diffusion is difficult to quantify due to the fundamental difference in structure. In Guérin et al. (2011a), the authors find that motor number fluctuations can result in an effective diffusion when the number of motors involved in transport is large.

A characteristic quantity in validating bidirectional transport models is the reversal or switching time of the system: the time between runs of each direction. In our model, the correlation structure of the effect of noise on each population allows for the reduction to an invariant manifold and consequently, a one dimensional mean first passage time problem in a double-well potential. Classical tools can then be used to numerically solve and analytically approximate the corresponding boundary value problem. The switching time is considered as a function of the cargo drag coefficient, which leads to complex behavior as the wells steepen but diffusion strengthens as the drag decreases. Ultimately, the mean switching time is found to be non-monotonic in the cargo drag coefficient, a feature not expected for switching due to motor dynamics. This non-monotonicity provides an experimental test to validate (or refute) our diffusion-driven switching hypothesis.

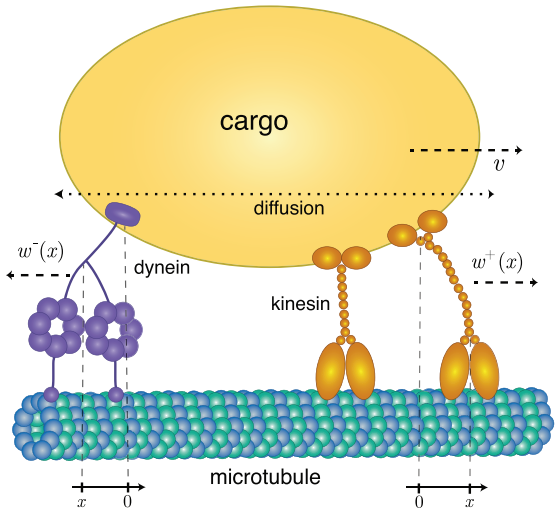

Fig. 1. A diagram of the mean-field model setup. The quantity, x, denoting the distance a motor is stretched is always measured with respect to the orientation of the microtubule.

2. Methods

2.1. Model formulation

Consider a cargo being pulled by two different populations of motors, denoted + and −. Let $m^{\pm}(x, t)$ be the density of type + or − motors at time t and stretched from their unstretched distance x units. The + or − labeling of the motor families denotes their preferred directionality. That is, m^+ corresponds to the density of motors preferring to walk in the positive direction (e.g. kinesin) and m^- the density of motors preferring to walk in the negative direction (e.g. dynein) as seen in Fig. 1. Although the negatively oriented motors are depicted as dynein in the figure, this need not be the case. The negatively oriented motors could be, for instance, another set of kinesin motors on an opposing microtubule. The framework presented is sufficiently general to accommodate both. The evolution of each motor population is then described by

$$\frac{\partial m^{\pm}}{\partial t} + \underbrace{\frac{\partial}{\partial x}\left\{\left[w^{\pm}(x) - v(t)\right]m^{\pm}\right\}}_{\text{stepping}} = \underbrace{\left(M^{\pm} - \int_{-\infty}^{\infty} m^{\pm}(x,t)\,\mathrm{d}x\right)\Omega_{\text{on}}^{\pm}(x)}_{\text{binding}} - \underbrace{\Omega_{\text{off}}^{\pm}(x)m^{\pm}(x,t)}_{\text{unbinding}}. \tag{1}$$

Although (1) appears as only one equation, m^+ and m^- each have their own equation that are structurally identical but may contain different parameters or functional forms. The quantity x, describing the distance the motor is stretched from its unstretched

displacement is always measured with respect to the microtubule, even though each motor type walks in a different direction, see Fig. 1. This choice of frame of reference is convenient, as it causes the two equations to be structurally identical (as opposed to having to reverse the sign of v).

It is worth noting that this PDE has been studied in other contexts and is referred to as the Lacker–Peskin PDE (Srinivasan and Walcott, 2009), which is an extension of the Huxley crossbridge model (Huxley, 1957; Keener and Sneyd, 2008). In that literature, the particular form of the PDE is derived from the limit of a large number of discrete binding sites or a large number of motors. However, in the present context, it is well established that the number of motors is quite small (Hendricks et al., 2010; Rai et al., 2013), hence a different interpretation for the mean-field model must be taken. If $M = 1$, Eq. (1) is a Chapman–Kolmogorov equation, corresponding to the behavior of a single motor and describes the probability of finding a motor stretched distance at x at time t. This process is inherently random by the stochastic nature of the binding dynamics, which is entirely accounted for in the binding and unbinding terms of the mean-field equation.

Cargo mediated transport is a multi-motor phenomenon, and consequently, we are interested in the behavior of an ensemble of motors. However, we point out the observation that (ignoring crowding effects) the motors interact solely through the cargo. For this reason, the motors can be treated as acting identically and independently, and hence, a mean-field model, which can be thought of as a rescaling of the Chapman–Kolmogorov equation for a single motor, is applicable. To elaborate, we can regard $m(x, t)$ as the *expected* (or mean, hence the name *mean-field*) number of motors bound at a given x and t. By construction, $0 \leq \int m\,dx \leq M$, and therefore the interpretation of M is a maximum number of motors bound. Thus, we have effectively averaged over the stochasticity in the binding dynamics to study a mean-field description of motor ensembles.

Before describing, in detail, each term in (1), we state a driving assumption for several of the functional forms appearing in the equation. The force generated due to the linker stretching is assumed to be Hookean, that is force $\sim kx$, where k is the spring constant or stiffness of the motor linker attachment to the cargo. The force-displacement curve of molecular motors has been studied experimentally (Kawaguchi et al., 2003; Lindemann and Hunt, 2003) and, although not perfectly linear, seems to be well-approximated by this assumption.

We now discuss each term of the equation in more detail. Broadly, the motor population can change in three ways: motors stepping (walking), binding or unbinding.

1. **stepping**: We assume that the rate of stepping for motors is dependent on the force exerted on the motor, typically characterized by a force-velocity curve. The force on the motor is generated by the linker displacement x in a Hookean manner, $F = kx$. Consequently, the walking rate of a motor is more naturally thought of as a *displacement*-velocity relationship, which is qualitatively the same as the force-velocity curve by the linearity of the force generation. Denote this displacement-velocity curve by $w(x)$ and take it to be of the linear form

$$w(x) := -ax + b, \tag{2}$$

where $a > 0$. At $x = 0$, which corresponds to the motor being unstretched, the motor walks with some velocity b. For the + directed motor, for instance, $b > 0$. As the motor walks farther from its unstretched position ($x > 0$), the force exerted on it causes the velocity to decrease until it eventually stalls at $x_{\text{stall}} := b/a$. If $x < 0$, that is, the cargo is ahead in the direction the motor seeks to walk, the velocity is assumed to be greater as the linker exerts a force in the direction of motion of the motor. If $x > x_{\text{stall}}$, then the force exerted by the linker is greater than the stall force, meaning the motor moves opposite its preferred direction.

Force-velocity relationships have been qualitatively observed experimentally for kinesin (Gennerich et al., 2007; Kunwar et al., 2008) and dynein (Belyy et al., 2014). One notable observation is a dramatic difference in behavior between motors in high ATP environments (Carter and Cross, 2005; Visscher et al., 1999) and ATP starved motors (Gross et al., 2007; Mitchell and Lee, 2009). For this work, we assume the motors operate with sufficient ATP. The force-velocity curve is visibly nonlinear, with main deviation from linearity occurring at superstall forces, where motors velocities become negative (as in this model), but with much smaller magnitude. Motors operating with an assisting force ($x < 0$ in this model) also appear to operate with sub-linear velocities. For this reason, a sigmoidal form (due to its saturating behavior) is deemed appropriate and used in a number of other modeling papers (Bouzat, 2016; Kunwar et al., 2011; McKinley et al., 2012; Müller et al., 2008). However, in this work, we assume that motors operate in a regime of the force-velocity curve that can be approximated by its linearization. This assumption is explored and discussed further in Section 3.1.

2. **binding**: The functional form of the binding term is set to be

$$\Omega_{\text{on}}(x) := k_{\text{on}}\,\delta(x),$$

where k_{on} is the constant describing the rate of binding of a molecular motor to the cargo. The $\delta(x)$ functional form corresponds to the assumption that motors are initially unstretched ($x = 0$) when they bind, thus only binding at $x = 0$. That is, the motors only bind in a non-force-producing state. This assumption can be relaxed (and is for later numerical simulations) to a Gaussian approximation of the delta function.

3. **unbinding**: The unbinding rate of molecular motors has experimentally been found to be related to the force exerted on them (Kawaguchi et al., 2003; Kunwar et al., 2011), however the nature of this dependency is complex and varies from motor to motor. Dynein is found to a have a catch-bond behavior (Kunwar et al., 2011; Nicholas et al., 2015). Both kinesin (Andreasson et al., 2015) and dynein (Nicholas et al., 2015) have been observed to have asymmetric force dependence in their unbinding.

Due to the complexity and variation in unbinding dependence, we take the simplest form that still behaves in a way that qualitatively matches experimental results, which is

$$\Omega_{\text{off}}(x) = k_{\text{off}}\,\exp\left\{\frac{k|x|}{F_D}\right\},$$

where again, the force exerted is assumed to be Hookean ($\sim kx$), and independent of direction (hence the absolute value). F_D is a characteristic force fit to experimental observations, and k_{off} is the unstretched detachment rate. This form is often referred to as Bell's Law, which is known to need corrections in some scenarios (Walcott, 2008). The overall behavior of this function establishes that motors detach at a faster rate the farther they are stretched due to the force exerted on their microtubule binding sites.

This functional form (or similar) has been used in other motor population models (Srinivasan and Walcott, 2009; Walcott, 2008). In Kunwar et al. (2011), the authors account for the stalling of motors and the catch-bond behavior of dynein by taking a non-monotonic dependence on the force. In our unbinding rate, neither the catch-bond behavior nor is the asymmetric dependence on force is included. The consequence of excluding these phenomena is purely quantitative, as they are not

dramatic enough effects (in the regimes that motors operate for transport) to produce a qualitative effect in our model.

It is also worth noting that Ω_{off} and Ω_{on} have different units, as the off-rate is multiplied by m, a motor density and the on-rate is multiplied by a total number of motors $\int m\,dx$.

We then can define the average force exerted by each motor population, recalling the assumption of a Hookean force,

$$F^{\pm}(t) := \int_{-\infty}^{\infty} k^{\pm} x m^{\pm}(x,t)\,dx. \tag{3}$$

This time-varying quantity requires knowledge of the full density of motors $m(x, t)$, which makes it difficult to study directly.

2.2. Steady-state analysis

This time-dependent force, described by (3) is difficult to compute in practice, so we turn our attention to the steady-state force. We consider the steady state ($dm^{\pm}/dt = 0$) and behavior of (1) with some steady-state velocity $\tilde{v}$, which leads to the pair of equations for the steady state densities $\tilde{m}^{\pm}$

$$\frac{\partial}{\partial x}\left\{\left[w^{\pm}(x) - \tilde{v}\right]\tilde{m}^{\pm}\right\} = \left(M^{\pm} - \int_{-\infty}^{\infty} \tilde{m}^{\pm}(x)\,dx\right)\Omega^{\pm}_{\text{on}}(x) - \Omega^{\pm}_{\text{off}}(x)\tilde{m}^{\pm}(x). \tag{4}$$

Exploiting the linearity of (4), along with the partitioning nature of the delta function, (4) can be solved analytically, resulting in a solution with an integrable singularity at the stall distance dependent on the velocity

$$x_{\text{stall}} := \frac{b - \tilde{v}}{a}.$$

For details of this calculation, see *Supplementary Section S1*. This allows us to define the steady state force exerted by each population of motor

$$\tilde{F}^{\pm}(\tilde{v}) := \int_{-\infty}^{\infty} k^{\pm} x \tilde{m}(x;\tilde{v})\,dx, \tag{5}$$

where we parameterize this force as a function of the steady state cargo velocity $\tilde{v}$ which appears in (4).

We now need an equation governing the cargo velocity, which is determined by the forces exerted on the cargo

$$\mathcal{M}\dot{v} + \gamma v = \sqrt{2\gamma k_B T}\xi(t) + \text{forces exerted by motors}. \tag{6}$$

In (6), $\mathcal{M}$ is the mass of the cargo, γ is the drag coefficient of the cargo and $\xi(t)$ is the white-noise process due to thermal fluctuations (diffusion) of the cargo which satisfies $\langle \xi(t)\xi(\tau)\rangle = \delta(t-\tau)$. The magnitude of these fluctuations is determined by the fluctuation-dissipation theorem (Gardiner, 2009).

2.3. Forces exerted by motors

A perhaps natural choice for the force terms in (6) could be the steady-state force, $\tilde{F}^{\pm}(v)$, found in (5). The use of a *force-velocity* relationship (which $\tilde{F}$ is) to study motors has a long history (e.g. Huxley (1957)) but there is a problem with this choice. Although v is changing instantaneously, the position of the cargo is not. The forces exerted by the motors are due to stretching of the linker (determined by their displacement), which does *not* change instantaneously as the velocity changes. In other words, it is impossible to completely infer *dynamics* from a *steady-state* force-velocity relationship. Thus, parameterizing the force with time-varying velocity would not produce the physical behavior we desire. For this reason, we turn to a simpler model to understand what to use for the force terms in (6) that accounts for this issue.

In Bouzat (2016), the authors make the observation that including cargo noise produces this described difficulty: motors should not react instantaneously to velocity and classical models produce results inconsistent with experimental observations if this is the case. To overcome this issue, the authors hypothesize that the motors respond to a time-windowed-average force, suggesting some "memory" property of the motors. Here, we directly compute a physiological, mechanistic delay stemming from the stepping of the motor, instead of a phenomenological "memory."

2.3.1. Ornstein–Uhlenbeck motivation

To understand motor response to fluctuations in the cargo velocity, we now turn our attention the behavior of an ensemble of M motors on a *single run*: after binding and before unbinding. This focus stems from the observation that force generation can only occur while the motors are bound. The dynamics of force generation are of interest as these dictate the cargo behavior. In McKinley et al. (2012), the authors also study the behavior of motors without binding dynamics and find that multiple motors can actually produce a lower cargo velocity than a single motor. However, in our model, we reiterate that the motors act identically and independently aside from interaction with the cargo, which is addressed separately. Hence, it is sufficient to describe the behavior of a single motor. Let $p_1(x, t)$ describe the probability density of finding a motor stretched distance x from its unstretched position at time t and let $x_1(t)$ be the corresponding Langevin random process.

The behavior follows almost identically with the mean-field model (1), but now binding and unbinding can be neglected due to the analysis only being of a single run. The only remaining dynamics are the motor stepping (still at its force dependent velocity w) and diffusion (the magnitude of which is lumped into a parameter D). The resulting process is an Ornstein–Uhlenbeck process Gardiner (2009), which can be described by the Langevin equation

$$\dot{x}_1 = [w(x_1) - v(t)] + \sqrt{2D}\,\xi(t),$$

or the corresponding Fokker–Planck equation

$$\frac{\partial p_1}{\partial t} = -\frac{\partial}{\partial x}\{[w(x) - v(t)]p_1\} + D\frac{\partial^2 p_1}{\partial x^2}. \tag{7}$$

To quantify the motor's ability to respond to instantaneous fluctuations in the cargo velocity, we consider the mean position of a motor while still attached, denoted μ_1,

$$\mu_1 := \langle x_1(t)\rangle.$$

From the Fokker–Planck equation (7), we find the relationship describing the temporal evolution of the mean of this process to be (assuming w is a linear function)

$$\dot{\mu}_1 = w(\mu_1) - v(t). \tag{8}$$

For details of the calculation, see Appendix A.

However, again recalling the assumption of a Hookean force (that is, force from a single motor stretched distance x_1 is kx_1), the average force exerted by a single motor under evolving under this process with density $p(x_1, t)$ is then

$$F_1 = k\int_{-\infty}^{\infty} x_1 p(x_1,t)\,dx_1 = k\mu_1.$$

and, since we have M motors in our ensemble, the total average force is immediate from linearity

$$F_{tot} = Mk\mu_1. \tag{9}$$

In other words, *for a bound ensemble of motors*, the mean force exerted can be parameterized by the mean distance stretched μ, where μ "tracks" the velocity through (8). This illustrates that the magnitude of the delay in motor response to fluctuations in cargo velocity is determined by the motor velocity. In other words, changes in force are only due to changes in displacement, not

velocity. This resolves the aforementioned issue about the force changing instantaneously. Now, the mean force tracks, with some delay as determined by (8), the velocity and evolves continuously.

2.3.2. Force evolution approximation

The previous calculation showed that while still attached, the mean force generation for a population of motors could be collapsed down to a single parameter μ_1. However, relating the mean-field model to this single-run analysis presents an obvious issue: how to account for binding dynamics? We now make the major approximation of the paper: even with binding and unbinding, the mean force generated by each population of motors can be collapsed to a single parameter μ (for each population) with a similarly structured delay. This leads us to the set of equations (with one motor family for illustration)

$$\mathcal{M}\dot{v} + \gamma v = \hat{F}(\mu) + \sqrt{2\gamma k_B T}\xi(t), \qquad \dot{\mu} = w(\mu) - v. \tag{10}$$

We assume the cargo velocity v fluctuates with the forces exerted on it, but the force exerted by the motors is not directly prescribed by the current v but rather some parameter μ which tracks v with a delay. We note that, in the previous section, we have proven that this delay structure exists while the motors are attached. However, we posit that this delay structure is still appropriate even when binding dynamics are incorporated because force generation on the cargo requires the motors to be attached. In the previous analysis, μ had a physical meaning: the average distance a motor is stretched. However, we lose this meaning and consider μ a "characteristic distance." The force exerted by these motors is also no longer $Mk\mu_1$ because not all motors are bound at any given time, so we give the force a general form $\hat{F}(\mu)$ that is specified later. It is also important to reiterate that (10) is written for a single parameter μ, meaning a single motor population to demonstrate the structure but we later incorporate parameters μ_1, μ_2, one for each population.

The particular choice of the parameterized force $\hat{F}_j(\mu)$ (for $j = 1, 2$, corresponding to each population) must not neglect unbinding and binding of the motors and must account for the fact that not all motors are bound at a given time. We conjecture that a sufficient approximation is the steady-state force $\tilde{F}(\tilde{v})$, originally parameterized by a steady-state cargo velocity $\tilde{v}$, described by (5).

It does not seem immediately clear how to construct a mapping between a value of μ and $\tilde{v}$ to plug into $\tilde{F}$. We recall that $\tilde{F}$ was computed assuming the cargo velocity $\tilde{v}$ was fixed (in steady-state), whereas the true quantity $v(t)$ is constantly fluctuating and never in steady-state. Utilizing the fact that $\tilde{v}$ corresponds to steady-state, we can construct a mapping between μ and $\tilde{v}$ by ensuring that the equilibria of our approximation match the equilibria of the original system. That is, if we are in steady-state, $\dot{\mu} = 0$ and consequently

$$\dot{\mu} = 0 = -a\mu + b - \tilde{v} \quad \Rightarrow \quad \tilde{v} = -a\mu + b.$$

This then provides a mapping between a steady-state cargo velocity $\tilde{v}$ and a particular μ value. Hence, we can now evaluate our force as a function of μ

$$\hat{F}_j(\mu_j) = \tilde{F}_j(-a_j\mu_j + b_j). \tag{11}$$

We reiterate that this approximate system is still inherently out-of-equilibrium, but now, by construction, has equilibria that match the original model since $\dot{\mu} = 0$ corresponds to a particular $\tilde{v}$, a steady-state velocity from which the force was originally computed.

In other words, the motors track the steady state force-velocity curve $\tilde{F}$ with some delay. This particular choice of the force structure allows for the complexity of the mean-field model, including all binding and unbinding to be embedded into the $\hat{F}(\mu)$ terms. However, the dynamics of the reduced "characteristic distance" model are easier to study due to being an ordinary differential equation rather than a partial differential equation. Our analysis shows that this delay structure is exact for bound motors and this approximation posits an extension of the structure to account for binding and unbinding. We explore the validity of this approximation numerically in Section 3.2.

2.4. Full model

The parameter regime we are considering deals with cargo with negligible mass, thus suggesting we are in a viscous or near-viscous regime. Exploiting this fact, we can perform an adiabatic (quasi-steady state) reduction on (10) to eliminate v. For details of this calculation, see *Supplementary Section S3*. The result of performing this reduction (with a single motor population) is

$$\dot{\mu} = w(\mu) - \frac{\hat{F}(\mu)}{\gamma} + \sqrt{\frac{2k_BT}{\gamma}}\xi(t), \tag{12}$$

or equivalently, in Fokker–Planck form

$$\frac{\partial p}{\partial t} = -\frac{\partial}{\partial \mu}\left\{w(\mu) - \frac{1}{\gamma}\hat{F}(\mu)\right\} + \frac{k_BT}{\gamma}\frac{\partial^2 p}{\partial \mu^2}. \tag{13}$$

One important note from the calculation detailed in *Supplementary Section S3* is that although v is eliminated from the system, v relaxes quickly to a Gaussian centered around

$$\hat{v} \sim \hat{F}(\mu)/\gamma, \tag{14}$$

thus the value of μ directly determines the (mean) velocity of the cargo at any time.

Combining all of the previous observations, we now propose the full model. In the derivation of (12,13), only one motor population was considered, but in bidirectional transport, there are two populations evolving separately, resulting in two equations with identical structure but different parameters. From this, we get the full model

$$\begin{aligned}\dot{\mu}_1 &= -a_1\mu_1 + b_1 - \frac{1}{\gamma}\{F_1(\mu_1) + F_2(\mu_2)\} + \sqrt{\frac{2k_BT}{\gamma}}\xi(t),\\ \dot{\mu}_2 &= -a_2\mu_2 + b_2 - \frac{1}{\gamma}\{F_1(\mu_1) + F_2(\mu_2)\} + \sqrt{\frac{2k_BT}{\gamma}}\xi(t).\end{aligned} \tag{15}$$

Note that we have switched the two populations to labels $j = 1, 2$ instead of $+/-$ and dropped the hat notation from $\hat{F}_j$ for notational convenience. Because the motor populations were originally coupled through the forces, the force terms in (12,13) must be replaced with the sum of forces from each family, and consequently, the Eqs. (15) are coupled. We have also used the functional form of the motor force velocity curve $w(x) = -ax + b$ and that the net force exerted by the motors is simply the sum of the force exerted by each population.

To emphasize the ability of this model to produce bidirectional motion without asymmetry between the motor populations, we take the parameters describing each of the populations to be the same (unless noted otherwise), described in Table 1. These parameters are chosen as physiologically reasonable parameters in the range of reported values of both kinesin and dynein, taken from Kunwar et al. (2008),Schnitzer et al. (2000) and Klumpp et al. (2015). The viscosity of cytoplasm is reported to be higher than water (Luby-Phelps, 2000; Mitchell and Lee, 2009). Although a potentially large viscosity is used in this work, any smaller would only make the magnitude of the fluctuations larger, further magnifying the importance of cargo diffusion.

2.5. Dimensional reduction

An important observation must be made about the noise structure of (15): the white noise term in each equation is exactly the

Table 1
"Typical" motor values used for both populations of motors in the symmetric case of the mean field model. Values used are within reported ranges of kinesin and dynein.

F_{stall} [pN]	v_0 $[\text{nm}\cdot\text{s}^{-1}]$	k_{off} $[\text{s}^{-1}]$	$\lvert F_d\rvert$ [pN]	k_{on} $[\text{s}^{-1}]$	M	k $[\text{pN}\cdot\text{nm}^{-1}]$	γ $[\text{pN}\cdot\text{s}\cdot\text{nm}^{-1}]$
5	1000	1	1	5	10	0.4	0.001

same (fully correlated). From a biophysical perspective, this is because the two motors feel the same fluctuations from the cargo diffusion. Hence, this is truly a one-dimensional diffusion rather than two dimensional as it currently appears. The Fokker–Planck equation corresponding to the system (15) has a non-invertible diffusion tensor, which further illustrates this point. To make the one-dimensional structure more apparent, we perform a change of variables, taking

$$\zeta := \mu_1 + \mu_2, \quad \eta := \mu_1 - \mu_2$$

Under this coordinate change, the system (15) becomes, abbreviating $D := k_B T/\gamma$

$$\dot{\zeta} = -\frac{a_1}{2}(\zeta+\eta) + b_1 - \frac{a_2}{2}(\zeta-\eta) + b_2 - \frac{2}{\gamma}\sum_j F_j + 2\sqrt{2D}\xi(t)$$

$$\dot{\eta} = -\frac{a_1}{2}(\zeta+\eta) + b_1 + \frac{a_2}{2}(\zeta-\eta) - b_2.$$

By taking the two populations to be symmetric, which corresponds to $a_1 = a_2 = a$ and $b_1 = -b_2 = b$, the η equation becomes

$$\dot{\eta} = -a\eta + 2b,$$

which has an invariant manifold described by $\tilde{\eta} = 2b/a$. Since the equilibria of the system must lie on this invariant manifold, all dynamics of interest evolve on the manifold and consequently reduces the problem to the one-dimensional evolution

$$\dot{\zeta} = -a\zeta - \frac{2}{\gamma}\left[F_1\left(\frac{\zeta+\tilde{\eta}}{2}\right) + F_2\left(\frac{\zeta-\tilde{\eta}}{2}\right)\right] + 2\sqrt{2D}\xi(t), \qquad (16)$$

where again, $\tilde{\eta} = 2b/a$.

Thus, we have fully reduced the dynamics of the system to a single time-varying quantity ζ, which again does not seem to have a physical meaning but can be thought of as the *characteristic distance* of the system. Although a considerable number of reductions have been made, the physical behavior of the system is still recoverable by recalling that the instantaneous mean cargo velocity, $\hat{v}$, of the system can be recovered from (14). In other words, $\zeta(t)$ is a proxy for $\hat{v}(t)$ which is the biophysical quantity of interest. It is worth noting that the analysis exploits the existence of an invariant manifold, but it does not seem to be the case that such a manifold exists if the populations are asymmetric. Hence, the asymmetric population problem is considerably more difficult to study (as only Monte Carlo simulations seem to be feasible) and not within the scope of this work.

3. Results

3.1. Linear motor force–velocity curve

We briefly explore the consequences of approximating the motor force-velocity curve $w(x)$ as a linear function described in (2). Recall that $w(x)$ is really a *displacement*-velocity curve but force generation is assumed to be Hookean, so the qualitative shape remains the same as the force-velocity curve. We reiterate that a sigmoidal force-velocity relationship seems to be in closer agreement to experimentally observed measurements and used it on other models. However, we posit that the motors operate primarily in a region of the force-velocity curve that can be approximated by its linearization. To assess the validity of this approximation, we relaxed the assumption of linearity on $w(x)$ and changed the functional form to be of the form $\tilde{w}(x) = \alpha_0 + \alpha_1 \tanh(\alpha_2(x-\alpha_3))$, a particular sigmoidal function utilized in previous work (McKinley et al., 2012). We then compare the steady-state ensemble force-velocity described by (5) produced by the linear $w(x)$ and two different parameter choices of the sigmoidal form that vary only by how quickly they saturate. The result of this comparison can be seen in Fig. 2. From this figure, we can see that the force-velocity curves produced for the ensemble (on the right) vary very little when the form of $w(x)$ is changed. There is excellent qualitative agreement and even good quantitative agreement, seeming to only differ for sufficiently large velocities outside the scope of the model. Thus, we conclude the use of the linearized $w(x)$ is suitable for the analysis, particularly noting that $\tilde{F}$ is the effectively only quantity used from the mean-field model and remains virtually the same. We conjecture this result can be interpreted intuitively, as superstall velocities are larger in magnitude by our approximation, meaning that the motors relax back to stall faster and therefore generate a smaller force due to displacement. This is offset by the motors unbinding less rapidly (due to a lower force), and consequently the net force generated is approximately the same.

3.2. Force delay approximation

The form of the system (10) is an approximation which describes a delay structure, where the force generated by a family of motors can be parameterized by a single dynamic quantity, μ. We prove this to be the case while the motors are bound with (9) and (12), but the heart of the approximation is that this extends to when binding dynamics are incorporated. We posit that a sufficient approximation to the instantaneous force generated is the steady-state ensemble force $\tilde{F}(\tilde{v})$ with a particular mapping between μ and $\tilde{v}$ described by (11). We seek to assess the validity of the collapse of the force generated by the mean-field equation to a force parameterized by μ. Specifically, we compare numerical simulations of the full mean-field model (1,3) and the reduced model (10). This numerical simulation is *not* an assessment of the validity of the mean-field model, but rather the validity of the force generated by collapsing the PDE behavior down to a single ODE for μ.

We simulate only a single motor family (+ direction) and no thermal noise for illustration. The approximation fundamentally is one of how motors (and the force generated by them) respond temporally, so a numerical experiment is performed by applying instantaneous external forces to both the mean field model of motors and the reduced model, both of which have cargo dynamics determined by (6). Both models are started at the completely unloaded state and run to equilibrium. Once at equilibrium, a -5 pN force (and later +5 pN) external force is applied to the cargo for 5 ms and then removed. The mean-field PDE was simulated using a Lax–Wendroff scheme and the remaining ODEs are computed using a Runge–Kutta 4(5) scheme. The dynamics of the force generated by the motor population and the resulting cargo velocity are tracked and shown in Fig. 3.

From Fig. 3 we are able to make a number of observations about the validity of the "characteristic distance" approximation. For one, the equilibria of the full model and reduced model are the same, which is immediate by the choice of (11), but also indicates

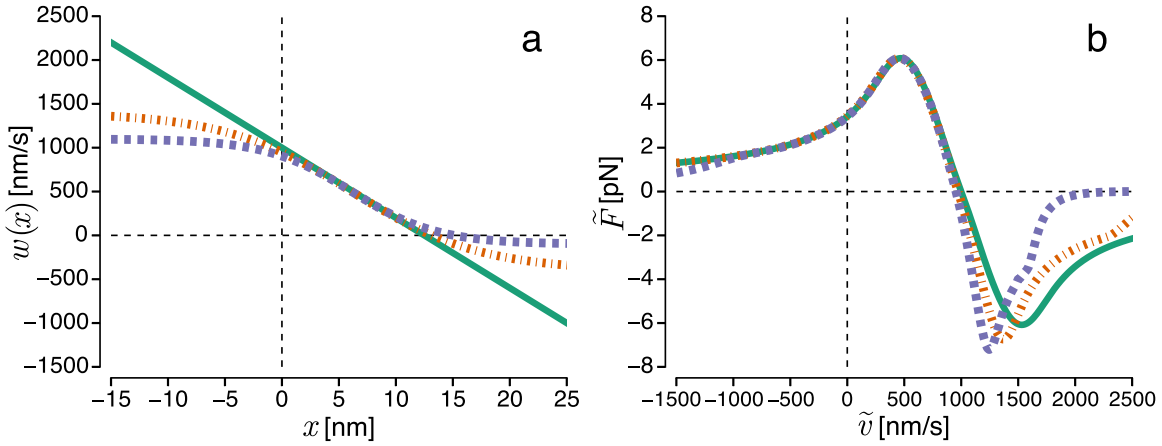

Fig. 2. **a:** the linear form (green, solid) of the displacement-velocity relationship of individual motors $w(x)$ used throughout the paper and two different sigmoidal versions for comparison (dotted). **b:** the resulting steady-state force-velocity curves for the ensemble of motors described by (5) for the different choices of $w(x)$. (For interpretation of the references to colour in this figure legend, the reader is referred to the web version of this article.)

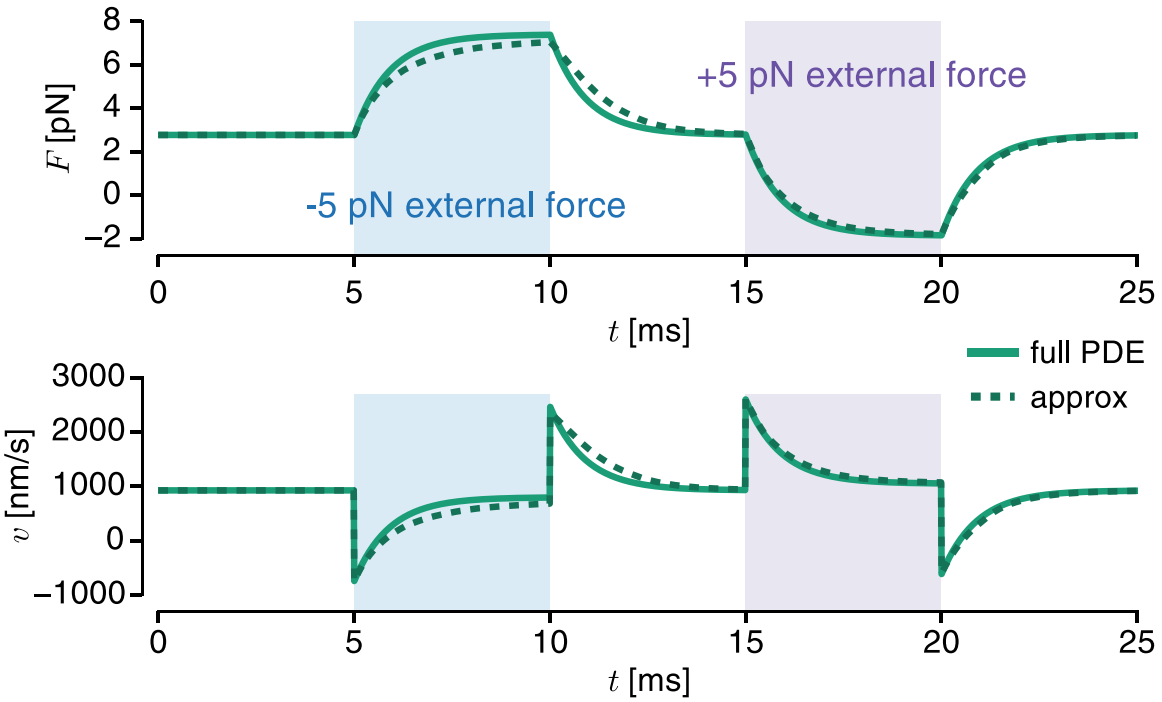

Fig. 3. A numerical comparison of the forces and cargo velocity generated by the full mean field motor model (1,3) with the "characteristic distance" approximation described by (10) for one motor population and no thermal noise. In both models, the evolution of the cargo velocity is described by (6). External forces are applied to the cargo and removed to illustrate the ability of the reduced model to respond to temporal changes in force.

that the reduced and full models have agreement on long time scales. As the external force changes instantaneously, both models behave (quantitatively and qualitatively) similarly regardless of the directionality of the force, and therefore, suggests there is also agreement on short time scales. Other external inputs (e.g. sinusoid) were also investigated and yielded similar results. Thus, we have collapsed the force generated by the PDE mean-field description of motors (1,3) into an ODE (10) in a "characteristic distance" variable and the approximation appears to be valid. We remind the reader that the binding dynamics are built into the mean-field structure, and therefore are accounted for in both the full model and reduced.

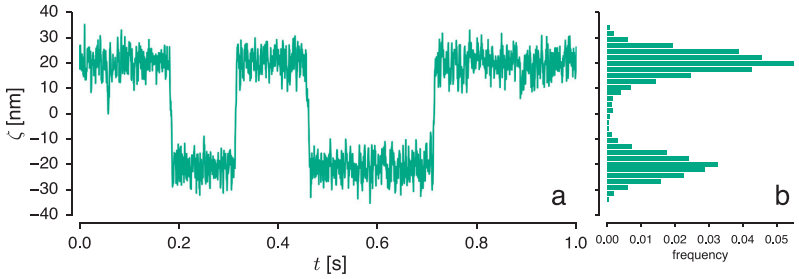

Fig. 4. **a:** A typical simulation of (16) performed with the Euler–Maruyama scheme. The system notably switches between two configurations. **b:** A histogram of the values of the simulation, which demonstrates bimodality.

3.3. Metastable behavior

We perform simulations of (16) with the parameters specified in Table 1 with the Euler–Maruyama scheme (Kloeden and Platen, 1992). The results of a typical simulation can be seen in Fig. 4a. From this simulation, we see a curious behavior: the characteristic distance ζ switches between two configurations, or is said to be *metastable*. Elaborating on this, ζ takes on values near some particular point and then, due to the noise of the system, randomly switches to values centered around another point. The histogram of ζ values during the simulation, which can also be seen in Fig. 4b is clearly bimodal, which is a characteristic sign of metastability. Although the two peaks in the figure appear different, this is a consequence of the short time for which the simulation was performed. If more switches were recorded, the two peaks of the histogram would be identical due to the symmetric population assumption, however this time frame was chosen to demonstrate the time-scale on which switching occurs.

The metastable behavior of the system is apparent from simulations, but can be further elucidated. To do so, consider the corresponding Fokker–Planck equation to (16), which describes the probability density $p(\zeta, t|\zeta_0, 0)$. That is, the probability density of (16) given that it started at ζ_0, which is described by

$$\partial_t p = -\partial_\zeta \{A(\zeta)p\} + 4D\partial_{\zeta\zeta} p, \tag{17}$$

where we are abbreviating

$$A(\zeta) := -a\zeta - \frac{2}{\gamma}\left[F_1\left(\frac{\zeta+\tilde{\eta}}{2}\right) + F_2\left(\frac{\zeta-\tilde{\eta}}{2}\right)\right], \qquad D := \frac{k_B T}{\gamma}. \tag{18}$$

A bifurcation diagram of the equilibria of $A(\zeta)$ is constructed by varying γ, the drag coefficient. Since ζ is not the physical quantity of interest, we translate the equilibria of ζ into the corresponding mean cargo velocity $\tilde{v}$ under the transformation described by (14). The resulting bifurcation diagram can be seen in Fig. 5a. This figure captures exactly the phenomenon described as *bidirectional motion* (Hancock, 2014). We see that for a robust range of γ, the system is *bistable*: there are stable positive and negative mean cargo velocities, which we will denote v_+, v_- respectively. In this same regime, the zero velocity v_0 is unstable. Interestingly, in small window of γ values, the system is actually *tristable*: two new equilibria emerge in a bifurcation and cause v_0 to turn stable. This may correspond to the experimental observation (Kunwar et al., 2011) that the system can spend long periods of time in a "pause" state, also noting that this same experimental work suggests velocities that agree with those predicted by our model. For large values of γ, the system only has one stable equilibrium, v_0.

From, Fig. 5a, the tristable region in γ-space is fairly narrow. It is possible that other parameters (or more detailed functional forms) would allow for this region to be more robust, but this is not observed. In fact, increasing motor processivity by lowering the baseline unbinding rate by an order of magnitude ($k_{\text{off}} = 1\,[\text{s}^{-1}] \to 0.1\,[\text{s}^{-1}]$) resulted in a *smaller* region of tristability, but larger region of bistability. For this reason, we instead focus our study toward the bistable region, where we study the time to switch between the positive and negative velocities. Then, the corresponding potential can be defined by

$$U(\zeta) := -\int A(\chi)\,\mathrm{d}\chi. \tag{19}$$

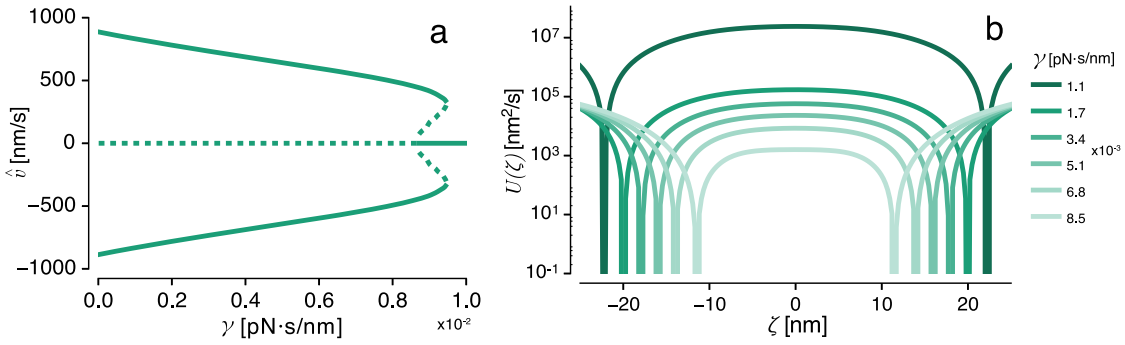

Fig. 5. **a:** A bifurcation diagram (as a function of the cargo drag, γ) for the system, which is computed from the equilibria of (18) and then translated into mean cargo velocities by (14). Dotted lines correspond to unstable equilibria and solid lines are stable. In a wide range of γ, the system demonstrates a stable positive and negative velocities, or bidirectional motion. **b:** the double-well potential structure (19) as a function of the drag coefficient γ. As γ decreases, the wells get steeper and farther apart.

This potential $U(\zeta)$ can be plotted as a function of γ in the bistable region of Fig. 5a and the result is seen in Fig. 5b. From the figure, we see that $U(\zeta)$ is a double-well potential. That is, there are two distinct well locations and a peak in the center, all three of which are roots of $A(\zeta)$. Denote the two well locations (stable fixed points of $A(\zeta)$) as ζ_{S1} and ζ_{S2}, where $\zeta_{S1} < \zeta_{S2}$ and the middle peak (a hyperbolic fixed point of $A(\zeta)$) as ζ_H.

The effect of the drag coefficient γ on the potential is non-trivial. Particularly, as γ decreases, the wells of the potential $U(\zeta)$ deepen and split farther apart, which alone would suggest an increase in time to switch. However, we later see that there is a counteracting effect in the strength of diffusion.

3.4. Mean first passage time analysis

One natural quantity to study in bidirectional systems is the time to switch directions, or the reversal time. Because of the double-potential well structure, this can be thought of as the mean time from one of the metastable points to the hyperbolic point, from which the system relaxes quickly to the other metastable point. Due to the symmetric motor population assumption, the time to switch states is independent of state. Thus, without loss of generality, we compute the mean first passage time from $\zeta_{S1} \to \zeta_{S2}$ where, again, $\zeta_{S1} < \zeta_H < \zeta_{S2}$.

The analysis of a mean first passage time in a one-dimensional potential is classical (Bressloff, 2014; Gardiner, 2009) and is briefly summarized here. Define $G(z, t)$ to be the probability that the system described by (17) is in the leftmost potential well at time t given the initial state $p(\zeta, 0) = z$. That is, the survival probability density is described by

$$G(z,t) := \int_{\zeta_{S1}}^{\zeta_H} p(\zeta, t \,|\, z, 0)\, \mathrm{d}\zeta .$$

Then, let $T(z)$ define the random variable describing the exit time from this potential well , which satisfies

$$\mathbb{P}[T(z) \le t] = 1 - G(z,t). \tag{20}$$

Taking a derivative of (20) yields the density for exit time $f(z, t)$

$$f(z,t) = -\partial_t G(z,t) = -\int_{\zeta_{S1}}^{\zeta_H} \partial_t p(\zeta, t \,|\, z, 0)\, \mathrm{d}\zeta .$$

From this, we can define the mean first exit time from the potential well, starting at the point z by

$$\tau(z) := \langle T(z) \rangle = \int_0^\infty t f(z,t)\, \mathrm{d}t = \int_0^\infty G(z,t)\, \mathrm{d}t. \tag{21}$$

The survival probability $G(z, t)$ satisfies the backward Fokker–Planck equation (Gardiner, 2009), which we can integrate and use (21) to yield the governing equation for the mean exit time density of the system starting at $\zeta_0 = z$, which is

$$A(z)\tau' + 4D\tau'' = -1, \qquad \tau(\zeta_H) = 0, \qquad \tau'(\zeta_{S1}) = 0. \tag{22}$$

The reflecting boundary at ζ_{S1} is a consequence of starting the system in the well corresponding to this point, as any excursions to the left will quickly relax back to the bottom of the well. The exit location, the hyperbolic point ζ_H, is an absorbing state due to the fast relaxation to the other potential well once the system transverses the peak between them.

The boundary value problem (22) does not appear to be solvable analytically due to the complexity of the force curves. However, $\tau(z)$ can be computed numerically in a straightforward manner (in a single integration) by exploiting the linearity of the system. Alternatively, a deep-well approximation can be made for the potential and the classical *Arrhenius formula* can be used to approximate the mean first passage time. For details on both of these methods, see Appendix B.

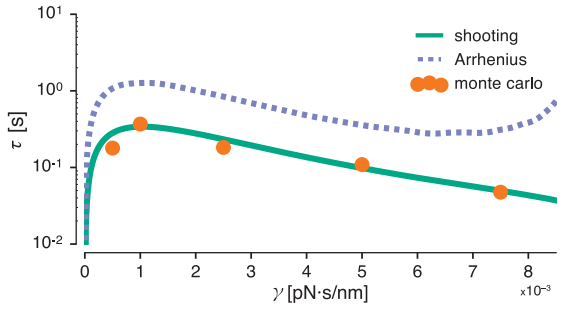

Fig. 6. Mean first passage times corresponding to the cargo switching directions. Two approaches to solving (22) are illustrated: a shooting technique, and the deep-well Arrhenius approximation. The results of an Euler-Maruyama simulation of (16) are also shown, where switching is considered passing through the hyperbolic point.

The two aforementioned techniques of evaluating $\tau(\zeta_{S1})$ are computed and compared against Monte Carlo simulations of (16), again using the Euler-Maruyama scheme, where switching is considered passing the hyperbolic point. The result of these techniques can be seen in Fig. 6. From this, we see that the shooting technique agrees with Monte Carlo simulations and the deep-well approximation is, although qualitatively similar, an overestimate of the switching time. This result is intuitive, as in reality, the wells may not be sufficiently deep for the approximation to work well and therefore allow escape much faster.

The behavior of the mean first passage times as a function of the drag, γ is quite interestingly, non-monotonic. That is, as the drag coefficient increases (which can be thought of as the cargo increasing in size), the time to switch initially goes up, but then ultimately goes back down. Mathematically, this complexity stems from γ scaling both the potential and the diffusion strength differently, explicitly in (18). As γ decreases, the potential wells deepen and spread apart as $\sim 1/\gamma$, but the strength of diffusion simultaneously scales by $\sim \sqrt{1/\gamma}$. which are competing effects for the switching time. The resulting behavior is therefore a complex competition between the scaling of the potential and the noise strength, which produces non-monotonicity. Switching due to motor binding and unbinding is *not* expected to demonstrate this same non-monotonicity, as this is a feature of the mismatched scaling in the strength of the driving noise source (diffusion) and the depth of the potential wells. In other words, γ does not scale the driving noise source the same way for motor binding dynamics. In other theoretical works that compute the switching time, monotonicity is seen (Guérin et al., 2011a; 2011b).

From a biophysical perspective, it should be noted that the predicted mean first passage times are on the order of ~ 0.5[s], which agrees with experimentally observed values (Kunwar et al., 2011). This agreement supports the hypothesis that cargo diffusion is the noise source for bidirectionality. The non-monotonicity of the curve also provides a testable experimental prediction. That is, bidirectional motion via molecular motors could be observed for different cargo drag values (which, could be obtained by varying bead size). If the resulting mean time to switch directions is found to be non-monotonic, this would further strengthen our theory that cargo diffusion, not motor binding dynamics are indeed the noise source of bidirectionality.

4. Discussion & conclusion

In this work, we have proposed a mean-field, unequally distributed load description of motor-mediated transport. To under-

stand the behavior of this complex model, we perform a series of reductions. To justify the first reduction, we take an aside to study only motors that are bound. Of these bound motors, we find that the force generated displays a delay structure that collapses the dimensionality of the system greatly. We posit that, since bound motors are the only contributor to force generation, this delay structure is applicable to the full system even when binding dynamics are incorporated. This allows for the reduction of a PDE describing each motor population to a single ODE for each, describing a "characteristic distance." Secondly, we use the small mass of the cargo to perform an adiabatic (quasi-steady state) reduction of the system. Due to a correlated noise structure and symmetry in the system, the final result is a one-dimensional system, the value of which is a proxy for the instantaneous cargo velocity. This resulting stochastic dynamics are observed to be "metastable", switching between two distinct states exclusively due of cargo diffusion. These states are associated with positive and negative cargo velocities, meaning the system is bidirectional. To quantify the reversal time of the system, a mean-first passage time analysis is performed and the results are explored as a function of the cargo drag, an experimentally tunable quantity. We find that the predicted switching time agrees with experimental values and also has a non-monotonic dependence on cargo drag, a claim that can be experimentally verified.

The use of a mean-field model in this work was not rigorously justified, and could perhaps be made so by starting with a discrete motor model akin to McKinley et al. (2012). Despite this, the mean-field model is able to accurately reproduce experimentally observed ensemble switching times and mean velocities from single-motor parameters. For this reason, we believe the mean-field model to be an appropriate description of the system, but the extent to which it is appropriate could be explored in future work. One notable behavior of our mean-field model is the instability of the pause state for a wide range of parameter values. Intuitively, any small perturbation away from the pause state will produce asymmetry in the system and ultimately result in one motor population "winning." However, it is well established experimentally that bidirectional systems spend a non-trivial amount of time in the paused state (Belyy et al., 2016; Derr et al., 2012), which has also been reproduced in discrete motor simulations such as Müller et al. (2008). This perhaps gives a clue toward when the mean-field model may break down. In the pause state, the motor number may be so low that the mean-field model is not appropriate and consequently, deviates from a discrete motor description. However, we see that in some parameter regimes, the mean-field model is even able to produce a metastable pause state (and consequently, a tristable system). Hence, this conjectured relationship between the use of a mean-field model and the instability of the pause state must be explored further.

The Ornstein-Uhlenbeck analysis for quantifying the ability of a motor to react to instantaneous changes in cargo velocity is of interest in other recent work (Bouzat, 2016) and in general, causes issue in any work that seeks to use a force-velocity relationship (which is inherently a steady-state analysis) to infer dynamics. In Bouzat (2016), the authors hypothesize a "motor memory" and conclude that models only agree with experimental values appropriately if the motors react to a windowed-time-average velocity. By examining only bound motors, we have quantified this "memory" physiologically, noting a distinct delay structure. Because bound motors are the force-generators of the system, we proposed a novel approximation to the full dynamics that satisfies the same delay structure, the validity of which was supported by numerical simulations. A more elegant approach to this approximation may be possible and could perhaps be related to the more detailed analysis of bound motor dynamics found in McKinley et al. (2012).

In Bouzat (2016), the authors also cite the importance of cargo diffusion in models producing results that match experimental values. In our work, we have further illustrated the importance of cargo diffusion by illustrating its ability to produce qualitative changes in motor-mediated transport. Specifically, the fundamental noise driving switching in our model is cargo diffusion, unlike previous unequally distributed load models which depended on a discrete motor description. This raises the possibility of the importance of diffusion in other aspects of motor-mediated transport.

Thus, we have illustrated that common features of previous work: discreteness of the motors, asymmetry of motor populations, equally distributed loads are *not* necessary to produce a physiologically reasonable model of bidirectional motor transport. This raises uncertainty of which key ingredients may be essential for tug-of-war, making it even more difficult to compare to the alternative regulatory hypothesis of bidirectionality. However, we have provided an experimentally testable prediction of the reversal time as a function of the drag coefficient, which can be tuned by the bead size in experimental setups. If indeed thermal noise is the driver of this switching, then agreement with this experiment would help strengthen the validity of this theory since this feature is not expected from motor binding dynamics as the driving noise source.

Acknowledgments

This research was partially supported by NSF grant DMS 1122297 and DMS-RTG 1148230.

Appendix A. Ornstein–Uhlenbeck Mean Evolution

In this section, we show that if the advection term of an Ornstein–Uhlenbeck has a time dependence, a differential equation can be obtained for the mean of the process, demonstrating an effective delay.

Consider a Fokker–Planck equation of the form

$$\partial_t p = -\partial_x[\{w(x) - v(t)\}p] + D\partial_{xx}p. \tag{A.1}$$

Denote $\mu(t)$ to be the mean of the process, that is $\mu = \langle p \rangle$. Then, we have:

$$\dot{\mu} = \frac{\mathrm{d}}{\mathrm{d}t}\int_{-\infty}^{\infty} x\, p(x,t)\,\mathrm{d}x = \int_{-\infty}^{\infty} x\partial_t p\,\mathrm{d}x.$$

However, we can use (A.1) to find that

$$\dot{\mu} = -\int_{-\infty}^{\infty} x\partial_x[\{w(x) - v(t)\}p]\,\mathrm{d}x + \int_{-\infty}^{\infty} xD\partial_{xx}p\,\mathrm{d}x,$$

which, after integration by parts, yields

$$\dot{\mu} = \langle w(x)\rangle - v.$$

Jensen's inequality states that for a convex w

$$\langle w(x)\rangle \geq w(\langle x\rangle),$$

however, if we assume $w(x)$ is *linear* (as we have done in the model), then Jensen's inequality attains equality and the result is

$$\dot{\mu} = w(\mu) - v(t).$$

Appendix B. Methods for 1D MFPT Problems

For the sake of generality, consider the one dimensional SDE

$$\mathrm{d}x = A(x)\mathrm{d}t + \sqrt{2B(x)}\,\mathrm{d}W,$$

which has a corresponding Fokker–Planck equation

$$\partial_t p = -\partial_x\{A(x)p\} + B(x)\partial_{xx}p.$$

We are assuming that $A(x)$ has three fixed points, two stable and one hyperbolic, denote x_S and x_H.

We are then interested in the mean first passage time starting from a point y, which we denote $\tau(y)$, and satisfies

$$A(y)\tau' + B(y)\tau'' = -1, \qquad \tau'(x_S) = 0, \qquad \tau(x_H) = 0. \tag{B.1}$$

B1. Shooting method

In this section, we exploit the linearity of (B.1) to construct a numerical shooting method for constructing a solution. First, we write the system as a first order system, by taking $\sigma = \tau'$,

$$\begin{bmatrix}\tau'\\ \sigma'\end{bmatrix} + \begin{bmatrix}0 & 1\\ 0 & \frac{A(x)}{B(x)}\end{bmatrix}\begin{bmatrix}\tau\\ \sigma\end{bmatrix} = \begin{bmatrix}0\\ -\frac{1}{B(x)}\end{bmatrix}, \qquad \begin{bmatrix}\tau(x_H)\\ \sigma(x_S)\end{bmatrix} = \begin{bmatrix}0\\ 0\end{bmatrix}. \tag{B.2}$$

To construct a solution to (B.2), we obtain two solutions of initial value problems of the same form and utilize the linearity of the equation to solve the boundary value problem via superposition. Thus, consider the following two systems:

$$\begin{bmatrix}p_1'\\ p_2'\end{bmatrix} + \begin{bmatrix}0 & 1\\ 0 & \frac{A(x)}{B(x)}\end{bmatrix}\begin{bmatrix}p_1\\ p_2\end{bmatrix} = \begin{bmatrix}0\\ -\frac{1}{B(x)}\end{bmatrix}, \qquad \begin{bmatrix}p_1(x_S)\\ p_2(x_S)\end{bmatrix} = \begin{bmatrix}0\\ 0\end{bmatrix}$$

$$\begin{bmatrix}q_1'\\ q_2'\end{bmatrix} + \begin{bmatrix}0 & 1\\ 0 & \frac{A(x)}{B(x)}\end{bmatrix}\begin{bmatrix}q_1\\ q_2\end{bmatrix} = \begin{bmatrix}0\\ 0\end{bmatrix}, \qquad \begin{bmatrix}q_1(x_S)\\ q_2(x_S)\end{bmatrix} = \begin{bmatrix}1\\ 0\end{bmatrix}$$

We now claim $\Upsilon = \begin{bmatrix}\tau & \sigma\end{bmatrix}^T$ is a linear combination of $P = \begin{bmatrix}p_1 & p_2\end{bmatrix}^T$ and $Q = \begin{bmatrix}q_1 & q_2\end{bmatrix}^T$. In other words, there exists some γ such that $\Upsilon = P + \gamma Q$. The value of γ is to be determined by making sure the right boundary condition is satisfied

$$\tau(x_H) = p_1(x_H) + \gamma q_1(x_H) = 0 \Rightarrow \gamma = -\frac{p_1(x_H)}{q_1(x_H)}.$$

Thus, our mean first passage time from $x_S \to x_H$ is then

$$\tau(x_S) = p_1(x_S) + \gamma q_1(x_S) = \gamma.$$

It is worth noting that this actually only requires a *single* ODE integration, as Q is identically constant by construction with $q_1 \equiv 1$ and $q_2 \equiv 0$, and consequently

$$\gamma = -p_1(x_H).$$

B2. Arrhenius (deep well) approximation

The deep-well approximation is a classical technique used to compute the mean first passage time from a potential well. Here, we briefly summarize the technique but additional details can be found in Gardiner (2009) and Bressloff (2014). Following the latter reference, define the potential function $U'(y) := -A(y)$, so $U = -\int A(y)\,dy$. After using an integrating factor and assuming B is constant for simplicity, we have

$$\tau = \frac{1}{B}\int_{x_S}^{x} e^{U(x')/B}\,dx' \int_0^{x'} e^{-U''(x'')/B}\,dx'',$$

noting that we have also taken $0 < x_S < x_H$ for convenience. Assuming the potential is deep-welled, the first integral is sharply peaked around $x' = x_H$, where the second integral is slowly varying. For this reason, we can interchange the limits of the integral to obtain

$$\tau = \frac{1}{B}\left[\int_0^{x_H} e^{-U(x'')/B}\,dx''\right]\left[\int_{x_S}^{x} e^{U(x')/B}\,dx'\right].$$

Now, the first integral is dominated around $x'' = x_H$, whereas the second is dominated around $x' = x_S$ so that the limits can be taken to infinity with little error. Using the method of steepest descent (or simply, a Taylor expansion), we finally have the classical *Arrhenius formula*

$$\tau \sim \frac{2\pi}{\sqrt{|U''(x_H)|U''(x_S)}} e^{(\Delta U)/B}, \qquad \Delta U := U(x_H) - U(x_S).$$

Supplementary material

Supplementary material associated with this article can be found, in the online version, at 10.1016/j.jtbi.2017.04.032.

References

Andreasson, J.O., Milic, B., Chen, G.-Y., Guydosh, N.R., Hancock, W.O., Block, S.M., 2015. Examining kinesin processivity within a general gating framework. Elife 4, e07403. doi:10.7554/eLife.07403.

Belyy, V., Hendel, N.L., Chien, A., Yildiz, A., 2014. Cytoplasmic dynein transports cargos via load-sharing between the heads. Nat. Commun. 5, 5544. doi:10.1038/ncomms6544.

Belyy, V., Schlager, M.A., Foster, H., Reimer, A.E., Carter, A.P., Yildiz, A., 2016. The mammalian dyneindynactin complex is a strong opponent to kinesin in a tug-of-war competition. Nat. Cell Biol. 18 (9), 1018–1024. doi:10.1038/ncb3393.

Bouzat, S., 2016. Models for microtubule cargo transport coupling the langevin equation to stochastic stepping motor dynamics: caring about fluctuations. Phys. Rev. E 93 (1), 012401. doi:10.1103/PhysRevE.93.012401.

Bressloff, P.C., 2014. Stochastic Processes in Cell Biology. Interdisciplinary Applied Mathematics, 41. Springer International Publishing doi:10.1007/978-3-319-08488-6.

Bressloff, P.C., Levien, E., 2015. Synaptic democracy and vesicular transport in axons. Phys. Rev. Lett. 114 (16), 1–5. doi:10.1103/PhysRevLett.114.168101.

Brooks, H.A., Bressloff, P.C., 2016. A mechanism for turing pattern formation with active and passive transport. SIAM J. Appl. Dyn. Syst. 15 (4), 1823–1843. doi:10.1137/16M1061205.

Carter, N.J., Cross, R.A., 2005. Mechanics of the kinesin step. Nature 435 (7040), 308–312. doi:10.1038/nature03528.

Derr, N.D., Goodman, B.S., Jungmann, R., Leschziner, A.E., Shih, W.M., Reck-Peterson, S.L., 2012. Tug-of-War in motor protein ensembles. Science 338, 662–666. doi:10.1126/science.1226734.

Fu, M.-M., Holzbaur, E.L.F., 2014. Integrated regulation of motor-driven organelle transport by scaffolding proteins. Trends Cell Biol. 24 (10), 564–574. doi:10.1016/j.tcb.2014.05.002.

Gardiner, C., 2009. Stochastic Methods: A Handbook for the Natural and Social Sciences. Springer Series in Synergetics, 13, 4th Springer Berlin Heidelberg doi:10.1007/978-3-662-02377-8.

Gennerich, A., Carter, A.P., Reck-Peterson, S.L., Vale, R.D., 2007. Force-Induced bidirectional stepping of cytoplasmic dynein. Cell 131 (5), 952–965. doi:10.1016/j.cell.2007.10.016.

Gross, S.P., Vershinin, M., Shubeita, G.T., 2007. Cargo transport: two motors are sometimes better than one. Curr. Biol. 17 (12), R478–R486. doi:10.1016/j.cub.2007.04.025.

Guérin, T., Prost, J., Joanny, J.-F., 2011a. Bidirectional motion of motor assemblies and the weak-noise escape problem. Phys. Rev. E 84 (4), 041901. doi:10.1103/PhysRevE.84.041901.

Guérin, T., Prost, J., Joanny, J.-F., 2011b. Motion reversal of molecular motor assemblies due to weak noise. Phys. Rev. Lett. 106 (6), 068101. doi:10.1103/PhysRevLett.106.068101.

Hancock, W.O., 2014. Bidirectional cargo transport: moving beyond tug of war. Nat. Rev. Mol. Cell Biol. 15 (9), 615–628. doi:10.1038/nrm3853.

Hendricks, A.G., Perlson, E., Ross, J.L., Schroeder, H.W., Tokito, M., Holzbaur, E.L.F., 2010. Motor coordination via a tug-of-War mechanism drives bidirectional vesicle transport. Curr. Biol. 20 (8), 697–702. doi:10.1016/j.cub.2010.02.058.

Howard, J., 2001. Mechanics of Motor Proteins and the Cytoskeleton. Sinauer Associates.

Huxley, A.F., 1957. Muscle structure and theories of contraction. Prog. Biophys. Biophys. Chem. 7, 255–318.

Kawaguchi, K., Uemura, S., Ishiwata, S., 2003. Equilibrium and transition between single- and double-Headed binding of kinesin as revealed by single-Molecule mechanics. Biophys. J. 84 (2), 1103–1113. doi:10.1016/S0006-3495(03)74926-1.

Keener, J.P., Sneyd, J., 2008. Mathematical Physiology. Springer Science & Business Media doi:10.1007/978-0-387-79388-7.

Kloeden, P.E., Platen, E., 1992. Numerical Solution of Stochastic Differential Equations. Stochastic Modelling and Applied Probability, 23. Springer doi:10.1080/17442509408833885.

Klumpp, S., Berger, F., Lipowsky, R., 2015. Molecular motors: cooperative phenomena of multiple molecularmotors. In: De, S., Hwang, W., Kuhl, E. (Eds.), Multiscale Model. Biomech. Mechanobiol. chapter 3. Springer London, London, p. 287. doi:10.1007/978-1-4471-6599-6.

Kunwar, A., Tripathy, S.K., Xu, J., Mattson, M.K., Anand, P., Sigua, R., Vershinin, M., McKenney, R.J., Yu, C.C., Mogilner, A., Gross, S.P., 2011. Mechanical stochastic tug-of-war models cannot explain bidirectional lipid-droplet transport. Proc. Natl. Acad. Sci. 108 (47), 18960–18965. doi:10.1073/pnas.1107841108.

Kunwar, A., Vershinin, M., Xu, J., Gross, S.P., 2008. Stepping, strain gating, and an unexpected force-Velocity curve for multiple-Motor-Based transport. Curr. Biol. 18 (16), 1173–1183. doi:10.1016/j.cub.2008.07.027.

Lindemann, C.B., Hunt, A.J., 2003. Does axonemal dynein push, pull, or oscillate? Cell Motil. Cytoskeleton 56 (4), 237–244. doi:10.1002/cm.10148.

Lipowsky, R., Beeg, J., Dimova, R., Klumpp, S., Müller, M.J., 2010. Cooperative behavior of molecular motors: cargo transport and traffic phenomena. Physica E 42 (3), 649–661. doi:10.1016/j.physe.2009.08.010.

Lipowsky, R., Chai, Y., Klumpp, S., Liepelt, S., Müller, M.J., 2006. Molecular motor traffic: from biological nanomachines to macroscopic transport. Physica A 372 (1), 34–51. doi:10.1016/j.physa.2006.05.019.

Luby-Phelps, K., 2000. Cytoarchitecture and physical properties of cytoplasm: volume, viscosity, diffusion, intracellular surface area. Int. Rev. Cytol. 192, 189–221.

McKenney, R.J., Vershinin, M., Kunwar, A., Value, R.B., Gross, S.P., 2010. LIS1 And nude induce a persistent dynein force-Producing state. Cell 141 (2), 304–314. doi:10.1016/j.cell.2010.02.035.

McKinley, S.A., Athreya, A., Fricks, J., Kramer, P.R., 2012. Asymptotic analysis of microtubule-based transport by multiple identical molecular motors. J. Theor. Biol. 305, 54–69. doi:10.1016/j.jtbi.2012.03.035.

Mitchell, C.S., Lee, R.H., 2009. A quantitative examination of the role of cargo-exerted forces in axonal transport. J. Theor. Biol. 257 (3), 430–437. doi:10.1016/j.jtbi.2008.12.011.

Müller, M.J., Klumpp, S., Lipowsky, R., 2008. Tug-of-war as a cooperative mechanism for bidirectional cargo transport by molecular motors. Proc. Natl. Acad. Sci. 105 (12), 4609–4614. doi:10.1073/pnas.0706825105.

Nadrowski, B., Martin, P., Julicher, F., 2004. Active hair-bundle motility harnesses noise to operate near an optimum of mechanosensitivity. Proc. Natl. Acad. Sci. 101 (33), 12195–12200. doi:10.1073/pnas.0403020101.

Nicholas, M.P., Höök, P., Brenner, S., Wynne, C.L., Vallee, R.B., Gennerich, A., 2015. Control of cytoplasmic dynein force production and processivity by its c-terminal domain. Nat. Commun. 6, 6206. doi:10.1038/ncomms7206.

Osunbayo, O., Butterfield, J., Bergman, J., Mershon, L., Rodionov, V., Vershinin, M., 2015. Cargo transport at microtubule crossings: evidence for prolonged tug-of-war between kinesin motors. Biophys. J. 108 (6), 1480–1483. doi:10.1016/j.bpj.2015.02.016.

Rai, A.K., Rai, A., Ramaiya, A.J., Jha, R., Mallik, R., 2013. Molecular adaptations allow dynein to generate large collective forces inside cells. Cell 152 (1–2), 172–182. doi:10.1016/j.cell.2012.11.044.

Schnitzer, M.J., Visscher, K., Block, S.M., 2000. Force production by single kinesin motors. Nat. Cell Biol. 2 (10), 718–723. doi:10.1038/35036345.

Shojania Feizabadi, M., Janakaloti Narayanareddy, B.R., Vadpey, O., Jun, Y., Chapman, D., Rosenfeld, S., Gross, S.P., 2015. Microtubule C-Terminal tails can change characteristics of motor force production. Traffic 16 (10), 1075–1087. doi:10.1111/tra.12307.

Soppina, V., Rai, A.K., Ramaiya, A.J., Barak, P., Mallik, R., 2009. Tug-of-war between dissimilar teams of microtubule motors regulates transport and fission of endosomes. Proc. Natl. Acad. Sci. USA 106 (46), 19381–19386. doi:10.1073/pnas.0906524106.

Srinivasan, M., Walcott, S., 2009. Binding site models of friction due to the formation and rupture of bonds: state-function formalism, force-velocity relations, response to slip velocity transients, and slip stability. Phys. Rev. E - Stat. Nonlinear Soft Matter Phys. 80 (4), 1–15. doi:10.1103/PhysRevE.80.046124.

Visscher, K., Schnitzer, M.J., Block, S.M., 1999. Single kinesin molecules studied with a molecular force clamp. Nature 400 (6740), 184–189. doi:10.1038/22146.

Walcott, S., 2008. The load dependence of rate constants. J. Chem. Phys. 128 (21), 215101. doi:10.1063/1.2920475.

CHAPTER 3

JUMP LOCATIONS OF JUMP-DIFFUSION PROCESSES WITH STATE-DEPENDENT RATES

The article in this chapter is reprinted with permission from *Journal of Physics A: Mathematical & Theoretical*, **50** (2017) 425003.

IOP Publishing Journal of Physics A: Mathematical and Theoretical
J. Phys. A: Math. Theor. **50** (2017) 425003 (17pp) https://doi.org/10.1088/1751-8121/aa8a90

Jump locations of jump-diffusion processes with state-dependent rates

Christopher E Miles[1] **and James P Keener**[1,2]

[1] Department of Mathematics, University of Utah 201 Presidents Circle, Salt Lake City, UT 84112, United States of America
[2] Department of Bioengineering, University of Utah 201 Presidents Circle, Salt Lake City, UT 84112, United States of America

E-mail: miles@math.utah.edu

Received 27 June 2017, revised 24 August 2017
Accepted for publication 6 September 2017
Published 22 September 2017

Abstract

We propose a general framework for studying statistics of jump-diffusion systems driven by both Brownian noise (diffusion) and a jump process with state-dependent intensity. Of particular natural interest in many physical systems are the jump locations: the system evaluated at the jump times. As an example, this could be the voltage at which a neuron fires, or the so-called 'threshold voltage'. However, the state-dependence of the jump rate provides direct coupling between the diffusion and jump components, making it difficult to disentangle the two to study individually. In this work, we provide an iterative map formulation of the sequence of distributions of jump locations. The distributions computed by this map can be used to elucidate other interesting quantities about the process, including statistics of the interjump times. Ultimately, the limit of the map reveals that knowledge of the stationary distribution of the full process is sufficient to recover (but not necessarily equal to) the distribution of jump locations. We propose two biophysical examples to illustrate the use of this framework to provide insight about a system. We find that a sharp threshold voltage emerges robustly in a simple stochastic integrate-and-fire neuronal model. The interplay between the two sources of noise is also investigated in a stepping model of molecular motor in intracellular transport pulling a diffusive cargo.

Keywords: jump-diffusion, stochastic processes, integrate-and-fire, state-dependent rates

(Some figures may appear in colour only in the online journal)

1. Introduction

Stochastic models driven by both Brownian noise (diffusion) and a discrete jump component, or so-called *jump-diffusion* models, have been used to describe a wide variety of phenomena. Perhaps most prominently, jump-diffusion has seen widespread use in mathematical finance [4, 23, 35, 36, 56] to describe frequent small transactions with occasional larger movements. Jump-diffusion has also served useful in mathematical biology, describing the integrate-and-fire nature of neuronal dynamics [15, 27, 50]. Other applications include biophysical descriptions of movement of chromosomes [51], interaction between soil moisture and rainfall events [11], and the occurrence of radio pulsar glitches [25]. Also relevant to the results described in this paper is a subset of jump-diffusion models that neglect diffusive noise and are driven by deterministic dynamics between jumps. This type of model appears in an equally eclectic variety of applications [3, 13, 17, 53].

Of particular interest in this work are jump-diffusion processes with state-dependent jump rates. This subset is seen in all the aforementioned applications, including finance [4, 28], ecology [17], biology [12], and astronomy [25]. This is often a natural supposition to make of a model, as the rate at which the jump event occurs may not remain constant on the timescale of interest, but instead depend on the state of the system. For instance, a neuron firing is dependent on the current voltage or a financial asset is often more likely to crash as it rises in price.

For many of these applications, the inclusion of a jump component means that it is a significant feature to the modeler. Thus, it is natural to ask: when (in some sense) do these jumps occur? While this often leads to studying the interjump *times*, a different possible interpretation (and the focus of this work) is to study the *jump locations*: the system evaluated at the jump times. This could be the voltage at which the neuron fires (the 'threshold voltage') or the price at which a stock crashes. Because the jump intensity is state-dependent, and the state itself is governed by a stochastic process, these locations are inherently random and difficult to disentangle from the full process. This raises another question: in what sense is knowledge (e.g. statistics) of the full process equivalent to knowledge of the jump locations? Does knowledge of the jump locations provide other insight to the behavior of the system? In this work, we seek to investigate these issues.

Previous studies have thoroughly investigated jump-diffusion models for constant jump rates [11, 29], as the two sources of noise can be independently superimposed. The interjump time distributions for processes with no diffusive noise have also been studied [12, 13] primarily using renewal theory or exploiting the deterministic nature between jumps. However, in general, state-dependent jump-diffusion is *not* deterministic between jumps, nor a renewal process, as sequential distributions are not independent, hence previous approaches do not apply. The theory of Cox processes [10] is also well-established and refers to a diffusion process driving a state-dependent Poisson process, but this does not complete the feedback loop of the jump process further modifying the state, which our framework allows. Diffusion with switching, which bears a resemblance to jump-diffusion, has also been studied [40] but is distinctly different in the role of discrete noise and not addressed in this work. Although efficient Monte Carlo methods exist for jump-diffusion and Lévy processes [28, 55], the jump component may be rare and therefore expensive to find an accurate distribution empirically. The solution to the full PDE describing this process can also be computed, but it is seemingly unknown how to disentangle the jump component alone from this description.

In this work, we present a general (accommodating a wide variety of models) framework for studying jump-diffusion systems and focus particularly on studying the sequence of jump locations. We present an iterative map formulation explicitly describing the distribution of the ith jump location. Fron this sequence of jump locations, statistics of the interjump times

can be extracted even with diffusion, overcoming a limitation of previous works [13]. By taking the limit of the map, assuming the process reaches stationery, we find that the density of the full process *differs* from that of the jump locations if and only if the jump rate is state-dependent. An explicit relationship between these two distributions is established, meaning that knowledge of one immediately provides knowledge of the other.

A few examples are discussed, illustrating when this framework can be used to elucidate interesting behavior of a system. The first example, a stochastic model of neuronal integrate-and-fire, is used to demonstrate that the jump locations themselves (in this case, the firing voltages) may be interesting. For the second example, we propose a simple model of a molecular motor (such as kinesin [30]) taking force-dependent steps pulling a diffusive cargo. Because the stepping rate is state dependent, but steps (and cargo diffusion) also modify the state, the effective stepping rate (a proxy for the motor's ability to produce transport) is non-trivial and can be studied using the proposed framework.

2. Formulation

2.1. Jump-diffusion

Let X_t denote a state-dependent jump-diffusion process and $\tilde{p}(x,t)$ be the probability density (PDF) of the full process, defined formally as

$$\tilde{p}(x,t)\,\mathrm{d}x := \mathsf{P}\left[X_t \in (x, x+\mathrm{d}x)\right].$$

The evolution of the density is described by the forward Champman–Kolmorgov equation [6, 26]

$$\partial_t \tilde{p}(x,t) = \mathbb{L}\tilde{p} - \lambda(x)\tilde{p} + \mathbb{J}\lambda\tilde{p}, \tag{1}$$

where the operator $\mathbb{L}$ characterizes the diffusion component, $\lambda(x)$ is the state-dependent intensity at which the jump process occurs, and the operator $\mathbb{J}$ describes the jump. A feature we seek to emphasize is the state dependence of the jump-rate $\lambda(x)$, resulting in direct coupling between the diffusion and jump components of the process.

The particular choices of $\mathbb{L}, \mathbb{J}, \lambda$ significantly change the behavior and characteristics of the process, but the description (1) is flexible enough to accommodate a wide variety of models, upon which we now elaborate.

2.2. Diffusion component

Consider the classical one-dimensional Itô SDE driven by Brownian motion described by

$$\mathrm{d}Y_t = A(Y_t)\,\mathrm{d}t + \sqrt{2D(Y_t)}\,\mathrm{d}W_t, \tag{2}$$

where W_t is a Brownian motion. The Fokker–Planck (forward Chapman–Kolmogorov) equation describing the evolution of the probability density function $p(y,t)$ corresponding to the path-wise description (2) is

$$\partial_t p(y,t) = \mathbb{L}p := -\partial_y\left\{A(y)\,p\right\} + \partial_{yy}\left\{D(y)\,p\right\}.$$

We use the *Fokker–Planck operator* $\mathbb{L}$ to characterize the diffusion process for the remainder of the paper. Although the Itô interpretation is used here, we could also consider a Stratonovich interpretation by modifying the particular details of $\mathbb{L}$, as this description still produces a differential operator in the forward equation.

2.3. Jump component

Let the jump process be an inhomogeneous (state-dependent) Poisson process with intensity (rate) $\lambda(X_t)$. Also necessary is a description of what occurs at the jumps, sometimes referred to as the *reset map* [14]. The behavior of the reset map is characterized by the *jump operator* $\mathbb{J}$, which is a probability density flux, ensuring that (1) indeed describes the evolution of a probability density. We now describe a few possible choices of this operator, letting τ denote the jump time.

2.3.1. Jump operator examples.

(i) *Constant jump size*. At the jump times, the process increments by a fixed amount Δ, so

$$X_{\tau_+} = X_{\tau_-} + \Delta.$$

Then, the corresponding jump operator $\mathbb{J}$ is a shift by that fixed quantity

$$\mathbb{J}p(x,t) := p(x-\Delta,t).$$

(ii) *Reset*. Fundamentally different than the previous example, rather than jumping by a fixed displacement, the process resets to a specific position, η, so that

$$X_{\tau_+} = \eta.$$

The corresponding $\mathbb{J}$ operator is

$$\mathbb{J}p(x,t) := \delta(x-\eta)\int_{-\infty}^{\infty} p(x,t)\,\mathrm{d}x,$$

where $\delta(x)$ is the Dirac delta function. The integral scaling is necessary to preserve probability fluxes: $\int_{-\infty}^{\infty}\mathbb{J}p\,\mathrm{d}x = \int_{-\infty}^{\infty} p\,\mathrm{d}x$.

(iii) *Random jump size*. A generalization of the first example, the particle can jump a random displacement Δ, where the size of the jump is described by the probability density $\Delta\sim\mu(\Delta,x)$, which can also be state-dependent. The $\mathbb{J}$ operator is

$$\mathbb{J}p(x,t) := \int_{-\infty}^{\infty} p(x-\Delta,t)\mu(\Delta,x)\,\mathrm{d}\Delta.$$

(iv) *Other examples*. Although not directly considered in this paper, maps of the form

$$X_{\tau_+} = \gamma X_{\tau_-} \qquad \Longrightarrow \qquad \mathbb{J}p(x,t) := \gamma p(\gamma x,t),$$

have been studied elsewhere [14] and can be formulated in our framework in the described manner. A generalization of this case could also be made to allow for jumps to a random location, but this does not seem to provide additional interesting structure.

An example trajectory of the processes considered in this process can be seen in figure 1. In this example, the diffusion component is an Ornstein–Uhlenbeck process and the jump consists of a fixed size and Gaussian rate.

While diffusion with resetting fits within the proposed framework, this topic has a long, rich history of study [22, 44]. Included within this body of literature are investigations of: time-dependent resetting (t-dependent λ) [47], optimal resetting [21], resetting in bounded domains [8], resets with drift [45], characterizations of the stationary behavior [42], and path-integral formulations [49]. We do not seek to propose our framework as an alternative to this rich body

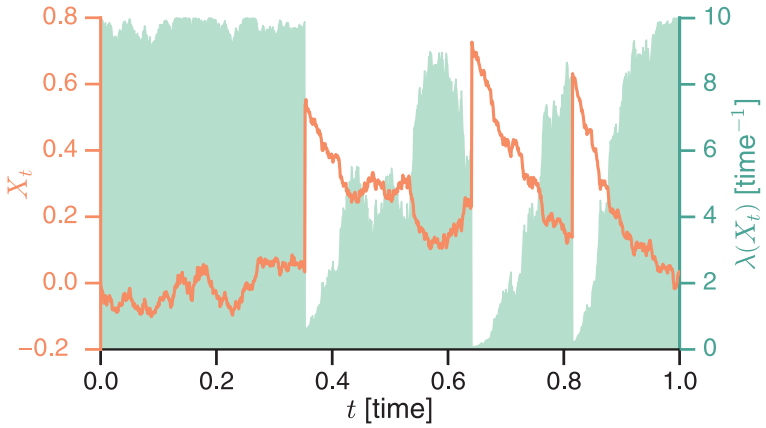

Figure 1. An example realization of a jump-diffusion process X_t with $\mathbb{L}p = \partial_x\{axp\} + Dp_{xx}$, $\lambda(x) = \alpha \exp\{-x^2/\beta\}$ and $\mathbb{J}p = p(x-\Delta)$. Also shown is the state dependent jump rate $\lambda(x)$. In this particular realization, 3 jumps occur. Parameter values used $a = .1, D = 1, \alpha = 10, \beta = 10, \Delta = 1$.

of literature, but merely identify that stochastic resetting fits within a family of models that otherwise lack this same level of attention and can be studied with the tools presented here.

3. Results In this section, we present the general theoretical results of the paper regarding the distributions of jump locations and interjump times.

3.1. Jump distributions

We begin by providing intuition for the construction of the sequence of jump locations. Rather than studying the full process including diffusion and jumps, a more convenient process to study is a survival formulation between jumps, which we denote the *absorbing process*,

$$\begin{cases} \partial_t p(x,t) = \mathbb{L}p - \lambda p \\ \partial_t q(x,t) = \lambda p. \end{cases} \tag{3}$$

Note that we distinguish between this and the full process $\tilde{p}(x,t)$, which we refer to henceforth as the *reinjected process*. While the absorbing process does not capture all the behavior of the full re-injected process (as it does not contain any information about $\mathbb{J}$), the absorbing process fixes the distribution (in both space and time) of jump events and consequently serves more fruitful in disentangling the jump component from the full process.

Theorem 1. *The densities of the jump location $p_\ell(x)$ and jump time $p_\tau(t)$ of (3) are described by*

$$p_\ell(x) = q(x,\infty) = \int_0^\infty \lambda(x)\, p(x,t)\, \mathrm{d}t,$$

and

$$p_\tau(t) = \int_{-\infty}^{\infty} \lambda(x)\, p(x,t)\, \mathrm{d}x.$$

Proof. Define the survival probability $s(t)$ to be the probability that the jump *has not* occurred by time τ

$$s(t) := \mathbb{P}[\tau > t] = \int_{-\infty}^{\infty} p(x,t)\,\mathrm{d}x,$$

which means the first jump time density $p_\tau(t)$ is then

$$p_\tau(t) = -\frac{\mathrm{d}s}{\mathrm{d}t} = -\int_{-\infty}^{\infty} \partial_t p\,\mathrm{d}x.$$

Then, using (3) and the fact that $p \to 0$ as $x \to \pm\infty$, we obtain

$$p_\tau(t) = \int_{\infty}^{\infty} \lambda p\,\mathrm{d}x = \int_{\infty}^{\infty} \partial_t q\,\mathrm{d}x.$$

Due to the lack of spatial flux in $q(x,t)$, the density of exit locations is $q(x,\infty)$, which can be obtained by integrating over all possible jump times

$$p_\ell(x) = \int_0^{\infty} \partial_t q\,\mathrm{d}t = q(x,\infty) - q(x,0) = q(x,\infty),$$

by noting that $q(x,0) \equiv 0$. For this proof (and the remainder of the results), we assume that $\lambda, \mathbb{L}, \mathbb{J}$ are chosen with sufficient regularity such that there are no explosions (i.e. the intensity stays finite. For more details on these conditions, see [2]. □

Although this provides useful information about the distributions (in time and space) at which a particular jump occurs, we are interested in studying the distributions of all jumps. This requires including the information embedded in $\mathbb{J}$ about how to re-inject the particle. triggered. A similar idea of studying the system between jumps was proposed in [46], in which the authors study the record statistics of the so-called Sisyphus random walk. However, the Sisyphus random walk is a discrete random walk on a lattice, rather than a continuous diffusion as discussed here, meaning the results are not directly applicable but strongly paralleled.

3.2. Jump location sequential mapping

We ystudy the interjump dynamics by noting that between jumps, the full process (1) can be described by the absorbing process (3). Define t_i to be the ith jump time and let $X_i := X_{t_i}$ be the ith jump location. Let $p_i(x)$ be the probability density of X_{t_i} formally defined to be,

$$p_i(x)\mathrm{d}x := \mathsf{P}[X_t \in (x, x+\mathrm{d}x) \,|\, t = t_i].$$

Theorem 2. *The distribution of the ith jump location, $p_i(x)$ is described by the following iterative relation*

$$\begin{cases} \partial_t \hat{p}_i(x,t) = \mathbb{L}\hat{p}_i - \lambda \hat{p}_i \\ \hat{p}_i(x,0) = \begin{cases} \mathbb{J}p_{i-1} & i > 1 \\ p_0 & i = 1 \end{cases} \\ p_{i+1}(x) = \int_0^{\infty} \lambda \hat{p}_i\,\mathrm{d}t, \end{cases} \tag{4}$$

where p_0 be some known starting distribution of the process.

This construction follows from directly from theorem 1. Effectively, $\hat{p}_i$ serves as intermediate quantity tracking the distribution of all possible jump locations (and times) for that particular iterate. That is, $\hat{p}_i$ is the survival density (in both time and space), tracking the process between jumps, so

$$\hat{p}_i(x,t)\mathrm{d}x := \mathsf{P}[X_{t+t_{i-1}} \in (x, x+\mathrm{d}x)\,,\; t + t_{i-1} < t_i].$$

Then, to start the next iterate, the distribution of jump locations must be modified by the jump procedure characterized by $\mathbb{J}$. Although tracking the jump locations rather than the jump times seems counterintuitive at first, no natural analogous formulation is apparent.

Define the more convenient quantity to study

$$u_i := p_i(x)/\lambda(x). \tag{5}$$

If $\lambda(x) = 0$ for some x, then necessarily $p_i(x) = 0$ since $\lambda(x) = 0$ implies no jump can occur at this location, hence this quotient causes no difficulties.

Theorem 3. *The description (4) is equivalent to*

$$\mathbb{T}u_{i+1} := [\lambda(x) - \mathbb{L}]\, u_{i+1} = \mathbb{J}\lambda u_i,$$

or more explicitly

$$u_{i+1} = \mathbb{T}^{-1}\mathbb{J}\lambda u_i. \tag{6}$$

Proof. Integrating both sides of (4) with respect to t and noting that $\hat{p}_i(x,\infty) = 0$ we are left with

$$\hat{p}_i(x,0) = \int_0^\infty \mathbb{L}\hat{p}_i\,\mathrm{d}t - \lambda(x)\int_0^\infty \hat{p}_i\,\mathrm{d}t.$$

The linear operator $\mathbb{L}$ is a differential operator in x and consequently commutes with the time integral. Using the initial condition and $p_i/\lambda = \int_0^\infty \hat{p}_i\,\mathrm{d}t$, we obtain the desired result. □

The map (6) provides an explicit description for the sequence

$$u_1(x) \to u_2(x) \to \cdots \to u_\star(x) \to u_\star(x) \to \cdots,$$

where, we assume $u_\star$ is the fixed point of of the map (6) and exists. Although we seek to not dwell on this aspect, a natural question to ask is under what conditions does $u_\star$ exist? Equivalently, when does the the process reach stationarity? In appendix B, we provide a brief commentary about how the relationship (6) can be thought of as an iterated linear non-negative integral operator which can be studied as such. Results from theoretical ecology literature are then cited which provide a heuristic analysis of conditions for convergence.

We proceed assuming that (6) has a fixed point, which must be of the following form.

Theorem 4. *The stationary distribution of the jump locations $p_\star(x)$ is described by*

$$0 = \mathbb{L}u_\star - \lambda u_\star + \mathbb{J}\lambda u_\star, \tag{7}$$

where $u_\star := p_\star/\lambda$.

Corollary 1. *The stationary distribution of the jump locations $p_\star$ is the same as the stationary distribution of the full process if and only if λ is constant.*

Proof. This is an immediate consequence of taking the full process to be in stationarity, so $\mathrm{d}\hat{p}/\mathrm{d}t = 0$ in (1), which satisfies

$$0 = \mathbb{L}\hat{p}_s - \lambda\hat{p}_s + \mathbb{J}\lambda\hat{p}_s. \tag{8}$$

This is exactly the same relationship as (7). Recalling that $\lambda u_\star = p_\star$ and that both $p_\star$ and $\hat{p}_s$ are probability densities, the only way that $p_\star = \hat{p}_s$ is if $u_\star$ is a rescaling of $p_\star$ or, equivalently, λ is constant. □

Elaborating a bit on this relationship: while (8) and (7) may appear to produce the same result, the solutions to each require different scalings. Since $\hat{p}_s$ is a probability density, it must be that

$$\int_{-\infty}^{\infty} \hat{p}_s \, \mathrm{d}x = 1. \tag{9}$$

However, $u_\star\lambda = p^\star$, where $p_\star$ is a probability density, so this means that

$$\int_{-\infty}^{\infty} u_\star(x)\lambda(x) \, \mathrm{d}x = 1. \tag{10}$$

It is worth pointing out that [13] derives similar results relating the jump locations and jump times, however, the justification used there depends on the trajectories being deterministic between jumps, i.e. without diffusion.

3.3. Moments

Define τ_i to be the ith interjump time, $\tau_i := t_i - t_{i-1}$. Also, let $\tau_\star$ be the interjump time for the stationary process.

Theorem 5. *The mean interjump time τ_i can be recovered from the distribution of the ith jump location and is*

$$\langle\tau_i\rangle = \int_{-\infty}^{\infty} u_i \, \mathrm{d}x = \int_{-\infty}^{\infty} \frac{p_i(x)}{\lambda(x)} \, \mathrm{d}x. \tag{11}$$

Also, the mean stationary interjump time can be computed from the stationary distribution of the jump locations $p_\star$

$$\langle\tau_\star\rangle = \int_{-\infty}^{\infty} u_\star \, \mathrm{d}x = \int_{-\infty}^{\infty} \frac{p_\star(x)}{\lambda(x)} \, \mathrm{d}x. \tag{12}$$

Proof. We integrate both sides of (4) with respect to x, again noting that $\hat{p}_i \to 0$ as $x \to \pm\infty$, resulting in

$$\partial_t \int_{-\infty}^{\infty} \hat{p}_i \, \mathrm{d}x = -\int_{-\infty}^{\infty} \lambda\hat{p}_i \, \mathrm{d}x.$$

However, from theorem 1, we see that the right-hand side is exactly the distribution of the interjump time p_{τ_i}, so we have

$$\partial_t \int_{-\infty}^{\infty} \hat{p}_i \, \mathrm{d}x = -p_{\tau_i}(t). \tag{13}$$

Taking the mean on both sides with respect to τ_i,

$$\langle \tau_i \rangle = -\int_0^\infty \int_{-\infty}^\infty t\partial_t \hat{p}_i \, \mathrm{d}x \, \mathrm{d}t,$$

after integrating by parts and noting that $\int_0^\infty \hat{p}_i \, \mathrm{d}t = p_i/\lambda$, we get the desired result. □

While the first moment (mean) of the interjump time can be computed directly with a quadrature of the presumed known jump location p_i, the higher order moments are less straightforward. Appendix A describes how, in theory, knowledge of the p_i can be used to extract higher order moments of τ_i. Solving for higher order moments using this approach requires solving a hierarchy of differential equations, which in practice, may not be so feasible. However, a more practical numerical approach may be to solve for p_i and then run the absorbing (3) process to extract explicitly p_{τ_i} using the relationships from theorem 1.

4. Examples

4.1. Neuronal integrate-and-fire

The behavior of individual neurons can roughly be thought of as an 'integration' process, which builds up voltage, and then 'fires', which describes the release of this voltage into an action potential [27], the full process of which is known as *integrate-and-fire*. The most classical version of this model involves a deterministic buildup of voltage until a fixed firing voltage threshold is reached.

Incorporating noise in various ways into this class of models has a rich body of literature [48, 50]. Some approaches include a so-called 'leaky' neuron, one that has diffusive noise in the integration phase [15, 18, 24], whereas others regard the threshold itself as stochastic [5, 12, 18, 41]. Our work provides a natural framework to consider both sources of noise and their effect.

We propose a simple model of neuronal integrate-and-fire. While this model is greatly simplified from the actual physiology, we take this approach to show that a minimal model, stripped of considerable details, is still able to produce interesting emergent behavior. In previous models with a stochastic threshold, there is some inherent threshold, say, v_0, where the firing rate $\lambda(v)$ is taken to be a Gaussian centered around v_0 [5, 12]. The justification for this that models such as Hodgkin–Huxley [34], which account for more fine-grained detail, predict a distinct firing threshold v_0. In our model, we find that this sharp threshold v_0 can also arise from stochasticity alone, even when no inherent threshold is defined in the model.

Let V_t denote the voltage at time t. Then, in the context of this framework, we take the forms

$$\mathbb{L}p = -\partial_v\{\alpha p\} + D\partial_{vv}p, \qquad \lambda(v) = \gamma \mathrm{e}^{\beta v}, \qquad \mathbb{J}p = \delta(v)\int_{-\infty}^\infty p(v,t)\,\mathrm{d}v.$$

In words: we take the buildup to be at a constant rate α and leaky with constant diffusivity. While it is typically more common to take evolution of the form $\dot{v} = -a + bv$, this defines an inherent voltage $\tilde{v} = b/a$, which we deliberately omit. The result of making this change is also qualitatively negligible. For the jump component, we take $\mathbb{J}$ to be the reset to zero case, a full fire. The rate at which the firing occurs is assumed to be monotonically increasing, where again, we emphasize the fundamental difference between this form and previously considered, where λ is a Gaussian centered around some voltage v_0. In our model, voltage simply builds up, and as it builds up, the system is more likely to fire. There is no prescribed firing threshold

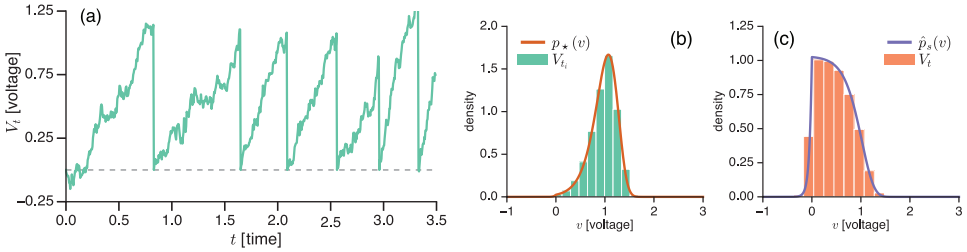

Figure 2. (a) an example trajectory of the proposed integrate-and-fire model. When the neuron fires, it resets back to $V = 0$ (dashed, gray). (b) the resulting stochastic firing voltages from Monte Carlo simulation (bars) and theoretically predicted (line). (c) the stationary density of the full process from Monte Carlo simulation (bars) and predicted (line).

as in classical work and its extensions. The justification for this form can be thought of as the underlying mechanism for firing: a discrete birth-death process (also with voltage dependent rates) of ion channels. At some fixed voltage v, the birth-death process is more likely to flip entirely 'on' and cause the neuron to fire. The relationship between models with explicit ion channels and integrate-and-fire has been explored previously [16].

An example simulation of the model can be seen in figure 2(a) with parameter values $\alpha = 2, D = .1, \gamma = .5, \beta = 2$. In the simulation, voltage builds up in a noisy (leaky) manner, and then the jump process fires, resetting back to $v = 0$, typical of an integrate-and-fire model. However, in this case, we emphasize that the firing voltage is inherently random and therefore of interest to study. Then, in stationarity, the fundamental relation in this work (7) becomes (noting $x \to v$)

$$0 = -\partial_v \{\alpha u_\star\} + D\partial_{vv} u_\star - \gamma e^{\beta x} u_\star + \delta(v) \int_{-\infty}^{\infty} \gamma e^{\beta v} u_\star \, dv.$$

From (10), the integral scaling on the δ function is equal to 1,

$$\delta(v) = -\partial_v \{\alpha u_\star\} + D\partial_{vv} u_\star - \gamma e^{\beta v} u_\star. \tag{14}$$

This can be computed in a similar manner to a Green's function, noting that for $v \neq 0$, we have

$$0 = -\partial_v \{\alpha u_\star\} + D\partial_{vv} u_\star - \gamma e^{\beta v} u_\star, \tag{15}$$

and integrating (14) from $(-\varepsilon, \varepsilon)$ and using the fact that $u_\star$ must be continuous, we get the matching condition

$$D\{u'(0^+) - u'(0^-)\} = -1. \tag{16}$$

Solving (15), we get that our solution is of the form

$$u_\star = \begin{cases} c_1 u_L(v) := c_1 e^{\frac{\alpha v}{2D}} I_{\alpha/(\beta D)}\left(\frac{2\sqrt{D\gamma e^{\beta v}}}{\beta D}\right) & v < 0 \\ c_2 u_R(v) := c_2 e^{\frac{\alpha v}{2D}} K_{-\alpha/(\beta D)}\left(\frac{2\sqrt{D\gamma e^{\beta v}}}{\beta D}\right) & v > 0, \end{cases}$$

where I, K are modified Bessel functions [1] such that $I \to 0$ as $v \to -\infty$ and $K \to 0$ as $v \to \infty$ (and are linearly independent). The jump condition (16) then becomes

$$D\{c_2 u_R'(0) - c_1 u_L'(0)\} = -1. \tag{17}$$

However, we also need to impose continuity of $u_\star$, so we also have the requirement

$$c_1 u_L(0) = c_2 u_R(0). \tag{18}$$

The conditions (17) and (18) provide us two equations for two unknowns, which yield

$$c_1 = \frac{2}{D\beta} 2K_{\alpha/(D\beta)}\left(\frac{2\gamma}{\beta\sqrt{D\gamma}}\right), \qquad c_2 = \frac{2}{\beta D} 2I_{\alpha/(\beta D)}\left(\frac{2\gamma}{\beta\sqrt{D\gamma}}\right).$$

Thus far, our solution is defined only up to a constant, but we know that $u_\star$ must satisfy the scaling (10), which our choice of c_1, c_2 serendipitously already satisfy. By computing $u_\star$ explicitly, we can use (5) to immediately obtain the distribution of jump locations $p_\star$. Finally, from corollary 1, we also have the stationary density of the full process, $\hat{p}_s$, which is a rescaling of $q_\star$ such that (9) is satisfied.

The stationary density $\hat{p}_s$ of the full process and the stationary jump distribution $p_\star$ are shown in figures 2(b) and (c). From this, we can see that $\hat{p}_s$, the stationary density of the full process provides no interesting information. It is relatively uniform through some range of voltages. If a PDE approach were taken to provide information about the full process, this is all that would be available. However, the jump locations $p_\star$, are noteworthy. Despite prescribing no explicit voltage threshold for firing, the state-dependent nature of the firing rate yields an effective threshold ($v_0 \approx 1$ for these parameter values) and persists through a wide range range of parameters. Hence, this is another, novel justification for models that take a deterministic firing threshold, as our minimal integrate-and-fire model produces this feature as a product of stochasticity, which is made apparent in the lens of the proposed framework.

4.2. Transport by a molecular motor

Consider a single molecular motor (e.g. kinesin [30]) attached to a cargo as in figure 3(a). Molecular motors produce transport by taking discrete steps along a track, exerting a force on a cargo. A notable feature of these steps is that the rate at which they are taken is well-established to be force-dependent [7]. That is, motors typically 'slow down' as force is exerted on them. As this discrete stepping process occurs, another source of noise is the diffusion of the cargo, which is also instantaneously changing the force applied to the motor, and consequently, the rate at which it steps. In our proposed simple motor of transport, we provide a preliminary investigation into this question.

We assume that the linker between the molecular motor and the cargo can be treated as a Hookean spring, where x denotes the distance stretched (from rest), as depicted in figure 3(a). Then, the diffusion component of this process is an Ornstein–Uhlenbeck process. We take the motor to take fixed step sizes, Δ and the rate at which motors step to be Gaussian $\lambda(x) = \sqrt{\frac{\alpha^2\beta}{2\pi}}\exp\{-\beta x^2/2\}$. Although there is evidence that the direction of the force is significant for motor stepping, we consider a symmetric stepping rate (and only forward stepping) for simplicity. A future investigation of the role of asymmetry in the rate is necessary. However, this simple model still produces interesting behavior.

The resulting stationary relationship (7) becomes

$$0 = \partial_x\{axu_\star\} + D\partial_{xx}u_\star - \lambda(x)u_\star + \lambda(x-\Delta)u_\star(x-\Delta). \tag{19}$$

There does not appear to be a fruitful approach to studying (19) analytically. However, we solve can it numerically using a Crank–Nicolson upwind scheme. From this, $u_\star$ and consequently $p_\star$ is obtained. The first moment of the interjump time $\langle\tau_\star\rangle$ is immediate after a quadrature (12).

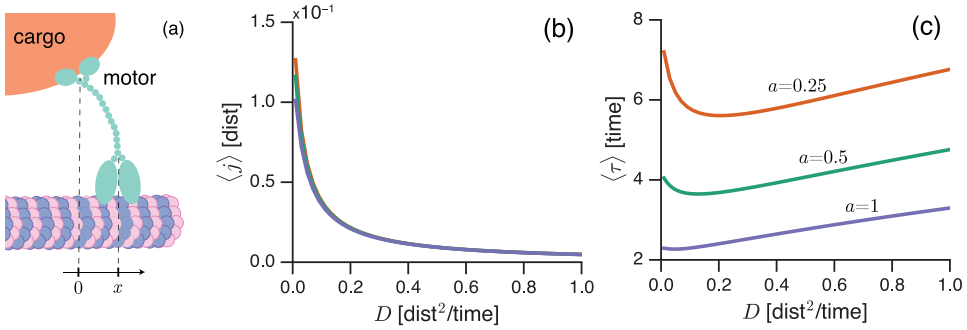

Figure 3. (a) a diagram illustrating the setup for the molecular motor model, where x denotes the distance the motor linker is stretched from rest. (b) the mean stationary jump location distribution for different values of a, linker strength as a function of the cargo diffusion coefficient D. (c) the mean stationary interjump time (stepping rate) for the motor.

We plot the mean value of x when a jump occurs, denoted $\langle j \rangle$ and the mean time between jumps, $\langle \tau \rangle$ as a function of the cargo diffusion coefficient D, for varying values of the linker strength, a. These results can be seen in figures 3(b) and (c) for parameter values $D = .1, \alpha = 1, \beta = 5$. The strength of diffusion appears to produce a curious effect on the other noise source. While the mean jump location, $\langle j \rangle$, remains effectively unchanged for varying values of linker strength, the mean interjump time exhibits very different behavior for different values of a. Specifically, we see that if the linker is weak, the interjump time can have a non-monotonic dependence on the diffusion coefficient. That is, the interaction between these two sources of noise (which can be studied as a result of this work) is non-trivial.

While this model is far simpler than the complex physiological it describes, the overall result (non-monotonic dependence on cargo diffusion) may be a feature that persists in a more detailed motor model (e.g. multi-motor), as other non-monotonic dependences on cargo noise have been seen [43]. Although the quantity $\langle j \rangle$ (the average distance a motor is stretched when stepping) is perhaps not the most useful in extracting information about more complex transport, it seems feasible that it it could be utilized in a reward-renewal framework akin to others utilized to study motor transport such as [31, 32, 39]. Motors also often have an asymmetric (state-dependent) unbinding rate, thought to be significant [52] and could perhaps provide a future application for this framework.

4.3. Independence of $\lambda(x)$

Lastly, we provide a short example (with no physical motivation in mind) that shows that our framework can be used with other tools (here, Fourier analysis) to glean interesting features of certain families of models. For this example, we consider a constant drift and diffusion with random jump size distribution $\mu(\Delta)$. Then, in stationarity (7), becomes

$$0 = -\partial_x \{a u_\star\} + D\partial_{xx} u_\star - \lambda(x) u_\star + \int_{-\infty}^{\infty} \mu(\Delta)\lambda(x-\Delta)u_\star(x-\Delta)\,\mathrm{d}\Delta. \tag{20}$$

One quantity of interest is the first moment of jump locations, so

$$\langle j_\star \rangle = \int_{-\infty}^{\infty} x p_\star \,\mathrm{d}x = \int_{-\infty}^{\infty} x u_\star \lambda \,\mathrm{d}x.$$

Although $\lambda(x)$ is arbitrary, surprisingly the Fourier transform can be used to gain some insight. Define the Fourier transform of $u_\star$ to be

$$U(k) := \mathcal{F}[u_\star] = \int_{-\infty}^{\infty} \mathrm{e}^{-\mathrm{i}kx} u_\star(x)\,\mathrm{d}x.$$

Also define the transformed quantities

$$\Lambda(k) := \mathcal{F}\left[\lambda u_\star\right], \qquad M(k) := \mathcal{F}[\mu],$$

from which, we note that

$$\Lambda'(0) = -\mathrm{i}\langle j\rangle, \qquad M'(0) = -\mathrm{i}\langle\mu\rangle.$$

Taking the transform of (20),

$$0 = -aikU - Dk^2U - \Lambda(k) + M(k)\Lambda(k), \tag{21}$$

which, evaluated at $k = 0$ yields

$$\left[1 - M(0)\right]\Lambda(0) = 0. \tag{22}$$

However, we know $\mu(\Delta)$ and $u_\star\lambda = p_\star$ are both probability densities and consequently $M(0) = 1$ and $\Lambda(0) = 1$. Thus, (22) is trivially satisfied. This is not useful on its own, but we can couple the higher order moments by taking a k derivative of (21) to yield

$$0 = -aikU' - aiU - 2DkU - 2k^2U' - \Lambda' + M'\Lambda + M\Lambda',$$

which, at $k = 0$ and using $M(0) = 1, \Lambda(0) = 1$ yields

$$0 = -aiU - \Lambda'(0) + M'(0) + \Lambda'(0),$$

which says that necessarily

$$M'(0) = -\mathrm{i}\langle\mu\rangle = aiU(0).$$

However, recall from (11) that $U(0) = \langle\tau_\star\rangle$, the mean interjump time, so

$$\langle\tau_\star\rangle = -\frac{\langle\mu\rangle}{a}. \tag{23}$$

This result is interesting for two reasons. For one, we have the mean interjump time is completely independent of the choice of $\lambda(x)$, aside from the requirement that the system reaches stationarity. Secondly, the sign of (23) narrows down the requirements for the process to reach stationarity. Since $\langle\tau_\star\rangle$ is an interjump time, it must be non-negative, meaning this quantity only exists if $a, \langle\mu\rangle$ differ in sign. This is intuitive as the drift and jump process must oppose each other to have a chance of reaching stationarity. We acknowledge that the linearity of this example (which allows us to perform the explicit Fourier analysis) also makes the result possible to derive through other methods (e.g. taking expectations of the SDE). However, we hope this analysis conveys that our framework provides a different lens (in junction with elementary tools) to study and possibly reveal behavior of a system.

5. Discussion and conclusion

In this work, we present a general framework for studying jump-diffusion systems with state-dependent jump rates, a class of models that were previously difficult or impossible to study otherwise due to the interaction between the two sources of noise. The formulation is flexible

enough to accommodate a variety of behaviors, providing relevance to a wide range of applications. The particular objects of study in this work are the distributions of the jump locations: the values of X_t evaluated at the jump times t_i.

We reformulate the full process into a survival description between jumps. Using this reformulation, the explicit distribution of jump locations can be extracted in a manner that depends on the previous jump location. This relation can be articulated as an iterated map, producing a sequence of jump locations. With explicit knowledge of the distribution of jump locations, statistics of the interjump times can be computed in more generality than previous work [13]. Taking this map to its limit, or equivalently, assuming the process reaches stationarity, the stationary distribution of the full process and the jump locations are shown to be closely related. An immediate consequence of this relation is that these two quantities differ if and only if the jump intensity is state dependent. That is, for the class of models studied in this work, the jump locations are distinct from the stationary density. Consequently, if the jump locations are of interest, the results of this work illustrate their relation to observations of the full process.

Although not the focus of this work, we provide a brief discussion of possible conditions on convergence to stationarity in the novel lens of this framework. This discussion utilizes tools from theoretical ecology motivated by the observation that the iterated map formulation is effectively a non-negative integral linear operator. This is in contrast to previous, more probabilistic approaches to studying finite time blowup of these models or similar [2, 9, 14, 54].

Finally, we provide three example applications of the framework. The first application, to a simple model of stochastic neuronal integrate-and-fire, is used to show a scenario where the jump locations themselves may be of interest. Our minimal model contains no inherent threshold voltage, but, as a product of stochasticity of the firing threshold, forms a robust, sharp peak of firing locations. This provides additional and novel support for the use of a deterministic threshold as in classical integrate-and-fire and its extensions. The second model, one of intracellular transport by a molecular motor is used to demonstrate how the two sources of noise (diffusion and jumps) interact. We ultimately find that the mean stepping rate of the motor can have a non-monotonic dependence on the strength of cargo diffusion, a consequence of the interaction between the two noise sources. Finally, a third example calculation shows that certain classes of models (in this case, constant drift, random jump size) can have curious behaviors. Specifically, we find that the mean interjump time for be *independent* of the choice of $\lambda(x)$, so long as the process does indeed reach stationarity.

This work proposes a preliminary framework for studying a wide class of problems. Although not explicitly studied here, we suspect that with more exotic diffusions (e.g. colored noise, which fits within the scope of these results), the interactions between the feedback between the noise sources can produce even more interesting behavior and will be explored in the future. Additionally, a more precise exploration is necessary of how an iterated map framework such as this can be used to provide conditions of stationarity.

Acknowledgments

This research was partially supported by NSF grant DMS 1515130 and DMS-RTG 1148230.

Appendix A. Higher order interjump time moments

In theory, higher order moments of the interjump times can be computed with knowledge of the sequence of jump distributions p_i as was discussed with the first moment in (11).

To illustrate this, consider (13) and take the second moment with respect to τ_i on both sides, resulting in

$$\langle \tau_i^2 \rangle = -\int_{-\infty}^{\infty} \int_0^{\infty} t^2 \partial_t \hat{p}_i \, \mathrm{d}t \, \mathrm{d}x.$$

Again, noting that $u_i = p_i/\lambda = \int_0^{\infty} \hat{p}_i \, \mathrm{d}t$, after integrating by parts, we get

$$\langle \tau_i^2 \rangle = -\int_{-\infty}^{\infty} v_i \, \mathrm{d}x,$$

which looks similar to (11), however, v_i is defined by the relation

$$[\lambda(x) - \mathbb{L}]v_i = u_i. \tag{A.1}$$

Thus, computation of the second moment requires solving the differential relationship (A.1), rather than just a quadrature as in the first moment. Continuing to higher order moments using same approach yields a further hierarchy coupled in a differential manner. Interestingly, the differential operator (left hand side) of (A.1) is exactly $\mathbb{T}$, the same as (6), meaning the Green's function (effectively $\mathbb{T}^{-1}$, discussed more in appendix B) could be used to compute these quantities.

Appendix B. Spectral properties of iterated map

Note that (6) involves the inverse of a differential linear operator $\mathbb{T}$, which is exactly determined by its corresponding Green's function. Let $G(x, \xi)$ be the corresponding Green's function to $\mathbb{T}$, meaning that

$$\mathbb{T}_x G(x, \xi) = \delta(x - \xi).$$

Then, (6) can be rewritten as

$$u_{i+1} = \int_{-\infty}^{\infty} G(x, \xi) \mathbb{J} \lambda u_i(\xi) \, \mathrm{d}\xi.$$

After a change of variables, define $\tilde{G}$ by

$$u_{i+1} = \int_{-\infty}^{\infty} \tilde{G}(x, \zeta) u_i(\zeta) \, \mathrm{d}\zeta := \int_{-\infty}^{\infty} G(x, \xi) \mathbb{J} \lambda u_i(\xi) \, \mathrm{d}\xi.$$

For example, for fixed jump sizes: $\mathbb{J}p = p(x - \Delta)$, then

$$\tilde{G}(x, \zeta) = G(x, \zeta + \Delta) \lambda(\zeta + \Delta).$$

Abbreviate this linear non-negative integral operator

$$\mathbb{A}q := \int_{-\infty}^{\infty} \tilde{G}(x, \zeta) q(\zeta) \, \mathrm{d}\zeta.$$

Now, iterations of our map correspond to iterating the integral operator $\mathbb{A}$ with kernel $\tilde{G}$. This formulation is exactly that of the so-called *integral projection models* (IPM) in theoretical ecology [20]. Stability results from the IPM literature can be used to understand the convergence of our iterative procedure.

The main result comes from [19] and is effectively a statement of the Krein–Rutman theorem [37, 38], the infinite dimensional analog of the Perron–Frobenius theorem. [6, 33]

Although L^1 seems like the natural function space to study the spectral properties of these operators, since they must preserve probability, L^2 turns out to be far more accessible due to issues establishing compactness in L^1. In appendix C of [20], the authors provide a more thorough commentary on these complications. we cite the main theorem which establishes the existence of a dominant eigenvalue for $\mathbb{A}$.

Theorem B.1 (Easterling 1998, [19]). *Suppose that $\tilde{G} \in L^2$ and is non-negative. If there exists an $\alpha > 0, \beta > 0, u_0$ such that*

$$\alpha(x)u_0(\xi) \leqslant \tilde{G}(x,\xi) \leqslant \beta(x)u_0(\xi),$$

for all x, ξ, then the integral operator $\mathbb{A}$ has a dominant eigenvalue with associated eigenfunction.

This establishes conditions for the existence of a dominant eigenvalue and eigenvector, which establish the long-term behavior.

Theorem B.2 (Easterling 1998, [19]). *Assuming that $\mathbb{A}$ satisfies the previous condition, then the stationary distribution $u_\star$ is given by the eigenfunction ϕ_1 associated with the dominant eigenvalue λ_1,*

$$\lim_{i\to\infty} \frac{u_i}{\lambda_1^i} = \kappa\phi_1,$$

where κ is a scaling parameter.

The previous theorem suggests that the sequence u_i converges if and only if $|\lambda_1| = 1$. Thus, this summary provides a rough heuristic, but possibly novel angle for determining whether the sequence u_i (and the full process) approach stationarity, although we reemphasize that this is not our focus.

ORCID iDs

Christopher E Miles https://orcid.org/0000-0001-5494-403X

References

[1] Abramowitz M and Stegun I A 1966 *Handbook of Mathematical Functions* (*Dover Books on Mathematics* vol 55) (New York: Dover)
[2] Bally V, Goreac D and Rabiet V 2017 arXiv: 1707.02713 [math.PR]
[3] Bartlett M S, Daly E, McDonnell J J, Parolari A J and Porporato A 2015 *Proc. R. Soc.* A **471** 20150389
[4] Bjork T, Kabanov Y and Runggaldier W 1997 *Math. Financ.* **7** 211–39
[5] Braun W, Matthews P C and Thul R 2015 *Phys. Rev.* E **91** 052701
[6] Bressloff P C 2014 *Stochastic Processes in Cell Biology* (*Interdisciplinary Applied Mathematics* vol 41) (New York: Springer)
[7] Carter N J and Cross R A 2005 *Nature* **435** 308–12
[8] Christou C and Schadschneider A 2015 *J. Phys. A: Math. Theor.* **48** 285003
[9] Cloez B and Hairer M 2015 *Bernoulli* **21** 505–36
[10] Cox D R 1955 *J. R. Stat. Soc. Ser.* B **17** 129–64
[11] Daly E and Porporato A 2006a *Phys. Rev.* E **73** 026108
[12] Daly E and Porporato A 2006b *Phys. Rev.* E **74** 041112
[13] Daly E and Porporato A 2007 *Phys. Rev.* E **75** 1–6
[14] DeVille L, Dhople S, Domínguez-García A D and Zhang J 2016 *SIAM J. Appl. Dyn. Syst.* **15** 526–56

[15] Di Maio V, Lánský P and Rodriguez R 2004 *Gen. Physiol. Biophys.* **23** 21–38
[16] Ditlevsen S and Greenwood P 2013 *J. Math. Biol.* **67** 239–59
[17] D'Odorico P, Laio F and Ridolfi L 2006 *Am. Nat.* **167** E79–87
[18] Dumont G, Henry J and Tarniceriu C O 2015 *J. Math. Biol.* **73** 1413–36
[19] Easterling M R 1998 The integral projection model: theory, analysis and application *PhD Thesis* North Carolina State University
[20] Ellner S P and Rees M 2006 *Am. Nat.* **167** 410–28
[21] Evans M R and Majumdar S N 2011a *J. Phys. A: Math. Theor.* **44** 435001
[22] Evans M R and Majumdar S N 2011b *Phys. Rev. Lett.* **106** 1–4
[23] Figueroa-López J 2011 Jump-diffusion models driven by Lévy processes *Handbook of Computational Finance* ed J Duan *et al* (Berlin: Springer) pp 61–88
[24] Fourcaud N and Brunel N 2002 *Neural Comput.* **14** 2057–110
[25] Fulgenzi W, Melatos A and Hughes B D 2017 *Mon. Not. R. Astron. Soc.* **470** 1–25
[26] Gardiner C 2009 *Stochastic Methods: a Handbook for the Natural and Social Sciences* 4th edn (*Springer Series in Synergetics* vol 13) (Berlin: Springer)
[27] Gerstner W and Kistler W M 2002 *Spiking Neuron Models: Single Neurons, Populations, Plasticity* (Cambridge: Cambridge University Press)
[28] Glasserman P and Merener N 2004 *Proc. R. Soc.* A **460** 111–27
[29] Hanson F B 2007 *Stochastic Processes and Control for Jump-Diffusions* (*Advances in Design and Control* vol 13) (Philadelphia: SIAM)
[30] Howard J 2001 *Mechanics of Motor Proteins and the Cytoskeleton* (Sunderland, MA: Sinauer Associates)
[31] Hughes J, Hancock W O and Fricks J 2011 *J. Theor. Biol.* **269** 181–94
[32] Hughes J, Hancock W O and Fricks J 2012 *Bull. Math. Biol.* **74** 1066–97
[33] Keener J P 2000 *Principles of Applied Mathematics: Tranformation and Approximation* (Boulder, CO: Westview Press)
[34] Keener J P and Sneyd J 2008 *Mathematical Physiology* (Berlin: Springer)
[35] Kou S G 2002 *Manage. Sci.* **48** 1086–101
[36] Kou S G 2007 *Handbooks in Operations Research and Management Science* vol 15 (Amsterdam: North-Holland) pp 73–116
[37] Krasnosel'skii M A 1964 *Positive Solutions of Operator Equations* (Groningen: Noordhoff)
[38] Krein M G and Rutman M A 1950 *Am. Math. Soc. Transl.* **26** 128
[39] Krishnan A and Epureanu B I 2011 *Bull. Math. Biol.* **73** 2452–82
[40] Lawley S D, Mattingly J C and Reed M C 2015 *SIAM J. Math. Anal.* **47** 3035–63
[41] Lindner B, Chacron M J and Longtin A 2005 *Phys. Rev.* E **72** 1–23
[42] Méndez V and Campos D 2016 *Phys. Rev.* E **93** 022106
[43] Miles C E and Keener J P 2017 *J. Theor. Biol.* **424** 37–48
[44] Montero M, Maso-Puigdellosas A and Villarroel J 2017 arXiv: 1706.04812 [math-ph]
[45] Montero M and Villarroel J 2013 *Phys. Rev.* E **87** 012116
[46] Montero M and Villarroel J 2016 *Phys. Rev.* E **94** 1–10
[47] Pal A, Kundu A and Evans M R 2016 *J. Phys. A: Math. Theor.* **49** 225001
[48] Plesser H E and Gerstner W 2000 *Neural Comput.* **12** 367–84
[49] Roldán É and Gupta S 2017 *Phys. Rev.* E **96** 022130
[50] Sacerdote L and Giraudo M T 2013 *Stochastic Biomathematical Models* (*Lecture Notes in Mathematics* vol 2058) (Berlin: Springer) pp 99–148
[51] Shtylla B and Keener J P 2010 *J. Theor. Biol.* **263** 455–70
[52] Takshak A and Kunwar A 2016 *Protein Sci.* **25** 1075–9
[53] Wu Y and Zhu W Q 2008 *Phys. Rev.* E **77** 1–9
[54] Xi F 2009 *Stoch. Process. Appl.* **119** 2198–221
[55] Xia Y and Giles M B 2012 *Springer Proc. in Mathematics and Statistics* vol 23 (Cham: Springer) pp 695–708
[56] Yan G and Hanson F B 2006 Option pricing for a stochastic-volatility jump-diffusion model with log-uniform jump-amplitudes *Amer. Control Conf. (Minneapolis, MN, 14–16 June 2006)* pp 2989–94

CHAPTER 4

DISENTANGLING ACTIVE AND PASSIVE DIFFUSION IN TRANSPORT DATA

The work in this chapter was done in collaboration with Michael D. Vershinin[12], Olaolu Osunbayo[1], and Babu J. N. Reddy.[3] A version of these contents are currently submitted as a manuscript under consideration.

4.1 Introduction

Intracellular cargo tracks tend to be highly complex because motion can be driven by a variety of causes, including mechanochemical enzymes [33] and passive diffusion [6] (equivalently, motion can be driven by causes that obey or break detailed balance [16]). The distinction between passive and active motion is crucial. For example, one might use positional fluctuations of an intracellular cargo to calibrate in vivo optical trapping [12], but it is essential to first establish that the chosen cargos are not subject to motor activity. On the other hand, if enzymatic contribution is established then one can proceed to probe the properties of molecular motors mediating the motility [30, 21]. It is thus desirable in many experimental contexts to have a simple way to distinguish between active and passive motility.

Mean-squared displacement (MSD) analysis [24] is commonly used to classify single particle motion. Pure Brownian motion leads to linear MSD curves whereas motion driven by individual mechanochemical enzymes often proceeds at constant velocity and produces a quadratic MSD dependence [24, 26]. An important subtlety is that Brownian motion is not the only stochastic process that leads to linear MSD curves [23, 35]. A linear MSD

[1]Department of Biology, University of Utah.

[2]Department of Physics & Astronomy, University of Utah.

[3]Department of Developmental & Cell Biology, University of California Irvine.

can very well arise from an active process, for example, with a balanced ensemble of mechanochemical enzymes that oppose each-others motion. MSD analysis may be convenient and easy to perform but it is not always able to distinguish active from passive motility.

Motility analysis and modeling is rapidly changing [35, 5]. Interest in active fluctuations and awareness of complications in practical data analysis is growing [28, 34]. Practical examples of enzymatically driven diffusion are now well established [21]. However, theoretical approaches to teasing out various diffusion and active motility modes from single particle tracking data [23] are still under active development [25, 22] and a single standardized approach has yet to emerge. It is, however, clear that in general mere tracking and associated analysis is insufficient to relate cargo-scale phenotype to constituent single molecule contributions. There is thus an acute need for new experimental probes of complex motility.

In this work, we construct a minimal model of an active but apparently diffusive process. We then examine the resulting motility and demonstrate that even in our minimal system the overall ensemble phenotype is complex. We then capture the fundamental dynamics in our system in a minimal theoretical model and further show how active contribution to the apparent diffusion can be isolated via a simple experimental approach.

4.2 Experimental basis

4.2.1 Bead assay

We have constructed a system for complex motility under controlled conditions by constructing a bead assay in which multiple microtubule-based motors could cross-bridge a cargo to a filament and subsequently engaged in a balanced tug-of-war. To keep the system minimal we have used a single type of motor: N340K mutant of kinesin-14 Ncd (nonclaret dysjunctional; [7]). Wildtype Ncd is nonprocessive with a bias for minus-end directed powerstroke [7, 9, 10, 36, 4]. The N340K mutant is a bidirectional motor, with more balanced preference for stepping in either direction. Ensembles of N340K Ncd motors were previously used in a microtubule gliding assay and showed ensemble bidirectional motility. Most of the motility was reported to be localized but some contiguous displacements in either direction were too long to be ascribed to diffusion even though overall motile

random process appeared roughly stationary [7]. The general view regarding this phenomenon is that the cooperative activity of Ncd motors is sufficient to temporarily power directed displacement [16] but the choice of direction occurs via spontaneous symmetry breaking and need not be biased in a specific direction. However, diffusive motion has not been fully ruled out [6].

We studied Ncd N340K driven motility in a bead assay to more closely model active bidirectional cargo motion, seen in **Figure 4.1**. The observed motility was consistent with gliding assay phenotype [7]: most beads exhibited limited localized motions while some beads had more extensive bidirectional motility. The MSD analysis of tracks revealed that the motion is strongly subdiffusive on short time scales but apparently diffusive on longer time scales, as in **Figure 4.1**.

We then wanted to examine whether the linear MSD lineshape could be directly attributed to the enzymatic activity of Ncd. The central idea behind our approach is that biological enzymes typically undergo dramatic changes in activity over a biologically relevant temperature range [15, 17, 8] whereas passive processes like diffusion show much less pronounced variation with temperature. We demonstrate in **Figures 4.2 and 4.3** that temperature-dependent single particle tracking is indeed a rapid and convenient approach

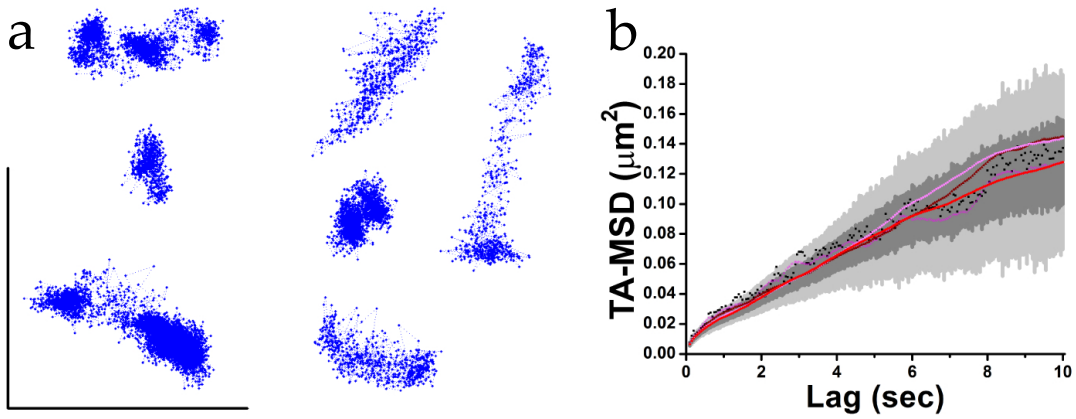

Figure 4.1. Experimental bead motility at room temperature. **a**: Representative weakly motile tracks. **b**: TA-MSD (time-averaged mean-squared displacement) for several measurement times: 0.05 sec (black), 0.5 sec (dark magenta), 2.5 sec (burgundy), 5 sec (light magenta), 10 sec (red). One sigma (68.3%) and two sigma (95%) confidence intervals were estimated for the 5 sec data via 1000 sample bootstrap for each lag point (dark and light grey respectively).

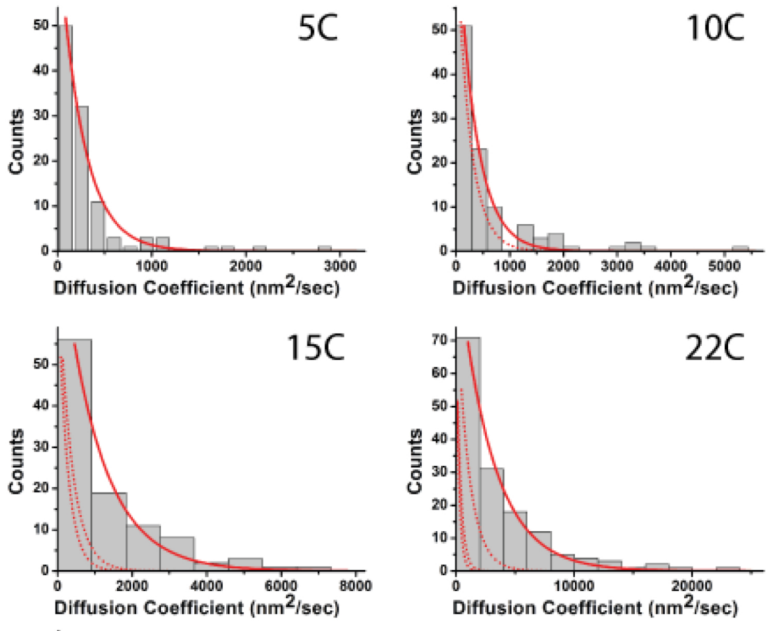

Figure 4.2. Temperature dependence of apparent diffusion coefficients for 5, 10, 15, 22 °C. In each panel, a fit to exponential density is shown (solid red). Because x-axis values needed to be rescaled for data at variable temperatures, fits to exponential densities at lower temperatures are shown for higher temperature panels (dashed red) for reference of overall scale.

to analysing the active contribution to apparent diffusion.

The linear fits [26] to long lag time portion of the MSD curves revealed that the distribution of the effective diffusion coefficients is not Gaussian. At all temperatures it is highly skewed and reasonably approximated by an exponential distribution, as in **Figure 4.2**. This feature is unexpected: approximately Gaussian distributions typically arise in this type of analysis due to the central limit theorem for large data sets. Indeed, this observation is in contrast to, for example, simple Brownian motion of beads in water, for which the distribution of diffusion coefficients is of course approximately Gaussian and varies slowly with temperature, as in **Figure 4.3**. Though exponential density is unusual, it does provide us with a decay scale which we can then use as the characteristic of diffusion at a given temperature.

We first highlight that the diffusion coefficient scale at room temperature is $0.008\mu\text{m}^2/\text{sec}$ more than an order of magnitude lower than the typical diffusion coefficients for regular diffusion of proteins along microtubules [6, 14]. This is consistent with the picture that

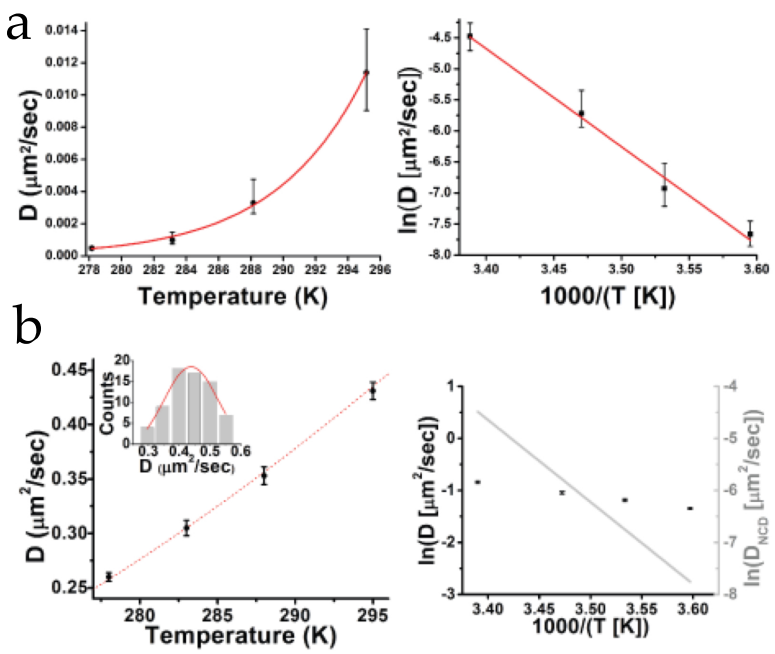

Figure 4.3. Characteristic diffusion coefficient for each temperature with best fit Arrhenius curve (red) on linear and Arrhenius style plots. **a**: Plots for motor-associated cargoes. **b**: Same plots for free diffusion of bead in water, showing only a weak dependence. Fit to Stokes-Einstein equation for radius 505 nm is shown (**b**; red dashed line); nominal bead radius is 499 ± 19 nm. **b**, inset: histogram of diffusion coefficients at 22 °C and a Gaussian fit (red). Arrhenius style plot: bead diffusion in water (black) is superimposed on linear trend for N340K Ncd diffusion.

random process generating the linear MSD is a complex multimotor interaction. Next, we observed that the characteristic diffusion coefficients extracted in this fashion yielded an excellent fit to the Arrhenius model but not to the linear one, as in **Figure 4.3**. The activation energy extracted from the Arrhenius fit was 130 KJ/mol somewhat high but within the range of activation energies observed for kinesin motors especially for a system of multiple motors where a stepping enzyme would see significant opposing load [3]. It is unlikely that another energy barrier relevant to our system is in this range. For example, the activation energies for protein diffusion along the microtubule lattice are not generally precisely known but are thought to be more than an order of magnitude lower [6]. The energy barriers relevant for the motor-microtubule detachment are of order 10 KJ/mol [32]. We conclude that the apparent diffusion is actually an active process.

4.2.2 Lipid droplet data

The last question we need to address is the unexpected finding that the distribution of effective diffusion coefficients in our assays is extremely skewed. To test whether this is a more general phenomenon associated with immotile but actively driven cargos we have examined a lipid droplet motility system in mammalian Cos-1 cells. Lipid droplet motility is known to be driven by kinesin-2 and dynein motors [13] and is also known to show a diverse array of phenotypes, from long distance directed motion to more stationary displacements, as in **Figure 4.4**. Moreover, lipid droplet motility in mammalian cells has been used as a probe of viscoelasticity of the cytoskeleton [37]. Indeed, subdiffusive behaviour has been found at short time scales but transition to linear MSD curves have been seen at longer time scales [37].

We examined the lipid droplet motility at long time scales only and focused on apparently diffusive transport. MSDs which conformed to a quadratic model better than linear as per Akaike information criterion were ignored in our analysis. The resulting tracks are not all stationary: linear or subdiffusive MSD curves can arise from active motion if it is saltatory, or if it is a minor part of a longer record. All these cases are seen in **Figure 4.4a**. The average MSD curve is broadly consistent with a linear trend, as in **Figure 4.4b**. Any minor subdiffusive curvature for short lags is not significant although such a feature would be expected from and consistent with a prior report [37]. However, the distribution of apparent diffusion coefficients (in **Figure 4.4c**) is inconsistent with Brownian motion and is instead highly skewed. The strong similarity between these observations and our in vitro data is of course insufficient to infer the microscopic picture of lipid droplet motility in cells. It is however sufficient to call into question whether viscoelastic contributions can be unambiguously attributed to the cytoskeletal filaments or cytosol in general. They may be partially or even wholly due to the motor contribution instead. It is also sufficient to call into question whether cytoskeletal motor contribution to nanoscale biomechanics in cells is purely elastic [11].

4.2.3 Subdiffusive behavior

The microscopic picture we have is bead-microtubule coupling via variable number of nonprocessive motors at a variety of relative binding positions and hence a variety of

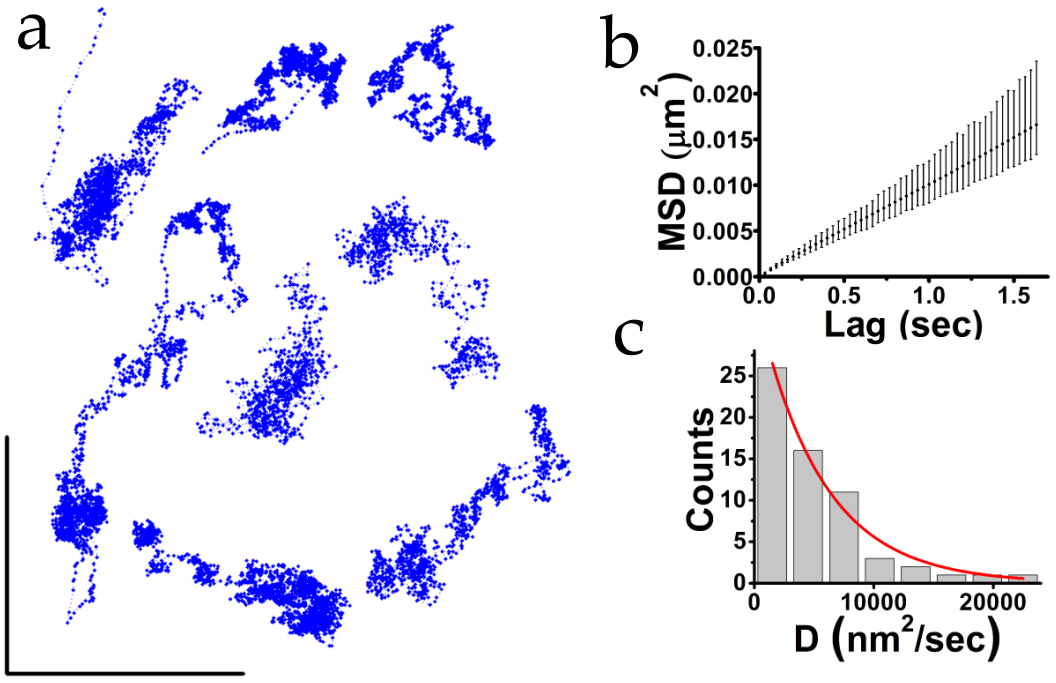

Figure 4.4. Lipid droplet motility in Cos-7 cells at 37 °C. **a**: example trajectory, showing apparently diffusive behavior, scale bar is 1μm. **b**: The average MSD curve and **c**: the distribution of effective diffusion coefficients.

coupling strengths. In this picture, when a motor detaches or attaches to the microtubule, the system slowly evolves to a new overall state. We would then expect that after some lag time, memory effects would become negligible. This is indeed seen in our data in **Figure 4.5**: Beyond about 1 second lag time, MSD curves do show a linear trend. Therefore, on long lag time scales the system becomes a good model of apparently diffusive behavior. Timeaveraged MSD (TA-MSD) analysis [29, 19, 31] of motility data for showed robust convergence, suggesting that the subdiffusive process is ergodic.

Our analysis also revealed a broad distribution of anomalous exponents from near zero to slightly above unity, in **Figure 4.6**. Generally, the distribution shifted lower with declining temperature. This is naturally explained by the above microscopic picture: as temperature gets lower, individual motor dynamics and thus also ensemble dynamics slow down leading to a flattening and leveling off of the MSD curve.

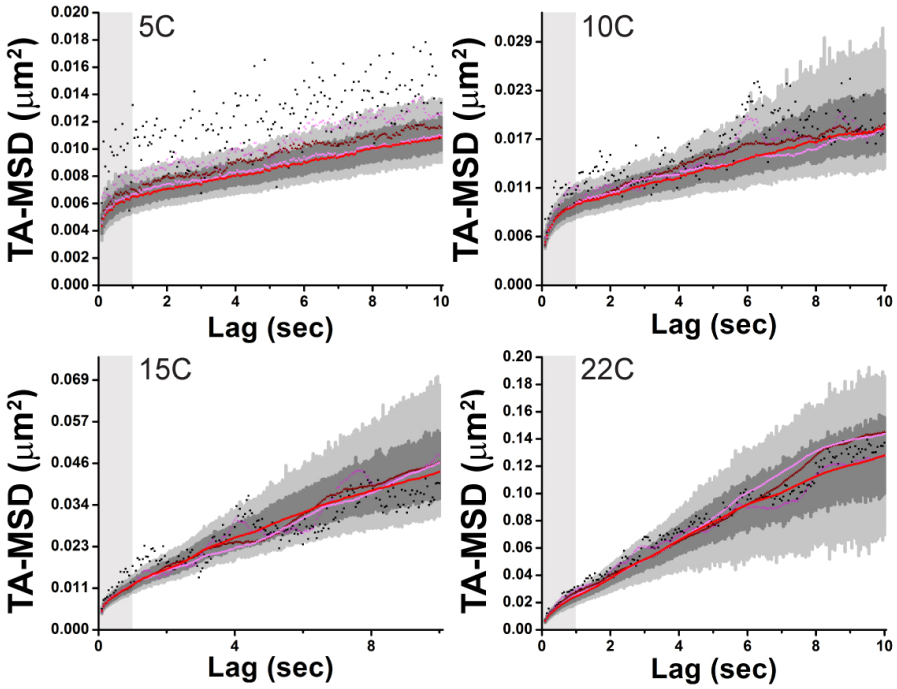

Figure 4.5. Anomalous features of bead motility. TA-MSD curves were computed for 5, 10, 15, 22 °C data as labeled. In each case average TA-MSD was computed for several measurement times: 0.05 sec (black), 0.5 sec (dark magenta), 2.5 sec (burgundy), 5 sec (light magenta), 10 sec (red). One sigma (68.3%) and two sigma (95%) confidence intervals were estimated for the 5 sec data via 1000 sample bootstrap for each lag point (dark and light grey respectively).

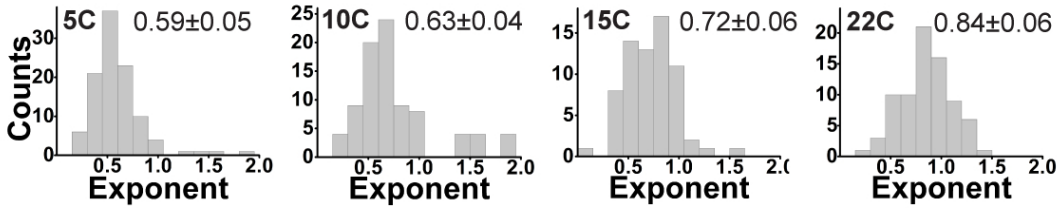

Figure 4.6. Subdiffusive anomalous exponents for MSD records below 1 second (grey regions in **Figure 4.5**) at 5, 10, 15, 22 °C as labeled. Peak locations and 95 confidence intervals are shown for each panel. Anomalous exponents were estimated via loglog linearization after adjustment for noise [18]. Each count corresponds to a full distinct bead trajectory

4.3 Jump–diffusion conceptual model

The observation of complex behaviour for nearly-immotile ensembles of molecular motors likely has some system-specific origins. At the same time, we might expect some skewness for the distribution of diffusion coefficients on very general grounds. The fundamental processes involved in all cases are ordinary diffusion (at the very least the diffusion of the cargo but also in some cases motor diffusion along the filament) and discrete jumps (binding, unbinding, and powerstroke events). For this reason, we seek to construct a minimal model that captures and elucidates the observed complex motility.

Let $p(x,t)$ be the probability density of a 1-dimensional jump-diffusion process in one dimension governed by the Fokker–Planck equation

$$\partial_t p(x,t) = D\partial_{xx} p(x,t) - 2\lambda p(x,t) + \lambda p(x-\delta,t) + \lambda p(x+\delta,t). \tag{4.1}$$

For simplicity, jumps in either direction are assumed to have fixed characteristic distance δ and occur at the same rate λ, so that the system is symmetric, in agreement with the N340K stepping data [7]. When the rate of jumps λ is set to zero, this describes the classical diffusion process. This system is highly reminiscent of the more general continuous-time random walk (CTRW) processes [23] but our model lacks the long-tailed correlations. While this model is minimal in its complexity, its simplicity allows for analytical tractability and deep understanding.

Ultimately, one primary feature we are interested in is the distribution of diffusion coefficients, as experimentally seen in **Figure 4.2**. We associate an empirical diffusivity with each trajectory, reflecting how the squared displacement scales with time. In other words, for a given trajectory we effectively are sampling the random variable

$$D_s(t) \coloneqq \frac{x(t)^2}{2t}, \tag{4.2}$$

where t is the sampling time, or the inverse of sampling frequency. One can think of the estimate of D for each path as an average of these samples. That is, a naïve estimator for the diffusivity is

$$D_{\text{est}} = \frac{1}{N}\sum_{i=1}^{N} D_s^{(i)}, \tag{4.3}$$

where N is the number of sample points on the path. Although the actual practice of estimating D for a path using these random variables is considerably more complicated

(a weighted linear regression [26]), this estimator provides the intuition for the curious statistics observed in experiments.

4.3.1 Moments

We are therefore interested in observations of the random variable D_s defined by equation (4.2). Moments of this variable are related to moments of x. Explicitly, the jth moment satisfies

$$\langle D_s^j \rangle = \frac{1}{(2t)^j} \langle x^{2j} \rangle = \frac{\mu_{2j}}{(2t)^j}, \qquad \mu_j \coloneqq \langle x^j \rangle, \tag{4.4}$$

The moments of x can be computed explicitly. Multiplying (4.1) by x^j and integrating, we find the explicit evolution of these moments

$$\frac{\mathrm{d}\mu_j}{\mathrm{d}t} = Dj(j-1)\mu_{j-2} + 2\lambda \sum_{k=1}^{\lfloor j/2 \rfloor} \binom{j}{2k} \delta^{2k} \mu_{j-2k},$$

where $\lfloor \cdot \rfloor$ is the floor operator.

This system of ODEs is "lower triangular" in the sense that μ_j only depends on μ_k where $k < j$. That is, we can solve these moments equations sequentially. The first, $\dot{\mu}_1 = 0$, so that $\mu_1 \equiv 0$ is intuitive, as diffusion and symmetric jumps produce no displacement on average. The remaining ODEs of interest are

$$\begin{aligned}
\frac{\mathrm{d}\mu_2}{\mathrm{d}t} &= 2D + 2\lambda\delta^2 \\
\frac{\mathrm{d}\mu_4}{\mathrm{d}t} &= 12\left[D + \lambda\delta^2\right]\mu_2 + 2\lambda\delta^4. \\
\frac{\mathrm{d}\mu_6}{\mathrm{d}t} &= 30\left[D + \lambda\delta^2\right]\mu_4 + 30\lambda\delta^4\mu_2 + 2\lambda\delta^6.
\end{aligned}$$

Immediately, we note that μ_2, the mean-squared displacement is indeed still linear even with the jump component. Moreover, the estimated diffusivity from this linear MSD is

$$\langle D_s \rangle = \frac{\mu_2}{2t} = D + \lambda\delta^2. \tag{4.5}$$

We can proceed on to the variance, using

$$\tilde{\sigma}^2 \coloneqq \mathrm{var}[D_s] = \frac{1}{(2t)^2}\left[\mu_4 - \mu_2^2\right] = 2\delta^4\lambda^2 + 2D^2 + 4\delta^2 D\lambda + \frac{\delta^4\lambda}{2t}. \tag{4.6}$$

Notably, if $\lambda = 0$ (no jumps, traditional diffusion), there is no dependence on t (the sampling time). However, with $\lambda \neq 0$, $\tilde{\sigma}^2 \to \infty$ as $t \to 0$.

The last moment, the skewness can be computed and is

$$\tilde{g} := \text{skew}\,[D_s] = \frac{32D^3t^2 + 96\delta^2D^2\lambda t^2 + 24\delta^4D\lambda t(4\lambda t+1) + \delta^6\lambda(8\lambda t(4\lambda t+3)+1)}{t\left(4D^2t + 8\delta^2D\lambda t + \delta^4\lambda(4\lambda t+1)\right)\sqrt{8D^2 + 16\delta^2D\lambda + \frac{2\delta^4\lambda(4\lambda t+1)}{t}}}. \tag{4.7}$$

This has the same features as the variance: if $\lambda = 0$ (no jumps, traditional diffusion), there is no t dependence. However, with $\lambda \neq 0$, as $t \to 0$, then $\tilde{g} \to +\infty$.

4.3.2 Relation to MSD analysis

We can relate the theoretical quantities to experimental observables by considering the observations of a single trajectory denoted

$$\{x_0, x_1, \ldots, x_N\},$$

where each observation occurs at a fixed time interval Δt, so $x(i) \approx x_0 + i\Delta t$. Then, each squared displacement, scaled by time, denoted $D_s^{(i)}$

$$D_s^{(i)} := \frac{[x_i - x_{i-1}]^2}{2\Delta t} \tag{4.8}$$

This is inherently a sample estimate of the diffusivity, the total estimator for which is (4.3).

Because each $D_s^{(i)}$ is independent, the statistics of the collection of diffusion coefficients over several paths each with N samples become

$$\langle D_{\text{est}}\rangle = \langle D_s\rangle, \qquad \text{var}\,[D_{\text{est}}] = \tilde{\sigma}^2/N, \qquad \text{skew}\,[D_{\text{est}}] = \tilde{g}/\sqrt{N}. \tag{4.9}$$

From (4.9) and (4.5), we reiterate the feature that this system indeed has a linear MSD curve, in agreement with the longer time measurements of the experimental system, as seen in vitro in **Figure 4.1** and in vivo in **Figure 4.4**.

The predicted diffusion coefficient is also of interest. We can also see that for enzymatically driven jumps, whose rate λ scales with temperature per Arrhenius law

$$\lambda \sim \exp\{-\Delta E/k_BT\},$$

and the passive diffusion scales linearly, by the fluctuation dissapation theorem

$$D \sim k_BT,$$

then the effective diffusion coefficient from (4.5) has identical scaling with the same activation energy. This suggests that our intuition is correct: if passive diffusion is dominant, the

empirical diffusivity should scale linearly, and if active, it will scale as a Boltzmann factor, which agrees directly with the experiments seen in **Figure 4.3**.

The higher order moments of D_{est} also provide insight toward the experimentally observed quantities. In the absence of jumps ($\lambda = 0$), we see from (4.9) the skewness of each sample is $2\sqrt{2}$, as expected for the chi-squared distribution with 1 degree of freedom. However, when $\lambda > 0$, the skewness grows. Furthermore, if $\lambda \gg 1/t$, that is, many jumps occur between samples, then the situation is similar in spirit to classical CTRW models: the tails become relatively long and lead to strong deviations from Brownian behavior. But the skewness is enhanced considerably even for $\lambda \sim 1/t$.

Although the skewness does indeed decay with the number of samples as predicted by the Central Limit Theorem, the rate of convergence is dependent on the magnitude of the skewness. Hence, as skewness is enhanced, convergence (to a Gaussian) becomes quite slow, even without violating the central limit theorem or ergodicity. This result is quite intuitive as a sampling issue. As experimental setups (and consequently, this random variable) are snapshots of the process and we have no memory effects built into our model, each sample is an independent identically distributed random variable representing diffusion and jumps occurring in a fixed amount of time (sampling time). The relationship between the sampling rate and the rate at which these jumps occur is therefore crucial in determining the statistics. In such cases, limited experimental data sets can still produce strongly skewed distributions for slopes of mean squared displacement curves without violating ergodicity. This observation has been made in other branches of scientific literature (for instance, finance [1]) but seems to be underappreciated in this context.

4.3.3 Comparison to simulations

While (4.9) describes the moments of the naïve estimator (4.3), in practice, the MSD, and associated diffusivity estimate is computed quite differently. Specifically, the MSD curve is computed using *overlapping* windows [26], so the MSD associated with a window of size $i\Delta t$ is averaged over all windows of that size,

$$\langle x_i^2 \rangle = \frac{1}{N_i} \sum_{j=1}^{N_i} \left[x_{ij} - x_{i(j-1)} \right]^2,$$

where N_i is the number of overlapping windows of size i, $N_i := \lfloor (N-1)/n \rfloor$. From there, a weighted linear regression is performed for $i\Delta t$ against x_i^2, with the weights $w(i)$ taken to be the inverse of the variance of all squared displacements of size i, that is

$$w(i) = \left(\text{var} \left[\left\{ \left[x_{ij} - x_{i(j-1)} \right]^2 \right\}_{j=1}^{N_i} \right] \right)^{-1}.$$

The estimate for D is then proportional to the slope of the linear regression line.

While this procedure does a notably good job at filtering out noise, its complexity makes predicting the output for even simple models, such as jump diffusion, intractable. For this reason, we perform simulations of jump-diffusion and compare the predicted skewness for the naïve estimator to that of the more complicated D estimator used in practice.

The comparison of these skewnesses can be seen in **Figure 4.7** and **Figure 4.8**. From the first, we see the dependence on the number of paths M, and the number of points on the path N agrees quite closely with the predicted values of (4.9). We do see an increase in the skewness for the simulated values, which is intuitive, as the overlapping windowed procedure introduces correlation in the estimate, which manifests as this difference. Of particular note, the jump-diffusion process ($\lambda \neq 0$) has considerably higher skewness than that of just classical diffusion for both the theoretical and simulated values.

Figure 4.8, we see the same features, with the noteworthy exception that simulated values differ from the predicted at small values of Δt. There is a technical limit on the number of samples (N) we can reasonably process, but we can fix N to be large and vary the sample time Δt (meaning that the total simulation time $N\Delta t$ also varies). Consequently, for any finite simulation it is always possible to examine low enough values of Δt, so that the length of simulation is not long enough to capture accurate statistics of the jump component.

4.4 Conclusion

We have demonstrated that tug-of-war events for cytoskeleton transport can lead to complex motile behaviours in the absence of the cytosol, in the absence of microtubule movement [19], and indeed even in the absence of multiple cytoskeletal filaments [27]. Some of the motility we observed (short lag times) is clearly in the class of anomalous

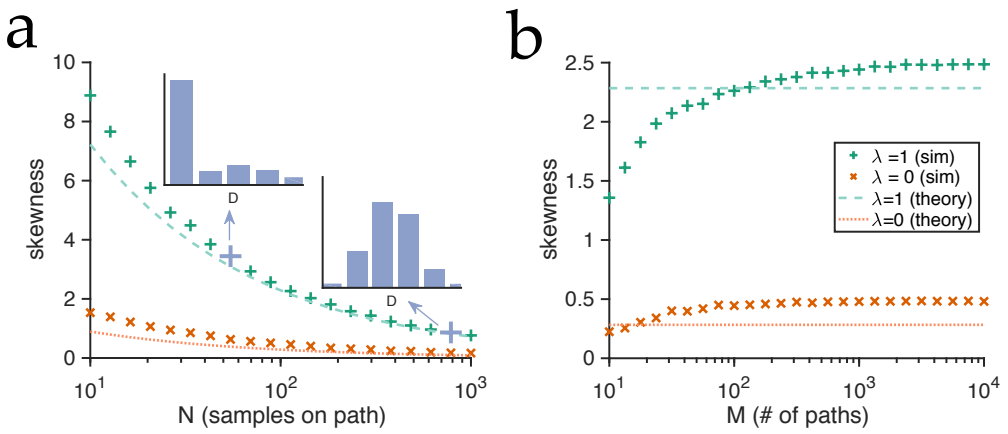

Figure 4.7. Analytically predicted and simulation values skewness of the distribution of empirical diffusion coefficients. Classical diffusion ($\lambda = 0$) and jump diffusion ($\lambda = 1$) cases are shown. **a:** Skewness decays asymptotically to zero as a function of the number of points on each path (N). **b**: Simulated skewness as a function of the number of trajectories (M) shows asymptotic convergence to analytic prediction (up to estimator bias) for large M. Analytic curves: dashed lines. Simulated results: crosses. Parameters (unless noted): $D = 1, M = 1000, N = 100, \Delta t = 10^{-3}, \delta = 0.8$.

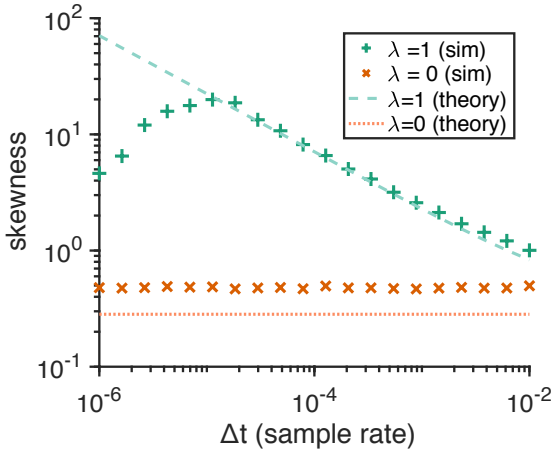

Figure 4.8. Simulated skewness as a function of Δt. As Δt becomes smaller than $1/\lambda$ the skewness should increase from analytical predictions. The simulated skewness does indeed grow as expected within a wide range of Δt, with a technical exception discussed in the text. Parameters (unless noted): $D = 1, M = 1000, N = 100, \delta = 0.8$.

diffusion while longer lag time motility remains to be fully understood. We also show that a tug-of-war process in the context of cytoskeletal transport can lead to linear MSD curves for longer lag times, however the apparent diffusion coefficients extracted from such MSD curves are likely to possess a highly skewed distribution. We note that inherently non-Gaussian distribution of apparent diffusion coefficients has been observed in many systems and has been recently modeled using the diffusing diffusivities approach [5]. This type of model does not easily map onto the case of enzymatically driven motion and is unlikely to be generally applicable for all in vitro and in vivo situations. However, when applicable, this type of a phenomenon is likely to further contribute to the skewness of the distribution of diffusion coefficients.

Subdiffusion (without aging effects, such as in [27]) observed in the context of cytoskeletal transport has often been conceptualized as a process of cargos getting trapped in small spatial compartments and occasional jumps between such compartments [31]. Our work suggests that stationary segments of cytoskeletal cargo motion may not always be due to compartment trapping but dynamic tug-of-war trapping instead and we establish two approaches for testing for this possibility. In addition, models of molecular motor transport often assume motor crosslinks to be purely elastic springs [2, 20]. This assumption is convenient, computationally efficient, and allows for reasonably faithful modeling of motor-driven transport. However, our observation of subdiffusive transport attributable directly to the motors (rather than the cytosolic influences) suggests that a more detailed model may be warranted.

On a practical level, we show that when dealing with cytoskeletal motility experiments which produce linear MSD curves, it is a good idea to examine the distribution of effective diffusion coefficients because deviations from Gaussian (or high-degree-of-freedom chi-squared) behaviour can be a signature of a more complex process. We further show that varying temperature is an excellent and easily experimentally accessible technique for probing active contributions to single particle motion in the cytoskeletal context.

4.5 References

[1] Y. Aït-Sahalia, *Disentangling diffusion from jumps*, J. Financ. Econ., 74 (2004), pp. 487–528.

[2] F. Berger, C. Keller, S. Klumpp, and R. Lipowsky, *Distinct transport regimes for two elastically coupled molecular motors*, Phys. Rev. Lett., 108 (2012), p. 208101.

[3] C. Bustamante, Y. R. Chemla, N. R. Forde, and D. Izhaky, *Mechanical processes in biochemistry*, Annu. Rev. Biochem., 73 (2004), pp. 705–748.

[4] A. E. Butterfield, R. J. Stewart, C. F. Schmidt, and M. Skliar, *Bidirectional power stroke by Ncd kinesin*, Biophys. J., 99 (2010), pp. 3905–3915.

[5] A. V. Chechkin, F. Seno, R. Metzler, and I. M. Sokolov, *Brownian yet non-Gaussian diffusion: From superstatistics to subordination of diffusing diffusivities*, Phys. Rev. X, 7 (2017), pp. 1–20.

[6] J. R. Cooper and L. Wordeman, *The diffusive interaction of microtubule binding proteins*, Curr. Opin. Cell Biol., 21 (2009), pp. 68–73.

[7] S. A. Endow and H. Higuchi, *A mutant of the motor protein kinesin that moves in both directions on microtubules.*, Nature, 406 (2000), pp. 913–6.

[8] A. L. Fink, S. J. Cartwright, and P. Douzou, *Cryoenzymology*, Crit. Rev. Biochem., 11 (1981), pp. 145–207.

[9] K. A. Foster, A. T. Mackey, and S. P. Gilbert, *A mechanistic model for Ncd directionality*, J. Biol. Chem., 276 (2001), pp. 19259–19266.

[10] K. Furuta and Y. Y. Toyoshima, *Minus-end-directed motor Ncd exhibits processive movement that is enhanced by microtubule bundling in vitro*, Curr. Biol., 18 (2008), pp. 152–157.

[11] I. Goychuk, V. O. Kharchenko, and R. Metzler, *Molecular motors pulling cargos in the viscoelastic cytosol: How power strokes beat subdiffusion*, Phys. Chem. Chem. Phys., 16 (2014), pp. 16524–16535.

[12] A. G. Hendricks, E. L. F. Holzbaur, and Y. E. Goldman, *Force measurements on cargoes in living cells reveal collective dynamics of microtubule motors*, Proc. Natl. Acad. Sci., 109 (2012), pp. 18447–18452.

[13] A. Herms, M. Bosch, B. J. Reddy, N. L. Schieber, A. Fajardo, C. Rupérez, A. Fernández-Vidal, C. Ferguson, C. Rentero, F. Tebar, et al., *Ampk activation promotes lipid droplet dispersion on detyrosinated microtubules to increase mitochondrial fatty acid oxidation*, Nat. Comm., 6 (2015), p. 7176.

[14] M. H. Hinrichs, A. Jalal, B. Brenner, E. Mandelkow, S. Kumar, and T. Scholz, *Tau protein diffuses along the microtubule lattice*, J. Biol. Chem., 287 (2012), pp. 38559–38568.

[15] W. Hong, A. Takshak, O. Osunbayo, A. Kunwar, and M. Vershinin, *The effect of temperature on microtubule-based transport by cytoplasmic dynein and kinesin-1 motors*, Biophys. J., 111 (2016), pp. 1287–1294.

[16] F. Jülicher and J. Prost, *Cooperative molecular motors*, Phys. Rev. Lett., 75 (1995), pp. 2618–2621.

[17] K. Kawaguchi, S. Ishiwata, and T. Yamashita, *Temperature dependence of the flexural rigidity of single microtubules*, Biochem. Biophys. Res. Commun., 366 (2008), pp. 637 – 642.

[18] E. Kepten, A. Weron, G. Sikora, K. Burnecki, and Y. Garini, *Guidelines for the fitting of anomalous diffusion mean square displacement graphs from single particle tracking experiments*, PLoS ONE, 10 (2015), pp. 1–10.

[19] I. M. Kulić, A. E. X. Brown, H. Kim, C. Kural, B. Blehm, P. R. Selvin, P. C. Nelson, and V. I. Gelfand, *The role of microtubule movement in bidirectional organelle transport*, Proc. Natl. Acad. Sci., 105 (2008), pp. 10011–10016.

[20] A. Kunwar, M. Vershinin, J. Xu, and S. P. Gross, *Stepping, strain gating, and an unexpected force-velocity curve for multiple-motor-based transport*, Curr. Biol., 18 (2008), pp. 1173–1183.

[21] C. Lin, M. Schuster, S. C. Guimaraes, P. Ashwin, M. Schrader, J. Metz, C. Hacker, S. J. Gurr, and G. Steinberg, *Active diffusion and microtubule-based transport oppose myosin forces to position organelles in cells*, Nat. Comm., 7 (2016), p. 11814.

[22] M. Lysy, N. S. Pillai, D. B. Hill, M. G. Forest, J. W. R. Mellnik, P. A. Vasquez, and S. A. McKinley, *Model comparison and assessment for single particle tracking in biological fluids*, J. Amer. Stat. Assoc., 1459 (2016), pp. 1413–1426.

[23] R. Metzler, J.-H. Jeon, A. G. Cherstvy, and E. Barkai, *Anomalous diffusion models and their properties: Non-stationarity, non-ergodicity, and ageing at the centenary of single particle tracking*, Phys. Chem. Chem. Phys., 16 (2014), pp. 24128–24164.

[24] H. Qian, M. Sheetz, and E. Elson, *Single particle tracking. Analysis of diffusion and flow in two-dimensional systems*, Biophys. J., 60 (1991), pp. 910–921.

[25] A. Robson, K. Burrage, and M. C. Leake, *Inferring diffusion in single live cells at the single-molecule level*, Philos. Trans. Roy. Soc. Ser. B, 368 (2012), pp. 20120029–20120029.

[26] M. J. Saxton, *Single-particle tracking: The distribution of diffusion coefficients*, Biophys. J., 72 (1997), pp. 1744–53.

[27] M. Scholz, S. Burov, K. L. Weirich, B. J. Scholz, S. M. Tabei, M. L. Gardel, and A. R. Dinner, *Cycling state that can lead to glassy dynamics in intracellular transport*, Phys. Rev. X, 6 (2016), pp. 1–9.

[28] S. Shinkai and Y. Togashi, *Energetics of single active diffusion trajectories*, EPL (Europhysics Letters), 105 (2014), p. 30002.

[29] J. Snider, F. Lin, N. Zahedi, V. Rodionov, C. C. Yu, and S. P. Gross, *Intracellular actin-based transport: How far you go depends on how often you switch*, Proc. Natl. Acad. Sci., 101 (2004), pp. 13204–13209.

[30] V. Soppina, A. K. Rai, A. J. Ramaiya, P. Barak, and R. Mallik, *Tug-of-war between dissimilar teams of microtubule motors regulates transport and fission of endosomes*, Proc. Natl. Acad. Sci., 106 (2009), pp. 19381–6.

[31] S. M. A. Tabei, S. Burov, H. Y. Kim, A. Kuznetsov, T. Huynh, J. Jureller, L. H. Philipson, A. R. Dinner, and N. F. Scherer, *Intracellular transport of insulin granules is a subordinated random walk*, Proc. Natl. Acad. Sci., 110 (2013), pp. 4911–4916.

[32] S. Uemura, K. Kawaguchi, J. Yajima, M. Edamatsu, Y. Y. Toyoshima, and S. Ishiwata, *Kinesin-microtubule binding depends on both nucleotide state and loading direction.*, Proc. Natl. Acad. Sci., 99 (2002), pp. 5977–5981.

[33] R. D. Vale, *The molecular motor toolbox for intracellular transport*, Cell, 112 (2003), pp. 467–480.

[34] H. Vandebroek and C. Vanderzande, *The effect of active fluctuations on the dynamics of particles, motors and dna-hairpins*, Soft Matter, 13 (2017), pp. 2181–2191.

[35] B. Wang, S. M. Anthony, S. C. Bae, and S. Granick, *Anomalous yet Brownian*, Proc. Natl. Acad. Sci., 106 (2009), pp. 15160–4.

[36] T. G. Wendt, N. Volkmann, G. Skiniotis, K. N. Goldie, J. Müller, E. Mandelkow, and A. Hoenger, *Microscopic evidence for a minus-end-directed power stroke in the kinesin motor Ncd*, EMBO J., 21 (2002), pp. 5969–5978.

[37] S. Yamada, D. Wirtz, and S. C. Kuo, *Mechanics of living cells measured by laser tracking microrheology*, Biophys. J., 78 (2000), pp. 1736–1747.

CHAPTER 5

COOPERATIVE TRANSPORT BY NONPROCESSIVE MOTORS

The work in this chapter was done in collaboration with Sean Lawley.[1] A version of these contents are currently submitted as a manuscript under consideration.

5.1 Introduction

In both experimental and modeling studies, *processive* motors have received considerable attention. Processive motors are characterized by taking hundreds of steps along a microtubule before unbinding. In contrast, *nonprocessive* motors (such as most members of the kinesin-14 family) take very few (1 to 5) steps before unbinding from a microtubule [4, 8]. Nonprocessive motors are crucial to a number of cellular processes, including directing cytoskeletal filaments [37], driving microtubule-microtubule sliding during mitosis [11], and retrograde transport along microtubules in plants [42]. Here, we focus on motor behavior during transport.

Some curious properties of nonprocessive motor transport were found in [13], seen in **Figure 5.1**. *One* nonprocessive (Ncd) motor has extremely limited transport ability, measured by both velocity and run length (distance traveled before detaching from a microtubule). However, *two* nonprocessive motors somehow act in unison to produce significant directed motion, a phenomenon termed "clustering." This observation is supported by the subsequent studies [23, 33], where similar experiments were performed creating a mutant of attached nonprocessive kinesin-14 motors, and processivity emerges. Moreover, the authors of [13] note that adding more Ncd motors beyond two further increases transport ability. In contrast, one processive motor (kinesin-1) is sufficient to produce transport, and additional motors do not significantly increase transport ability [13, 39]. Other interesting

[1]Department of Mathematics, University of Utah.

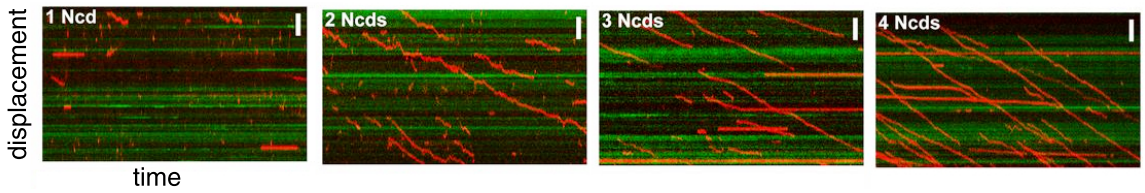

Figure 5.1. Adapted from [13], panels show kymographs of motor-associated beads for varying number of nonprocessive Ncd motors. A single motor is seemingly unable to produce robust transport, whereas teams of motors produce long run lengths.

facets of transport by nonprocessive motors include the emergence of processive transport in the presence of higher microtubule concentration [14] or opposing motors [19].

In this work, we formulate and analyze a mathematical model to investigate the natural question: How do nonprocessive motors cooperate to transport cargo? Our model predicts that nonprocessive motor stepping, binding, and unbinding rates must depend on the number of bound motors, and that this dependence is a key mechanism driving the collective transport of nonprocessive motors. We note that such dependence has been observed in experiments [10, 17] and in simulations of detailed computational models [26, 9, 31, 14], all stemming from geometric effects of cargo/motor configuration.

Nonprocessive motors are notoriously difficult to study experimentally, because they take only a few steps before detaching. For this same reason, it is not clear how to best model nonprocessive motors, or known if existing modeling frameworks, such as mean-field methods [24, 6] or averaging the stepping dynamics into an effective velocity [32], are appropriate. Hence, our model explicitly includes the discrete binding, unbinding, and stepping dynamics of each motor, as well as the continuous tethered motion of the cargo.

Mathematically, our model takes the form of a randomly switching stochastic differential equation (SDE), and thus merges continuous dynamics with discrete events. The continuous SDE dynamics track the cargo position, while the discrete events correspond to motor binding, unbinding, and stepping. Our model is thus a *stochastic hybrid system* [3], which are often two-component processes, $(J(t), X(t))_{t\geq 0} \in \mathcal{I} \times \mathbb{R}^d$, where J is a Markov jump process on a finite set $\mathcal{I}$, and X evolves continuously by

$$\mathrm{d}X(t) = F_{J(t)}(X(t))\,\mathrm{d}t + \sigma\,\mathrm{d}W(t), \tag{5.1}$$

where $\{F_j(x)\}_{j\in\mathcal{I}}$ is a given finite family of vector fields, $\sigma \geq 0$, and W is a Brownian

motion. That is, X follows an SDE whose righthand side switches according to the process J.

However, our model differs from most previous hybrid systems in some key ways. First, the set of possible continuous dynamics (e.g., possible righthand sides of (5.1)) for our model is infinite. Second, the new righthand side of (5.1) that is chosen when J jumps depends on the value of X at that jump time, although the rates dictating J are taken to be independent of X. We employ several techniques to analyze our model and make predictions regarding nonprocessive motor transport. First, we cast our model in a renewal theory framework, and generalize the classical renewal reward theorem [41] to apply to our setting, distinct from previous motor applications [27, 20, 21, 22, 38]. Next, we decompose the stochasticity in the system by averaging over the diffusion while conditioning on a realization of the jump process. This effectively turns the randomly switching SDE into a randomly switching ordinary differential equation (ODE), and thus a piecewise deterministic Markov process [5]. Finally, we observe that for biologically reasonable parameter values, the relaxation rate of the continuous cargo dynamics is much faster than the jump rates for the discrete motor behavior. We then exploit this timescale separation to find explicit formulas for key motor transport statistics.

The rest of the paper is organized as follows. We formulate the mathematical model in section 5.2. In section 5.3, we generalize the renewal reward theorem to apply to our model. In section 5.4, we derive explicit formulas to evaluate motor transport. In section 5.5, we use the model to make biological predictions. We conclude with a brief discussion and an Appendix that collects several proofs.

5.2 Mathematical model

We model the motion of a single cargo driven by $M \geq 1$ motors along a single microtubule. These motors are permanently attached to the cargo, but they can bind to and unbind from the microtubule. At any time $t \geq 0$, the state of our model is specified by

$$\big(X(t), \mathbf{Z}(t), \mathbf{J}(t)\big) \in \mathbb{R} \times \mathbb{R}^M \times \{u, b\}^M,$$

where $X(t) \in \mathbb{R}$ is the location of the center of the cargo, $\mathbf{Z}(t) = (Z_i(t))_{i=1}^M \in \mathbb{R}^M$ gives the locations of the centers of M motors, and $\mathbf{J}(t) = (J_i(t))_{i=1}^M$ specifies if each

motor is unbound or bound. Spatial locations are measured along the principal axis of the microtubule, which we identify with the real line.

The cargo position evolves continuously in time, while the positions and states of motors change by discrete events, which correspond to binding to the microtubule, stepping along the microtubule, or unbinding from the microtubule. Specifically, in between these discrete motor events, $X(t)$ follows an Ornstein-Uhlenbeck (OU) process centered at the average bound motor position,

$$\mathrm{d}X(t) = \frac{k}{\gamma} \sum_{i \in I(t)} \big(Z_i(t) - X(t)\big)\mathrm{d}t + \sqrt{2k_B T/\gamma}\,\mathrm{d}W(t). \tag{5.2}$$

Here, $I(t) = \{i : J_i(t) = b\} \subseteq \{1, \ldots, M\}$ gives the indices of motors that are bound at time $t \geq 0$, and $\{W(t)\}_{t \geq 0}$ is a standard Brownian motion. The SDE (5.2) stems from assuming a viscous (low Reynolds number) regime with drag coefficient $\gamma > 0$, and that each bound motor exerts a Hookean force on the cargo with stiffness $k > 0$. The Stokes-Einstein relation specifies the diffusion coefficient $k_B T/\gamma$, where k_B is Boltzmann's constant and T is the absolute temperature.

The discrete behavior of motors is as follows. Let $m(t) \in \{0, 1, \ldots, M\}$ denote the number of bound motors at time $t \geq 0$,

$$m(t) = \sum_{i=1}^{M} 1_{\{J_i(t) \neq u\}} \in \{0, 1, \ldots, M\},$$

where $1_{\{A\}}$ denotes the indicator function on an event A. Each unbound motor binds to the microtubule at rate $k_{\text{on}}(m(t)) > 0$. Since unbound motors are tethered to the cargo, if an unbound motor binds at time $t \geq 0$, then we assume that it binds to the track at $X(t)$ (motors can bind anywhere along the microtubule, not only binding sites). We could allow it to bind to a random position, but if the mean binding position is $X(t)$, then our results are unchanged. The position of each bound motor is fixed until it either steps or unbinds. Each bound motor unbinds at rate $k_{\text{off}}(m(t)) > 0$ and steps at rate $k_{\text{step}}(m(t)) > 0$. When a motor steps, we add $\delta > 0$ to its position, which is then fixed until it steps again or unbinds. This discrete motor behavior is summarized in **Figure 5.2**. We emphasize that the motor binding, unbinding, and stepping rates are allowed to depend on the number of bound motors, $m(t)$, but are otherwise independent of $X(t)$.

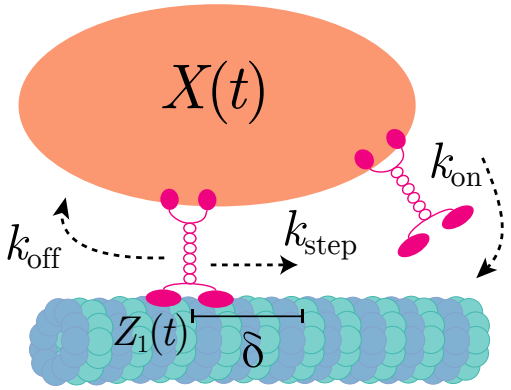

Figure 5.2. Schematic describing the binding, unbinding, and stepping of motors. The positions of cargo and bound motors are $X(t)$ and $Z_i(t)$, respectively, both measured with respect to the principal axis of the microtubule. The state of the motor can switch between bound or unbound, and while bound, the motor can step, incrementing $Z_i(t)$ by displacement δ.

5.2.1 Nondimensionalization and assumptions

We now give a dimensionless and more precise formulation of the model described above. First, we nondimensionalize the model by rescaling time by the rate $k_{\text{off}}(1)$ and space by the inverse length δ^{-1}. Next, we note that unbound motors do not affect the cargo position. Hence, for convenience we can take $Z_i(t) = X(t)$ if the i-th motor is unbound, meaning that we can include unbound motors in the sum in (5.2) with zero contribution, and make the sum over *all* motors. This yields the simplified dimensionless form

$$\mathrm{d}X(t) = \varepsilon^{-1} \sum_{i=1}^{M} \big(Z_i(t) - X(t)\big)\mathrm{d}t + \sigma \mathrm{d}W(t), \tag{5.3}$$

where

$$\varepsilon := k_{\text{off}}(1)\gamma/k, \qquad \sigma := \sqrt{2k_B T/(\delta^2 k_{\text{off}}(1)\gamma)},$$

and motors bind, unbind, and step at dimensionless rates

$$\lambda_{\text{on}}(m) := \frac{k_{\text{on}}(m)}{k_{\text{off}}(1)}, \quad \lambda_{\text{off}}(m) := \frac{k_{\text{off}}(m)}{k_{\text{off}}(1)}, \quad \lambda_{\text{step}}(m) := \frac{k_{\text{step}}(m)}{k_{\text{off}}(1)}. \tag{5.4}$$

We find it convenient for our analysis to track the number of steps taken by each motor before unbinding, so let us expand the state space of $\mathbf{J}(t)$ so that its components $(J_i(t))_{i=1}^{M}$ each take values in $\{u, 0, 1, 2, \dots\}$ with transition rates

$$u \overset{\lambda_{\text{on}}(m(t))}{\to} 0, \qquad j \overset{\lambda_{\text{step}}(m(t))}{\to} j+1, \qquad j \overset{\lambda_{\text{off}}(m(t))}{\to} u, \qquad j \neq u. \tag{5.5}$$

The components of $\mathbf{J}(t)$ are conditionally independent given $m(t)$. At time $t \geq 0$, the i-th motor is unbound if $J_i(t) = u$, bound if $J_i(t) \geq 0$, and steps when $J_i(t)$ transitions from j to $j+1$ for $j \geq 0$.

Under these assumptions, $m(t)$ is itself a Markov process on $\{0, 1, \ldots, M\}$ with transition rates

$$0 \underset{1}{\overset{M\lambda_{\text{on}}(0)}{\rightleftharpoons}} 1 \underset{2\lambda_{\text{off}}(2)}{\overset{(M-1)\lambda_{\text{on}}(1)}{\rightleftharpoons}} 2 \rightleftharpoons \cdots \rightleftharpoons M-2 \underset{(M-1)\lambda_{\text{off}}(M-1)}{\overset{2\lambda_{\text{on}}(M-2)}{\rightleftharpoons}} M-1 \underset{M\lambda_{\text{off}}(M)}{\overset{\lambda_{\text{on}}(M-1)}{\rightleftharpoons}} M. \tag{5.6}$$

For simplicity, we assume that the motors are initially unbound and that the cargo and motors start at the origin,

$$J_i(0) = u, \quad X(0) = Z_i(0) = 0, \quad i \in \{1, \ldots, M\}.$$

The position of the i-th motor is then

$$Z_i(t) = \big(X(\tau_i(t)) + J_i(t)\big)1_{\{J_i(t) \neq u\}} + X(t)1_{\{J_i(t)=u\}}, \quad i \in \{1, \ldots, M\}, \tag{5.7}$$

where $\tau_i(t)$ is the most recent binding time of the i-th motor,

$$\tau_i(t) = \sup\{s < t : J_i(s) = u\}, \quad i \in \{1, \ldots, M\}.$$

We assume the Brownian motion $W = \{W(t)\}_{t \geq 0}$ and the jump process $\mathbf{J} = \{\mathbf{J}(t)\}_{t \geq 0}$ are independent.

5.3 Cargo position as a renewal reward process

In order to analyze our model, we first show that $X(t)$ is a renewal reward process with partial rewards [41] and extend the classical renewal reward theorem to our case of partial rewards. This framework has an intuitive interpretation: The net displacement of cargo is determined by the displacement accrued at each epoch of being bound or unbound. However, there is a technical challenge. In the most classical setting, the reward-renewal theorem accrues rewards at the end of each epoch and boundedness of expectation of the rewards is sufficient to apply the reward-renewal theorem. In the case of partial rewards (which we have in our model), where rewards are accrued during an epoch, stronger conditions are required, which we prove are satisfied.

First, define the sequence of times in which the cargo completely detaches from the microtubule (off) and subsequently reattaches to the microtubule (on),

$$0 = \tau_{\text{on}}^0 = \tau_{\text{off}}^0 < \tau_{\text{on}}^1 < \tau_{\text{off}}^1 < \tau_{\text{on}}^2 < \tau_{\text{off}}^2 < \dots$$

by

$$\begin{aligned} \tau_{\text{off}}^k &:= \inf\{t > \tau_{\text{on}}^k : m(t) = 0\}, \quad k \geq 1, \\ \tau_{\text{on}}^k &:= \inf\{t > \tau_{\text{off}}^{k-1} : m(t) \geq 1\}, \quad k \geq 1. \end{aligned} \tag{5.8}$$

Next, define the sequence of cargo displacements when the cargo is attached to the microtubule (on) and detached from the microtubule (off),

$$R_{\text{on}}^k := X(\tau_{\text{off}}^k) - X(\tau_{\text{on}}^k), \quad R_{\text{off}}^k := X(\tau_{\text{on}}^k) - X(\tau_{\text{off}}^{k-1}), \quad k \geq 1, \tag{5.9}$$

and the corresponding times spent attached or detached,

$$T_{\text{on}}^k := \tau_{\text{off}}^k - \tau_{\text{on}}^k, \quad T_{\text{off}}^k := \tau_{\text{on}}^k - \tau_{\text{off}}^{k-1}, \quad k \geq 1. \tag{5.10}$$

It follows directly from the strong Markov property that $\{(T_{\text{off}}^k + T_{\text{on}}^k, R_{\text{off}}^k + R_{\text{on}}^k)\}_{k\geq 1}$ is an independent and identically distributed (iid) sequence of random variables.

In the language of renewal theory, $\{T_{\text{off}}^k + T_{\text{on}}^k\}_{k\geq 1}$ are the interarrival times and $\{R_{\text{off}}^k + R_{\text{on}}^k\}_{k\geq 1}$ are the corresponding rewards. Let $N(t)$ be the renewal process that counts the number of arrivals before time $t \geq 0$,

$$N(t) := \sup\{k \geq 0 : \tau_{\text{off}}^k \leq t\}. \tag{5.11}$$

Define the reward function, $R(t)$, and the partial reward function, $Y(t)$, by

$$R(t) := \sum_{k=1}^{N(t)} (R_{\text{on}}^k + R_{\text{off}}^k), \qquad Y(t) := X(t) - X(\tau_{\text{off}}^{N(t)}), \tag{5.12}$$

and observe that

$$X(t) = R(t) + Y(t).$$

In words, $R(t)$ describes rewards accrued during past epochs, and $Y(t)$ is the partial reward accrued during the current epoch. We show below that $\mathbb{E}[|R_{\text{on}} + R_{\text{off}}|] < \infty$ and $\mathbb{E}[T_{\text{on}} + T_{\text{off}}] < \infty$, and therefore the classical renewal reward theorem [41] ensures that

$$\lim_{t\to\infty} \frac{R(t)}{t} = \lim_{t\to\infty} \frac{\mathbb{E}[R(t)]}{t} = \frac{\mathbb{E}[R_{\text{on}}] + \mathbb{E}[R_{\text{off}}]}{\mathbb{E}[T_{\text{on}}] + \mathbb{E}[T_{\text{off}}]} \quad \text{almost surely.} \tag{5.13}$$

The following theorem verifies that this convergence actually holds for $X(t)$.

Theorem 5.1. The following limit holds,

$$\lim_{t\to\infty}\frac{X(t)}{t}=\lim_{t\to\infty}\frac{\mathbb{E}[X(t)]}{t}=\frac{\mathbb{E}[R_{\text{on}}]+\mathbb{E}[R_{\text{off}}]}{\mathbb{E}[T_{\text{on}}]+\mathbb{E}[T_{\text{off}}]}\quad\text{almost surely.}\tag{5.14}$$

To prove this theorem, we need several lemmas. We collect the proofs of these lemmas in Appendix B.1. The first lemma bounds the probability that the partial reward function $Y(t)$ in (5.12) is large when the cargo is detached from the microtubule.

Lemma 5.2. Define the sequence of iid random variables $\{Y_{\text{off}}^k\}_{k\geq 1}$ by

$$Y_{\text{off}}^k:=\sup_{t\in[\tau_{\text{off}}^{k-1},\tau_{\text{on}}^k]}\left|X(t)-X(\tau_{\text{off}}^k)\right|,\quad k\geq 1.$$

Then for any $C>0$ and $k\geq 1$, we have that

$$\mathbb{P}(Y_{\text{off}}^k\geq C)\leq\sqrt{\pi/x}(2x+1)e^{-x},\quad\text{where } x=\tfrac{C}{\sigma}\sqrt{2M\lambda_{\text{on}}(0)}>0.\tag{5.15}$$

Similarly, the next lemma bounds the probability that the partial reward function is large when the cargo is attached to the microtubule.

Lemma 5.3. Define the sequence of iid random variables $\{Y_{\text{on}}^k\}_{k\geq 1}$ by

$$Y_{\text{on}}^k:=\sup_{t\in[\tau_{\text{on}}^k,\tau_{\text{off}}^k]}|X(t)-X(\tau_{\text{on}}^k)|,\quad k\geq 1.$$

If $\Lambda:=\max_{m\in\{1,\dots,M\}}\lambda_{\text{step}}(m)$, then there exists $\lambda>0$ so that for $C>0$, $k\geq 1$,

$$\begin{aligned}\mathbb{P}(Y_{\text{on}}^k\geq C)\leq{}&\left(\frac{C}{2}\right)^{-C/2}e^{C/2}\frac{\lambda}{M\Lambda+\lambda}\left(\frac{M\Lambda}{M\Lambda+\lambda}\right)^{C/2}\Gamma(C/2+1)\\&+\exp(-\lambda C/(2M\Lambda))+\sqrt{\pi/x}(2x+1)e^{-x},\quad\text{with } x=\tfrac{C}{\sigma}\sqrt{\lambda/2}>0,\end{aligned}$$

where $\Gamma(c)$ is the Gamma function.

The next lemma uses Lemmas 5.2 and 5.3 to prove that the partial reward function gets large only finitely many times.

Lemma 5.4. Define the sequence of iid random variables $\{Y_k\}_{k\geq 1}$ by

$$Y_k:=\sup_{t\in[\tau_{\text{off}}^{k-1},\tau_{\text{off}}^k]}\left|X(t)-X(\tau_{\text{off}}^k)\right|,\quad k\geq 1.\tag{5.16}$$

Then

$$\mathbb{P}\Big(\lim_{K\to\infty}\bigcup_{k=K}^{\infty}\{Y_k>\sqrt{k}\}\Big)=0.$$

The last lemma checks that the mean of Y_k in (5.16) is finite.

Lemma 5.5. Define $\{Y_k\}_{k\geq 1}$ as in (5.16). Then $\mathbb{E}[Y_k] < \infty$ for all $k \geq 1$.

With these lemmas in place, we are ready to prove Theorem 5.1.

Proof of Theorem 5.1. It follows immediately from Lemma 5.5 that $\mathbb{E}[|R^k_{\text{on}} + R^k_{\text{off}}|] < \infty$. Furthermore, T^k_{off} is exponentially distributed with rate $M\lambda_{\text{on}}(0)$, and the proof of Lemma 5.3 shows that $\mathbb{E}[T^k_{\text{on}}] < \mathbb{E}[S]$ for an exponentially distributed random variable S with some rate $\lambda > 0$. Hence, $\mathbb{E}[T^k_{\text{on}} + T^k_{\text{off}}] < \infty$, and thus (5.13) holds by a direct application of the classical renewal reward theorem [41].

Therefore, it remains to check that

$$\lim_{t\to\infty} \frac{\mathbb{E}\left[X(t) - X(\tau^{N(t)}_{\text{off}})\right]}{t} = 0 = \lim_{t\to\infty} \frac{X(t) - X(\tau^{N(t)}_{\text{off}})}{t}, \quad \text{almost surely.} \tag{5.17}$$

The first equality in (5.17) follows immediately from Lemma 5.5.

To verify the second equality in (5.17), we note that Lemma 5.4 ensures that

$$\limsup_{k\to\infty} \frac{Y_k}{\sqrt{k}} \leq 1, \quad \text{almost surely.}$$

Therefore,

$$\lim_{t\to\infty} \frac{|X(t) - X(\tau^{N(t)}_{\text{off}})|}{t} \leq \lim_{t\to\infty} \frac{|Y_{N(t)}|}{t} \leq \lim_{t\to\infty} \frac{\sqrt{N(t)}}{t} = 0, \quad \text{almost surely,}$$

since

$$\lim_{t\to\infty} \frac{N(t)}{t} = \frac{1}{\mathbb{E}[T_{\text{on}} + T_{\text{off}}]}, \quad \text{almost surely,}$$

by the strong law of large numbers for renewal processes [41]. □

Consequently, the position of the cargo does indeed satisfy a classical reward-renewal structure with two different types of epochs: bound and unbound, each of which accrue some net displacement.

5.4 Mathematical analysis of transport ability

With the framework of renewal theory constructed in section 5.3, we are ready to analyze the transport ability of the model introduced in section 5.2. To assess the transport ability of the motor cargo ensemble, we analyze the expected *run length*, expected *run time*,

and asymptotic *velocity*. We define the run length to be the distance traveled by the cargo between the first time a motor attaches to the cargo until the next time that all motors are detached from the microtubule, which was defined precisely in (5.9) and denoted by R_{on}. The run time is the corresponding time spent attached to a microtubule, which was defined precisely in (5.10) and denoted by T_{on}. The asymptotic velocity is

$$V := \lim_{t\to\infty} \frac{X(t)}{t}. \tag{5.18}$$

The velocity V includes both the time the cargo is being transported along the microtubule and diffusing while unattached.

Applying Theorem 5.1, we have that

$$V = \frac{\mathbb{E}[R_{\text{on}}] + \mathbb{E}[R_{\text{off}}]}{\mathbb{E}[T_{\text{on}}] + \mathbb{E}[T_{\text{off}}]} \quad \text{almost surely.} \tag{5.19}$$

Now,

$$\mathbb{E}[R_{\text{off}}] = 0, \tag{5.20}$$

since the cargo is freely diffusing when no motors are bound, and since motor binding and unbinding is independent of Brownian motion $\{W(t)\}_{t\geq 0}$. Furthermore, when all of the M motors are unbound, each motor binds at rate $\lambda_{\text{on}}(0)$. Hence,

$$\mathbb{E}[T_{\text{off}}] = (M\lambda_{\text{on}}(0))^{-1}. \tag{5.21}$$

It therefore remains to calculate two of the three quantities, V, $\mathbb{E}[R_{\text{on}}]$, and $\mathbb{E}[T_{\text{on}}]$, since the third is given by (5.19). We calculate $\mathbb{E}[T_{\text{on}}]$ first since it is the simplest, as it is a mean first passage time of a continuous-time Markov chain

5.4.1 Expected run time

As we noted in section 5.2.1, the number of motors bound $m(t)$ is itself the Markov process (5.6). To compute the expected run time, we compute the mean time for $m(t)$ to reach state $m = 0$ starting from $m(0) = 1$.

Let $\widetilde{Q} \in \mathbb{R}^{(M+1)\times(M+1)}$ be the generator of the Markov chain $m(t)$ in (5.6). That is, the (i,j)-entry of $\widetilde{Q}$ gives the rate that $m(t)$ jumps from state i to state $j \neq i$, and the diagonal entries are chosen so that $\widetilde{Q}$ has zero row sums. Let $Q \in \mathbb{R}^{M\times M}$ be the matrix obtained from deleting the first row and column of $\widetilde{Q}$. The matrix Q is tridiagonal,

with the m-th row containing subdiagonal, diagonal, and superdiagonal entries $m\lambda_{\text{off}}(m)$, $-(m\lambda_{\text{off}}(m) + (M-m)\lambda_{\text{on}}(m))$, $(M-m)\lambda_{\text{on}}(m)$, respectively. The expected run time $\mathbb{E}[T_{\text{on}}]$ is (by Theorem 3.3.3 in [35]),

$$\mathbb{E}[T_{\text{on}}] = \mathbf{1}^T\mathbf{t}, \qquad \text{where} \quad Q^T\mathbf{t} = -\mathbf{e}_1, \tag{5.22}$$

where $\mathbf{1} \in \mathbb{R}^M$ is the vector of all 1's and $\mathbf{e}_1 \in \mathbb{R}^M$ is the standard basis vector.

5.4.2 Decomposing stochasticity

Having calculated $\mathbb{E}[T_{\text{on}}]$ in (5.22), we can determine V by determining $\mathbb{E}[R_{\text{on}}]$ (or vice versa). Two key steps allow us to analyze V and $\mathbb{E}[R_{\text{on}}]$: (i) we average over the diffusive dynamics while conditioning on a realization of the jump dynamics, and (ii) we take advantage of a timescale separation between the relaxation rate of the cargo dynamics and the jump rate of the motor dynamics.

5.4.2.1 Conditioning on jump realizations

Observe that the stochasticity in the model can be separated into a *continuous* diffusion part and a *discrete* part controlling motor binding, unbinding, and stepping. Mathematically, the continuous diffusion part is described by the Brownian motion W in (5.3), and the discrete motor state is described by the Markov jump process $\mathbf{J}$. We first average over the diffusion by defining the conditional expectations

$$x(t) := \mathbb{E}[X(t)|\mathbf{J}], \quad t \geq 0, z_i(t) := \mathbb{E}[Z_i(t)|\mathbf{J}], \quad t \geq 0,\ i \in \{1,\dots,M\}. \tag{5.23}$$

We emphasize that (5.23) are averages over paths of W given a realization $\mathbf{J}$. Thus, $\{x(t)\}_{t\geq 0}$ and $\{\{z_i(t)\}_{t\geq 0}\}_{i=1}^M$ are functions of the realization $\mathbf{J}$. This definition is convenient, because while $X(t)$ follows the randomly switching SDE (5.3), the process $x(t)$ follows a randomly switching ODE, whose solution is known explicitly.

Proposition 5.6. *For each $t > 0$, the expected cargo position $x(t)$ conditioned on a realization of the jump process satisfies*

$$\frac{d}{dt}x(t) = \varepsilon^{-1}\sum_{i=1}^{M}\big(z_i(t) - x(t)\big), \quad \textit{almost surely}. \tag{5.24}$$

Proof. Using the explicit solution of an OU process, we have that

$$X(t) = X(\tau)e^{-\theta(t-\tau)} + \mu(1 - e^{-\theta(t-\tau)}) + \mathcal{M}, \tag{5.25}$$

where τ is the most recent jump time of $\mathbf{J}$,

$$\tau = \sup\big\{\{0\} \cup \{s < t : \mathbf{J}(s-) \neq \mathbf{J}(s+)\}\big\},$$

$\theta = m(\tau)\varepsilon^{-1}$, $\mu = \frac{1}{m(\tau)}\sum_{i\in I(\tau)} Z_i(\tau)$, and $\mathcal{M}$ satisfies $\mathbb{E}[\mathcal{M}|\mathbf{J}] = 0$. We have used the notation $f(t\pm) := \lim_{s\to t\pm} f(s)$. Hence, taking the expectation of (5.25) conditioned on $\mathbf{J}$ yields

$$\begin{aligned} x(t) &= \mathbb{E}[X(\tau)e^{-\theta(t-\tau)}|\mathbf{J}] + \mathbb{E}[\mu(1 - e^{-\theta(t-\tau)})|\mathbf{J}] \\ &= e^{-\theta(t-\tau)}\mathbb{E}[X(\tau)|\mathbf{J}] + (1 - e^{-\theta(t-\tau)})\frac{1}{m(\tau)}\sum_{i\in I(\tau)} \mathbb{E}[Z_i(\tau)|\mathbf{J}], \end{aligned}$$

since τ are $\{m(s)\}_{s\geq 0}$ measurable with respect to the σ-algebra generated by $\mathbf{J}$. □

5.4.2.2 Separation of timescales

We next make an observation of disparate timescales. After averaging over the diffusive noise W, the model effectively depends on two timescales: the relaxation time of the continuous dynamics (5.24) (characterized by the dimensionless rate ε^{-1}) and the switching times of the discrete motor dynamics (5.5) (characterized by the dimensionless rates $\lambda_{\text{on}}, \lambda_{\text{step}}, \lambda_{\text{off}}$). Even for conservative parameter estimates, the continuous timescale is much faster than the discrete switching timescale. For instance, suppose a motor exerts a Hookean force with stiffness $k = 0.5$ pN/nm [13] on a spherical cargo with radius $r = 1$ μm in cytosol with viscosity η equal to that of water. It follows that $k/(6\pi\eta r) \approx 3 \times 10^4$ s^{-1}, whereas $k_{\text{off}}(1)$ is on the order of 10^{-1} to 10^1 s^{-1} [13]. Hence,

$$\varepsilon := k_{\text{off}}(1)\gamma/k \approx 3 < 10^{-4} \ll 1. \tag{5.26}$$

Further, $\lambda_{\text{on}}, \lambda_{\text{step}}, \lambda_{\text{off}}$ are roughly order one since $k_{\text{on}}, k_{\text{step}}, k_{\text{off}}$ have similar orders of magnitude [13].

Therefore, compared to the switching timescale, $x(t)$ quickly relaxes to an equilibrium between motor switches. Furthermore, we are interested in studying $\mathbb{E}[R_{\text{on}}]$ and V, which depend on the behavior of $x(t)$ over the course of several motor switches. Hence, we

approximate $x(t)$ by a jump process $\overline{x}(t)$ obtained from assuming $x(t)$ immediately relaxes to its equilibrium after each motor switch.

More precisely, let $(\overline{x}(t), \overline{z}_1(t), \ldots, \overline{z}_M(t)) \in \mathbb{R}^{M+1}$ be a $\mathbf{J}$-measurable, right-continuous process,

$$\overline{x}(t) = \overline{x}(t+), \quad \overline{z}_i(t) = \overline{z}_i(t+), \quad t \geq 0,\ i \in \{1, \ldots, M\},$$

with $\overline{x}(0) = x(0)$ and $\overline{z}_i(0) = z_i(0)$, $i \in \{1, \ldots, M\}$, that evolves in the following way. In light of (5.7), we define the effective motor positions by how they are modified through the jump process, binding at τ_i and then incrementing from stepping, or staying unbound at the cargo position $\overline{x}(t)$,

$$\overline{z}_i(t) = \big(\overline{x}(\tau_i(t)) + J_i(t)\big)1_{\{J_i(t) \neq u\}} + \overline{x}(t)1_{\{J_i(t)=u\}}, \quad i \in \{1, \ldots, M\}. \tag{5.27}$$

Due to the assumed fast relaxation, $\overline{x}(t)$ only changes when a motor steps or unbinds, as newly bound motors exert no force. That is, if $J_i(t+) = J_i(t-)$ for all $i \in \{1, \ldots, M\}$ satisfying $J_i(t-) \geq 0$, then $\overline{x}(t-) = \overline{x}(t+)$. Otherwise, $\overline{x}(t)$ evolves according to the following two rules, which describe how the cargo position $\overline{x}(t)$ changes when a motor steps or unbinds.

1. If the i-th motor steps ($J_i(t-) = j \geq 0$ and $J_i(t+) = j+1$), then $\overline{x}(t+) = \overline{x}(t-) + 1/m(t)$.

2. If the i-th motor unbinds ($J_i(t-) = j \geq 0$ and $J_i(t+) = u$), then $\overline{x}(t+) = \overline{x}(t-) + \Delta_{i,(\overline{z}_1,\ldots,\overline{z}_{m(t-)})}$, where $(\overline{z}_1, \ldots, \overline{z}_{m(t-)})$ gives the positions of the $m(t-)$ bound motors just before time t, and

$$\Delta_{i,(\overline{z}_1,\ldots,\overline{z}_{m(t-)})} = \frac{1}{m(t-)-1} \sum_{i'=1, i' \neq i}^{m(t-)} \overline{z}_{i'}(t-) - \frac{1}{m(t-)} \sum_{i'=1}^{m(t-)} \overline{z}_{i'}(t-). \tag{5.28}$$

In words, if either of these events occurs, the cargo position $\overline{x}(t)$ relaxes to the mean position of the motors. These two rules describe how the mean motor position changes in the two scenarios. If a single motor steps, incrementing its position by 1, the mean motor position increases by $1/m(t)$. If a motor unbinds, (5.28) is the change in the mean motor position from removing that motor.

It follows from these two evolution rules for $\overline{x}(t)$ that

$$\overline{x}(t) = \sum_{m=1}^{M} \frac{1}{m} S_m(t) + \chi(t), \tag{5.29}$$

where $S_m(t)$ is the number of steps taken when m motors are bound before time t (each of which modifies the position by $1/m$), and $\chi(t)$ accounts for changes in the cargo position that result from a motor unbinding,

$$\chi(t) = \sum_{k=1}^{N_{\text{off}}(t)} \Delta_{j_k,(\overline{z}_1(s^k_{\text{off}}-),\ldots,\overline{z}_{m(s^k_{\text{off}}-)}(s^k_{\text{off}}-)}, \tag{5.30}$$

where $0 = s^0_{\text{off}} < s^1_{\text{off}} < \ldots$ is the sequence of times in which a motor unbinds,

$$s^k_{\text{off}} := \inf\left\{t > s^{k-1}_{\text{off}} : J_i(t-) \geq 0 \text{ and } J_i(t) = u \text{ for some } i \in \{1,\ldots,M\}\right\} \quad k \geq 1,$$

and $N_{\text{off}}(t) := \sup\{k \geq 0 : s^k_{\text{off}} \leq t\}$ is the number of unbindings before time $t \geq 0$, and $j_k \in \{1,\ldots,M\}$ gives the (almost surely unique) index of the motor that unbinds at time s^k_{off}. That is, j_k satisfies $J_{j_k}(s^k_{\text{off}}-) \neq J_{j_k}(s^k_{\text{off}}) = u$.

The following proposition checks that $x(t)$ converges almost surely to the jump process $\overline{x}(t)$ as $\varepsilon \to 0$. The proof is in Appendix B.2.

Proposition 5.7. *If $T \geq 0$ is an almost surely finite stopping time with respect to $\{\boldsymbol{J}(t)\}_{t\geq 0}$, then*

$$\lim_{\varepsilon\to 0} x(T) = \overline{x}(T), \quad \textit{almost surely}.$$

From this proposition, we conclude that studying the mean behavior of the cargo position $X(t)$ can ultimately be reduced to studying the jump process $\overline{x}(t)$, where the jumps correspond to motor stepping and unbinding events.

5.4.3 Run length and velocity

Since $\varepsilon \ll 1$ for biologically relevant parameters, we investigate the run length and velocity of $X(t)$ by investigating the analogous quantities for $\overline{x}(t)$,

$$\overline{R} := \overline{x}(\tau^1_{\text{off}}) - \overline{x}(\tau^1_{\text{on}}), \qquad \overline{V} := \lim_{t\to\infty} \frac{\overline{x}(t)}{t}. \tag{5.31}$$

5.4.3.1 Run length

The following proposition checks that the mean run length of the full process $X(t)$ converges to the mean run length of the jump process $\overline{x}(t)$ as $\varepsilon \to 0$.

Proposition 5.8. $\mathbb{E}[R_{on}] \to \mathbb{E}[\overline{R}]$ *as* $\varepsilon \to 0$.

Proof. By the tower property of conditional expectation (Theorem 5.1.6 in [7]), we have that

$$\mathbb{E}[R_{\text{on}}] = \mathbb{E}[\mathbb{E}[R_{\text{on}}|\mathbf{J}]] = \mathbb{E}[\mathbb{E}[X(\tau^1_{\text{off}}) - X(\tau^1_{\text{on}})|\mathbf{J}]] = \mathbb{E}[x(\tau^1_{\text{off}}) - x(\tau^1_{\text{on}})].$$

Now, Proposition 5.7 ensures that

$$x(\tau^1_{\text{off}}) - x(\tau^1_{\text{on}}) \to \overline{R}, \quad \text{almost surely as } \varepsilon \to 0. \tag{5.32}$$

Let $N \geq 0$ be the number of steps taken between time τ^1_{on} and time τ^1_{off}. Since motors take steps of distance one, we have the almost sure bound, $x(\tau^1_{\text{off}}) - x(\tau^1_{\text{on}}) \leq N$. Steps are taken at Poisson rate $m(t)\lambda_{\text{step}}(m(t)) \leq M\Lambda$, and thus $\mathbb{E}[N] \leq \Lambda M \mathbb{E}[\tau^1_{\text{off}} - \tau^1_{\text{on}}] < \infty$. Thus, (5.32) and the bounded convergence theorem complete the proof. □

5.4.3.2 Velocity

Let us now investigate $\overline{V}$ in (5.31), observing that this quantity can be approached in two ways. The first exploits the observation that nonzero mean displacements only occur from motor stepping, so the velocity can be interpreted as the product of how often a step occurs with m motors and the size of the displacement. The second approach is again a reward-renewal argument, noting that the only nonzero displacements occur during epochs of bound cargo. The connection between these two approaches provides explicit relationships between the velocity, run lengths, and run times.

Recalling the decomposition of the jump process $\overline{x}$ in (5.29), we seek to compute the expected value

$$\mathbb{E}[\overline{x}(t)] = \sum_{m=1}^{m} \frac{1}{m} \mathbb{E}[S_m(t)] + \mathbb{E}[\chi(t)].$$

Using the definition of $\chi(t)$ in (5.30), we compute its expectation by summing over all possible displacements from one of m motors unbinding $\Delta_{j,(\overline{z}_1(t-),\ldots,\overline{z}_{m(s^k_{\text{off}}-)}(t-)}$, which yields

$$\sum_{j=1}^{m} \Delta_{j,(z_1,\ldots,z_m)} = \frac{1}{m-1} \sum_{j=1}^{m} \Big(-z_j + \sum_{i=1}^{m} z_j \Big) - \sum_{i=1}^{m} z_i = 0.$$

Since each of the bound motors is equally likely to unbind, it follows that $\mathbb{E}[\chi(t)] = 0$. This can be interpreted as the observation that the arithmetic mean does not change in

expectation when removing a randomly (uniformly) chosen element. In other words, the effects of motors unbinding ahead of the cargo are completely offset in the mean by motors unbinding behind the cargo. Therefore, the only long-term influence on $\overline{x}$ is stepping events.

Given a realization $\{m(s)\}_{s\geq 0}$, the number of steps taken with m motors bound before time $t \geq 0$ is Poisson distributed with mean $m\lambda_{\text{step}}(m)\int_0^t 1_{m(s)=m}\,ds$. Hence,

$$\mathbb{E}[S_m(t)] = m\lambda_{\text{step}}(m)\mathbb{E}\Big[\int_0^t 1_{m(s)=m}\,ds\Big].$$

Now, $\{m(s)\}_{s\geq 0}$ is an ergodic Markov process, so the occupation measure converges almost surely to the stationary measure (see Theorem 3.8.1 in [35])

$$\frac{1}{t}\sum_{n=1}^{M}\int_0^t 1_{m(s)=m}\,ds \to p_m, \quad \text{almost surely as } t\to\infty,$$

where $p_m := \lim_{t\to\infty}\mathbb{P}(m(t)=m)$ is the stationary probability m motors are bound. We note that p_m is the $(m+1)$-st component of the unique probability vector, $\mathbf{p}\in\mathbb{R}^{1\times(M+1)}$ satisfying (see Theorem 3.5.2 in [35])

$$\mathbf{p}\widetilde{Q} = 0, \tag{5.33}$$

where $\widetilde{Q}\in\mathbb{R}^{(M+1)\times(M+1)}$ is the generator matrix defined in section 5.4.1. Since the occupation measure is bounded above by one, the bounded convergence theorem gives

$$\lim_{t\to\infty}\frac{\mathbb{E}[\overline{x}(t)]}{t} = \lim_{t\to\infty}\sum_{m=1}^{M}\lambda_{\text{step}}(m)\mathbb{E}\Big[\frac{1}{t}\int_0^t 1_{m(s)=m}\,ds\Big] = \sum_{m=1}^{M}\lambda_{\text{step}}(m)p_m.$$

It is easy to see that the classical renewal reward theorem applies to $\overline{x}(t)$ so that

$$\sum_{m=1}^{M}\lambda_{\text{step}}(m)p_m = \lim_{t\to\infty}\frac{\mathbb{E}[\overline{x}(t)]}{t} = \lim_{t\to\infty}\frac{\overline{x}(t)}{t} = \frac{\mathbb{E}[\overline{R}]}{\mathbb{E}[T_{\text{on}}]+\mathbb{E}[T_{\text{on}}]}, \quad \text{almost surely.}$$

Furthermore, (5.19), (5.20), (5.21), and Proposition 5.8 yield

$$\lim_{\varepsilon\to 0}V = \lim_{\varepsilon\to 0}\frac{\mathbb{E}[R_{\text{on}}]}{(M\lambda_{\text{on}}(0))^{-1}+\mathbb{E}[T_{\text{on}}]} = \frac{\mathbb{E}[\overline{R}]}{(M\lambda_{\text{on}}(0))^{-1}+\mathbb{E}[T_{\text{on}}]} = \sum_{m=1}^{M}\lambda_{\text{step}}(m)p_m.$$

In summary, we now have explicit formulas for the velocity V and expected run length $\mathbb{E}[R_{\text{on}}]$ of $X(t)$ in the small ε limit,

$$\lim_{\varepsilon\to 0}V = \overline{V} = \sum_{m=1}^{M}\lambda_{\text{step}}(m)p_m \tag{5.34}$$

$$\lim_{\varepsilon\to 0}\mathbb{E}[R_{\text{on}}] = \mathbb{E}[\overline{R}] = \Big((M\lambda_{\text{on}}(0))^{-1}+\mathbb{E}[T_{\text{on}}]\Big)\sum_{m=1}^{M}\lambda_{\text{step}}(m)p_m, \tag{5.35}$$

where p_m is given by (5.33) and $\mathbb{E}[T_{\text{on}}]$ is given by (5.22). In **Figure 5.3**, we compare these formulas for $\mathbb{E}[\overline{R}]$ and $\overline{V}$ with estimates of $\mathbb{E}[R_{\text{on}}]$ and V from simulations of the full process $(X(t), \mathbf{Z}(t), \mathbf{J}(t))$ (for details on our statistically exact simulation method, see section 5.4.5).

Furthermore, some experimental works [13, 23] measure the average run velocity, $\mathbb{E}[\overline{R}/T_{\text{on}}]$. Now, if $\sigma(m)$ denotes the σ-algebra generated by $\{m(t)\}_{t\geq 0}$, then recalling (5.8) and (5.10) and using the tower property of conditional expectation yields

$$\begin{aligned}\mathbb{E}\Big[\frac{\overline{R}}{T_{\text{on}}}\Big] = \mathbb{E}\Big[\frac{1}{T_{\text{on}}}\mathbb{E}[\overline{R}|\sigma(m)]\Big] &= \mathbb{E}\Big[\frac{1}{T_{\text{on}}^1}\sum_{m=1}^{M}\frac{1}{m}\mathbb{E}[S_m(\tau_{\text{off}}^1)|\sigma(m)]\Big] \\ &= \sum_{m=1}^{M}\frac{1}{m}m\lambda_{\text{step}}(m)\mathbb{E}\Big[\frac{1}{T_{\text{on}}^1}\int_0^{\tau_{\text{off}}^1} 1_{m(s)=m}\,ds\Big].\end{aligned}$$

Hence, it follows from (5.34) that

$$\mathcal{V} := \mathbb{E}[\overline{R}/T_{\text{on}}] = \overline{V}/p_{\text{on}}, \tag{5.36}$$

where $p_{\text{on}} = \sum_{m=1}^{M} p_m$ is the stationary probability that $m(t) \geq 1$.

5.4.4 Cases $M = 1$, $M = 2$, and $M = 3$

In this subsection, we collect explicit formulas for the run length $\mathbb{E}[\overline{R}]$ and run velocity $\mathcal{V}$ when the total number of motors is $M = 1, 2, 3$. The run time $\mathbb{E}[T_{\text{on}}]$ and net velocity V can be easily deduced from these quantities using (5.34)-(5.35) but are omitted for brevity.

For $M = 1$ total motors, the quantities are simply

$$\mathbb{E}[\overline{R}] = \lambda_{\text{step}}(1), \quad \mathcal{V} = \lambda_{\text{step}}(1). \tag{5.37}$$

For $M = 2$ total motors, we find

$$\mathbb{E}[\overline{R}] = \lambda_{\text{step}}(1) + \frac{\lambda_{\text{on}}(1)\lambda_{\text{step}}(2)}{2\lambda_{\text{off}}(2)}, \quad \mathcal{V} = \frac{2\lambda_{\text{off}}(2)\lambda_{\text{step}}(1) + \lambda_{\text{on}}(1)\lambda_{\text{step}}(2)}{2\lambda_{\text{off}}(2) + \lambda_{\text{on}}(1)}. \tag{5.38}$$

For $M = 3$ total motors, we find

$$\begin{aligned}\mathbb{E}[\overline{R}] &= \lambda_{\text{step}}(1) + \frac{\lambda_{\text{on}}(1)(3\lambda_{\text{off}}(3)\lambda_{\text{step}}(2) + \lambda_{\text{on}}(2)\lambda_{\text{step}}(3))}{3\lambda_{\text{off}}(2)\lambda_{\text{off}}(3)}, \\ \mathcal{V} &= \frac{3\lambda_{\text{off}}(3)\left[\lambda_{\text{off}}(2)\lambda_{\text{step}}(1) + \lambda_{\text{on}}(1)\lambda_{\text{step}}(2)\right] + \lambda_{\text{on}}(1)\lambda_{\text{on}}(2)\lambda_{\text{step}}(3)}{3\lambda_{\text{off}}(3)\left[\lambda_{\text{off}}(2) + \lambda_{\text{on}}(1)\right] + \lambda_{\text{on}}(1)\lambda_{\text{on}}(2)}.\end{aligned} \tag{5.39}$$

To put these quantities in dimensional units, recall the jump rates (5.4) and multiply $\mathbb{E}[\overline{R}]$ by the dimensional step distance $\delta > 0$ and multiply $\mathcal{V}$ by $\delta k_{\text{off}}(1) > 0$.

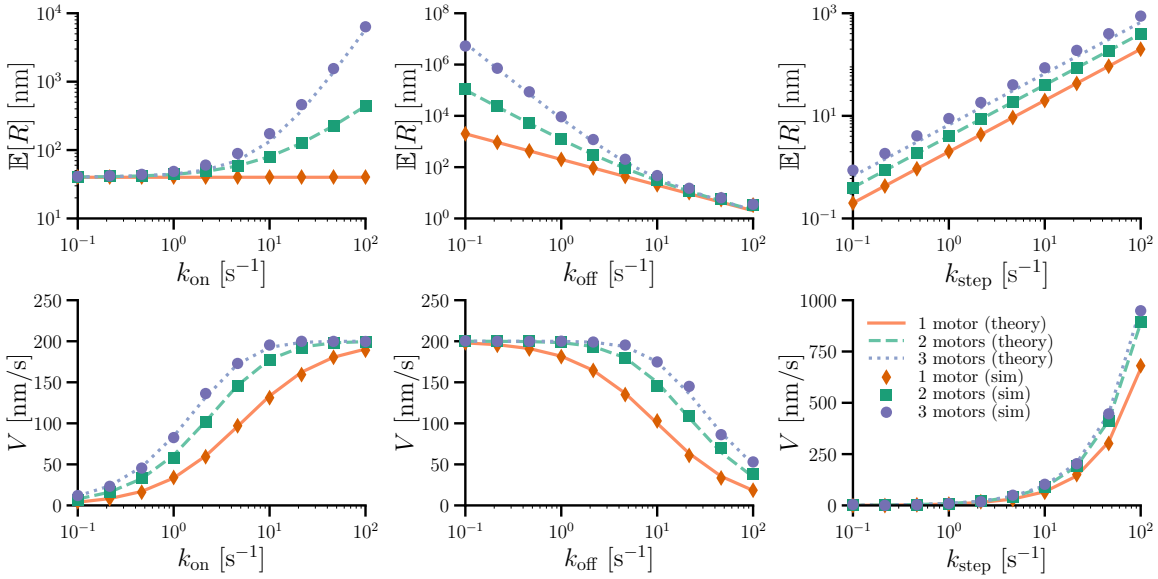

Figure 5.3. Expected run lengths $\mathbb{E}[R]$ and asymptotic velocities V as a function of the parameters $k_{\text{on}}, k_{\text{off}}, k_{\text{step}}$ for $M = 1, 2, 3$ total motors. The curves are the analytical formulas (5.34)-(5.35) for the $\varepsilon \to 0$ limit, and the dots are estimates from statistically exact realizations of the full process, $\{(X(s), \mathbf{Z}(s), \mathbf{J}(s))\}_{s=0}^{t}$, where the ending time t is such that $N(t) = 10^5$ where $N(t)$ is defined in (5.11). Unless noted otherwise, $k_{\text{on}}(m) = 10\,[\text{s}^{-1}]$, $k_{\text{step}}(m) = 20\,[\text{s}^{-1}]$, $k_{\text{off}}(m) = 5\,[\text{s}^{-1}]$ for each m. Further, k and γ are as in (5.26) and $k_B T = 4.1\,[\text{pN} \cdot \text{nm}]$.

5.4.5 Numerical simulations

To verify our predictions for the expected run lengths and velocities, we compare to statistically exact numerical simulations of the full process $(X(t), \mathbf{Z}(t), \mathbf{J}(t))$. In a given state, we use the classical Gillespie stochastic simulation algorithm to generate the time of the next transition for the Markov chain $\mathbf{J}(t)$ and to choose which transition occurs. For $m(t) \geq 1$, $X(t)$ is an OU process, generically described by

$$\mathrm{d}X(t) = \alpha\,[\mu - X(t)]\,\mathrm{d}t + \beta \mathrm{d}W(t).$$

To update $X(t)$ to the next time $t + \tau$, we use the statistically exact method described in [15], summarized by

$$X(t+\tau) = e^{-\alpha\tau} X(t) + (1 - e^{-\alpha\tau})\mu + \beta \sqrt{\frac{(1 - e^{-2\alpha\tau})}{2\alpha}}\,\mathfrak{n}$$

where $\mathfrak{n}$ is a standard normal random variable. When $m(t) = 0$, $X(t)$ is a pure diffusion process with $\alpha = 0$, so (5.4.5) becomes an Euler-Maruyama update. This procedure gener-

ates statistically exact sample paths of $X(t)$, sampled at the transition times of $\mathbf{J}(t)$. We use this scheme to generate a long realization of $(X(t), \mathbf{Z}(t), \mathbf{J}(t))$, thereby providing Monte Carlo estimates for $\mathbb{E}[R_{\text{on}}]$ and V for a given parameter set.

5.5 Biological application

We now use the formulas (5.37)-(5.39) for run velocity, $\mathcal{V}$, and run length, $\mathbb{E}[\overline{R}]$, to explore the behavior of nonprocessive motors. The behavior of individual nonprocessive motors is characterized by two observations: i) short attachment times, ii) the time it takes to hydrolyze ATP (and consequently, to step) coincides with this attachment time [4, 12, 34]. Concretely, Ncd motors in the kinesin-14 family take 1 to 5 steps before unbinding [1, 8]. In our model, $\lambda_{\text{step}}(1)$ gives the expected number of steps before unbinding, so we characterize nonprocessive motors as those with $\lambda_{\text{step}}(1) \in [1, 5]$.

Using this characterization, we explore the observation made in [13, 23, 42] that nonprocessive motors in the kinesin-14 family cooperate to produce long-range transport. This behavior is reported in [13, 23] in terms of a velocity that is analogous to the run velocity $\mathcal{V}$ in our model. Specifically, the primary manifestation of cooperativity is that $\mathcal{V}$ increases substantially when the total number of motors increases from $M = 1$ to $M = 2$. For $M \geq 2$, the velocity remains relatively constant.

We thus ask the question: What features are necessary to produce this behavior? Now, if the step rate is independent of the number of bound motors, m, then it follows immediately from (5.34) and (5.36) that $\mathcal{V}$ is independent of M. In particular, if the dimensional step rate is $k_{\text{step}}(m) \equiv k_0$ for all $m \in \{1, \ldots, M\}$, then in dimensional units $\mathcal{V}$ is simply δk_0, regardless of any other parameter values.

Therefore, our model predicts that the stepping rate must depend on the number of bound motors in order to produce the cooperative behavior seen in run velocities in [13, 23]. This prediction is bolstered by the simulation results of [13]. There, the authors constructed a detailed computational model of motor transport, and they had to improve motor stepping ability when two or more motors are bound in order for simulations of their computational model to match experimental run velocities.

The authors of [13] also describe motor cooperativity in terms of the average distance traveled by a cargo before all of its motors detach from a microtubule, which is analogous

to $\mathbb{E}[\overline{R}]$ in our model. Namely, they find that the run length $\mathbb{E}[\overline{R}]$ dramatically increases when M increases from 1 to 2. Our model can replicate this cooperativity if and only if we allow the binding rate, k_{on}, and/or the unbinding rate, k_{off}, to depend on the number of bound motors, m.

To illustrate, we find the parameter values needed for our model to match the measurements from [13]. However, we emphasize the qualitative results rather than the precise quantitative values of our parameters. Indeed, there are issues preventing an exact comparison of our model with the data in [13]. For example, as the authors point out, the length of the microtubules sometimes caused run lengths to be significantly altered (see Figures 1 and S6 in [13]). Furthermore, for a single motor ($M = 1$), the authors report average run lengths of approximately 300 [nm], and they note that this value is necessarily an overestimate since they were unable to measure very short runs. Furthermore, this value must also be an overestimate since a single nonprocessive motor takes only a few steps per run (by definition of nonprocessive), and each step is approximately 7 [nm] [8].

We thus assume that $\lambda_{\text{step}}(1) = 4$, based on [1, 8] and $\delta = 7\,[\text{nm}]$. This gives $\mathbb{E}[R] = 28\,[\text{nm}]$ for $M = 1$, which we use instead of the reported value in [13]. We then match the respective approximate run lengths of 1300 [nm] and 3300 [nm] for $M = 1, 2$ and the respective approximate run velocities of 100, 150, and 150 [nm/s] for $M = 1, 2, 3$ reported in [13]. Using the formulas in (5.37)-(5.39), this uniquely determines the stepping rates, $k_{\text{step}}(1) \approx 14$ [s^{-1}] and $k_{\text{step}}(2) \approx k_{\text{step}}(3) \approx 21$ [s^{-1}], and the unbinding rate $k_{\text{off}}(1) \approx 3.5$ [s^{-1}], which are all within the range of previously reported rates. The other binding/unbinding rates are not uniquely specified, but rather must satisfy the relations $k_{\text{off}}(2) \approx 0.02 k_{\text{on}}(1)$ and $k_{\text{off}}(3) \approx 1.1 k_{\text{on}}(2)$. Hence, if k_{off} were constant in m, then $k_{\text{on}}(1) \approx 200$ [s^{-1}] and $k_{\text{on}}(2) \approx 3$ [s^{-1}].

We make two observations about this result: i) the binding rate $k_{\text{on}}(1)$ is an order of magnitude larger than reported values [1, 13] and ii) the binding rate decreases as the number of bound motors increases from 1 to 2. Both of these points can be explained by geometry. First, the value of $k_{\text{on}}(1)$ is enhanced because the single bound motor tethers the unbound motors close to the microtubule, and thus allows those motors to bind more easily. This binding enhancement due to geometry has precedent in motor studies. Indeed, in a different family of kinesins, it was shown to be critical for determining run lengths

[10]. Further, it was shown to play a critical role in enabling dynein processivity [17], and it was posited as an explanation for why myosin motors can become processive when processive kinesin motors are present [19]. The authors in [2] report large k_{on} values in a model of microtubule sliding driven by kinesin-14 motors and also speculate that this is due to tethering effects. These effects are summarized in **Figure 5.4**.

This effect can also be understood in terms of rebinding. If two motors are bound and one unbinds, then that motor can rapidly rebind since the bound motor keeps it near the microtubule. Such rebinding was the mechanism posited in [14] to explain the processive behavior of nonprocessive motors along microtubule bundles. Further, rebinding is very important in enzymatic reactions [40, 16, 29, 30]. In that context, one incorporates rebinding by using an "effective" unbinding rate, which is the intrinsic unbinding rate multiplied by the probability that the particle does not rapidly rebind [28]. Hence, this effect could be included in our model by reducing $k_{\text{off}}(2)$ rather than (or in addition to) increasing $k_{\text{on}}(1)$. Importantly, this is exactly what is implied by the relation, $k_{\text{off}}(2) \approx 0.02 k_{\text{on}}(1)$, derived above.

Second, geometric exclusion effects can explain a decrease in binding rates as the number of bound motors increases from 1 to 2. When more motors are bound, it is more difficult for additional motors to bind because the range of diffusive search is reduced for unbound motors. In numerical investigations of motor transport systems, this exact effect is observed [26, 31]. Furthermore this decrease in binding rate can arise due to

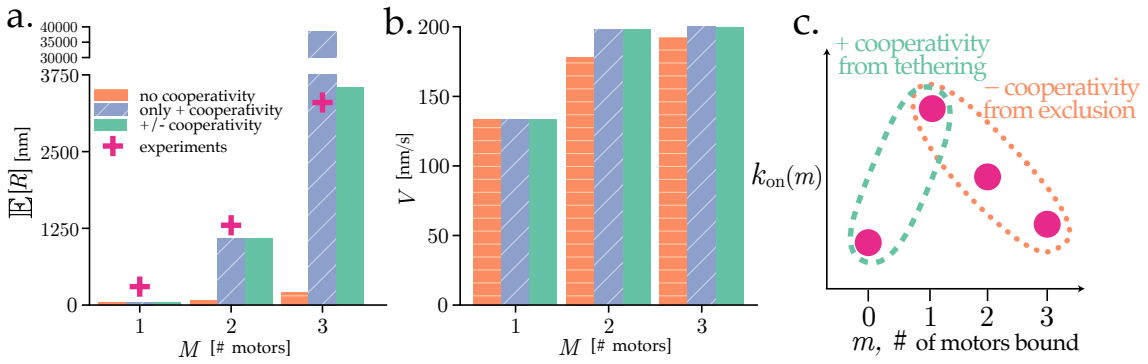

Figure 5.4. Summary of biological results. **a**: mean run length $\mathbb{E}[R]$ for different parameter sets, discussed in the text. **b**: mean run velocity V as a function of the same parameters. **c**: cartoon graph of motor binding rate $k_{\text{on}}(m)$ with hypothesized geometric effects.

motors competing for binding sites, a point posited in [25]. Interestingly, these authors find that negative cooperativity has little impact on transport velocity. The same is true in our model, as the value of $\mathcal{V}$ changes by less than 1 [nm/s] as $k_{\text{on}}(2)$ ranges from 0 to ∞ while keeping the other parameters fixed. However, we note that the run length for $M = 3$ is greatly affected by $k_{\text{on}}(2)$, and thus this highlights the importance of using both run velocity and run length to study motor transport.

5.6 Discussion

In this work, we formulated and analyzed a mathematical model of transport by nonprocessive molecular motors. We deliberately made our model simple enough to enable us to extract explicit formulas for experimentally relevant quantities, yet maintain agreement with detailed computational studies. One such simplification is to assume the motor stepping and unbinding rates are independent of force. The justification for this assumption is that since nonprocessive motors take only a few steps before unbinding (compared to hundreds of steps by processive motors), these motors are unlikely to be stretched long distances and therefore are unlikely to generate large forces. This assumption on the stepping rate has been made in other models involving nonprocessive motors [34] and did not appear to be a necessary feature in that context. Furthermore, how force affects stepping is not completely clear [36].

These limitations notwithstanding, our model makes some concrete predictions about motor number-dependent stepping, binding, and unbinding behavior and how these quantities contribute to transport by nonprocessive motors. Specifically, we observe that a complex cooperativity mechanism appears to be a necessary ingredient for nonprocessive motor transport, and these predictions align with several recent experimental and computational works. Furthermore, these predictions can be investigated experimentally. Indeed, we hope that the work here will spur further investigation into how geometry affects nonprocessive motor transport, especially given that kinesin-14 motors are known to transport a wide variety of cargo, including long, cylindrical microtubules [18, 11] and large, spherical vesicles in plants [42].

5.7 References

[1] R. D. Astumian and I. Derényi, *A chemically reversible Brownian motor: Application to kinesin and Ncd*, Biophys. J., 77 (1999), pp. 993–1002.

[2] M. Braun, Z. Lansky, A. Szuba, F. W. Schwarz, A. Mitra, M. Gao, A. Lüdecke, P. R. ten Wolde, and S. Diez, *Changes in microtubule overlap length regulate kinesin-14-driven microtubule sliding*, Nat. Chem. Biol., (2017), pp. 1245–1252.

[3] P. C. Bressloff, *Stochastic Processes in Cell Biology*, vol. 41 of Interdisciplinary Applied Mathematics, Springer International Publishing, 2014.

[4] R. B. Case, D. W. Pierce, N. Hom-Booher, C. L. Hart, and R. D. Vale, *The directional preference of kinesin motors is specified by an element outside of the motor catalytic domain*, Cell, 90 (1997), pp. 959–966.

[5] M. H. A. Davis, *Piecewise-deterministic Markov processes: A general class of non-diffusion stochastic models*, J. Roy. Stat. Soc. Ser. B, (1984), pp. 353–388.

[6] T. Duke, *Cooperativity of myosin molecules through strain-dependent chemistry.*, Philos. Trans. Roy. Soc. Ser. B, 355 (2000), pp. 529–38.

[7] R. Durrett, *Probability: Theory and Examples*, Cambridge University Press, 2010.

[8] S. A. Endow and H. Higuchi, *A mutant of the motor protein kinesin that moves in both directions on microtubules.*, Nature, 406 (2000), pp. 913–6.

[9] R. P. Erickson, Z. Jia, S. P. Gross, and C. C. Yu, *How molecular motors are arranged on a cargo is important for vesicular transport*, PLoS Comp. Biol., 7 (2011), p. e1002032.

[10] Q. Feng, K. J. Mickolajczyk, G.-Y. Chen, and W. O. Hancock, *Motor reattachment kinetics play a dominant role in multimotor-driven cargo transport*, Biophys. J., 114 (2017), pp. 1–12.

[11] G. Fink, L. Hajdo, K. J. Skowronek, C. Reuther, A. A. Kasprzak, and S. Diez, *The mitotic kinesin-14 Ncd drives directional microtubule-microtubule sliding*, Nat. Cell Biol., 11 (2009), pp. 717–23.

[12] K. A. Foster, A. T. Mackey, and S. P. Gilbert, *A mechanistic model for Ncd directionality*, J. Biol. Chem., 276 (2001), pp. 19259–19266.

[13] K. Furuta, A. Furuta, Y. Y. Toyoshima, M. Amino, K. Oiwa, and H. Kojima, *Measuring collective transport by defined numbers of processive and nonprocessive kinesin motors*, Proc. Natl. Acad. Sci., 110 (2013), pp. 501–506.

[14] K. Furuta and Y. Y. Toyoshima, *Minus-end-directed motor Ncd exhibits processive movement that is enhanced by microtubule bundling in vitro*, Curr. Biol., 18 (2008), pp. 152–157.

[15] D. T. Gillespie, *Exact numerical simulation of the Ornstein-Uhlenbeck process and its integral*, Phys. Rev. E, 54 (1996), pp. 2084–2091.

[16] I. V. Gopich and A. Szabo, *Diffusion modifies the connectivity of kinetic schemes for multisite binding and catalysis*, Proc. Natl. Acad. Sci., 110 (2013), pp. 19784–19789.

[17] D. A. Grotjahn, S. Chowdhury, Y. Xu, R. J. McKenney, T. A. Schroer, and G. C. Lander, *Cryo-electron tomography reveals that dynactin recruits a team of dyneins for processive motility*, bioRxiv, (2017), pp. 1–35.

[18] M. A. Hallen, Z.-Y. Liang, and S. A. Endow, *Ncd motor binding and transport in the spindle.*, J. Cell Sci., 121 (2008), pp. 3834–41.

[19] A. R. Hodges, C. S. Bookwalter, E. B. Krementsova, and K. M. Trybus, *A nonprocessive class V myosin drives cargo processively when a kinesin-related protein is a passenger*, Curr. Biol., 19 (2009), pp. 2121–2125.

[20] J. Hughes, W. O. Hancock, and J. Fricks, *A matrix computational approach to kinesin neck linker extension*, J. Theor. Biol., 269 (2011), pp. 181–194.

[21] ——, *Kinesins with extended neck linkers: A chemomechanical model for variable-length stepping*, Bull. Math. Biol., 74 (2012), pp. 1066–1097.

[22] J. Hughes, S. Shastry, W. O. Hancock, and J. Fricks, *Estimating velocity for processive motor proteins with random detachment*, J. Agric. Biol. Environ. Stat., 18 (2013), pp. 204–217.

[23] E. Jonsson, M. Yamada, R. D. Vale, and G. Goshima, *Clustering of a kinesin-14 motor enables processive retrograde microtubule-based transport in plants*, Nat. Plants, 1 (2015), p. 15087.

[24] F. Jülicher and J. Prost, *Cooperative molecular motors*, Phys. Rev. Lett., 75 (1995), pp. 2618–2621.

[25] S. Klumpp and R. Lipowsky, *Cooperative cargo transport by several molecular motors*, Proc. Natl. Acad. Sci., 102 (2005), pp. 17284–17289.

[26] C. B. Korn, S. Klumpp, R. Lipowsky, and U. S. Schwarz, *Stochastic simulations of cargo transport by processive molecular motors*, J. Chem. Phys., 131 (2009), p. 245107.

[27] A. Krishnan and B. I. Epureanu, *Renewal-reward process formulation of motor protein dynamics*, Bull. Math. Biol., 73 (2011), pp. 2452–2482.

[28] D. A. Lauffenburger and J. Linderman, *Receptors: Models for binding, trafficking, and signaling*, Oxford University Press, 1993.

[29] S. D. Lawley and J. P. Keener, *Including rebinding reactions in well-mixed models of distributive biochemical reactions*, Biophys. J., 111 (2016), pp. 2317–2326.

[30] ——, *Rebinding in biochemical reactions on membranes*, Phys. Biol., (2017).

[31] A. T. Lombardo, S. R. Nelson, M. Y. Ali, G. G. Kennedy, K. M. Trybus, S. Walcott, and D. M. Warshaw, *Myosin Va molecular motors manoeuvre liposome cargo through suspended actin filament intersections in vitro*, Nat. Comm., 8 (2017), p. 15692.

[32] S. A. McKinley, A. Athreya, J. Fricks, and P. R. Kramer, *Asymptotic analysis of microtubule-based transport by multiple identical molecular motors*, J. Theor. Biol., 305 (2012), pp. 54–69.

[33] C. Mieck, M. I. Molodtsov, K. Drzewicka, B. van der Vaart, G. Litos, G. Schmauss, A. Vaziri, and S. Westermann, *Non-catalytic motor domains enable processive movement and functional diversification of the kinesin-14 Kar3*, eLife, 4 (2015), pp. 1–23.

[34] B. Nitzsche, E. Dudek, L. Hajdo, A. A. Kasprzak, A. Vilfan, and S. Diez, *Working stroke of the kinesin-14, Ncd, comprises two substeps of different direction*, Proc. Natl. Acad. Sci., 113 (2016), pp. E6582–E6589.

[35] J. Norris, *Markov Chains*, Statistical & Probabilistic Mathematics, Cambridge University Press, 1998.

[36] E. Pechatnikova and E. W. Taylor, *Kinetics processivity and the direction of motion of Ncd.*, Biophys. J., 77 (1999), pp. 1003–1016.

[37] P. M. Shaklee, T. Idema, G. Koster, C. Storm, T. Schmidt, and M. Dogterom, *Bidirectional membrane tube dynamics driven by nonprocessive motors*, Proc. Natl. Acad. Sci., 105 (2008), pp. 7993–7997.

[38] B. Shtylla and J. P. Keener, *Mathematical modeling of bacterial track-altering motors: Track cleaving through burnt-bridge ratchets*, Phys. Rev. E, 91 (2015), p. 042711.

[39] G. T. Shubeita, S. L. Tran, J. Xu, M. Vershinin, S. Cermelli, S. L. Cotton, M. A. Welte, and S. P. Gross, *Consequences of motor copy number on the intracellular transport of kinesin-1-driven lipid droplets*, Cell, 135 (2008), pp. 1098–1107.

[40] K. Takahashi, S. Tanase-Nicola, and P. Rein Ten Wolde, *Spatio-temporal correlations can drastically change the response of a MAPK pathway*, Proc. Natl. Acad. Sci., 107 (2010), pp. 2473–2478.

[41] M. Vlasiou, *Regenerative processes*, in Wiley Encyclopedia of Operations Research and Management Science, J. J. Cochran, L. A. Cox, P. Keskinocak, J. P. Kharoufeh, and J. C. Smith, eds., American Cancer Society, 2011.

[42] M. Yamada, Y. Tanaka-Takiguchi, M. Hayashi, M. Nishina, and G. Goshima, *Multiple kinesin-14 family members drive microtubule minus end-directed transport in plant cells*, The J. Cell. Biol., 216 (2017), pp. 1705–1714.

CHAPTER 6

FUTURE DIRECTIONS

In this chapter, we outline plans for future work, both in pursuit of biological and mathematical questions. Extensions of the contents of this thesis are described, as well as distinct research directions.

6.1 Bidirectional transport with asymmetric populations

In **Chapter 2**, we considered the tug-of-war problem for *symmetric* populations. That is, the motors associated with each direction had identical properties (e.g., binding kinetics, velocities). In this scenario, the system displays interesting symmetry breaking behavior, but perhaps neglects biological evidence to the contrary. It is well established that in tug-of-war contexts (with kinesin and dynein [9, 34, 22] or by different types of kinesins [13]) the two populations are asymmetric. It is then of natural interest to investigate the influence of asymmetry on the metastable switching of this system.

However, the analysis described in **Chapter 2** hinged on the symmetry of the system, with the state of the system (ξ, η) evolving on an invariant manifold. However, if F_1, F_2 (the effective force generated by each population) differ, the problem becomes a singular metastable escape problem with a seemingly mathematical interesting structure.

Rather than study this problem directly, we instead turn to a minimal toy problem of the form $\mathbf{x} := (x, y) \in \mathbb{R}^2$

$$\frac{\mathrm{d}}{\mathrm{d}t}\mathbf{x} = A(\mathbf{x}) + B(\mathbf{x})\boldsymbol{\xi}(t), \tag{6.1}$$

where ¸(**t**) ∈ $\mathbb{R}^{\mathbf{2}}$ is a vector of independent white noise processes. We then take the drift A to be the classical Maier-Stein system [25, 26, 27]

$$A(\mathbf{x}) = \begin{bmatrix} x - x^2 - \alpha x y^2 \\ -y(1 + x^2) \end{bmatrix}. \tag{6.2}$$

The drift (6.2) produces three equilibria at $x = 0, \pm 1$ along $y = 0$. The noise matrix B is taken to be of the form

$$B = \begin{bmatrix} 1 & 0 \\ \gamma & \varepsilon \end{bmatrix}. \tag{6.3}$$

The noise matrix (6.3) shares features of the bidirectional transport problem described in **Chapter 2**. If $\varepsilon = 0, \gamma \neq 0$, the noise between the populations is perfectly correlated, as in the thermal fluctuation case. However, classical metastable escape theory considers the opposite: $\varepsilon \neq 0, \gamma = 0$. From the noise matrix B we define the diffusion tensor

$$D \coloneqq BB^T = \begin{bmatrix} 1 & \gamma \\ \gamma & \gamma^2 + \varepsilon^2 \end{bmatrix}. \tag{6.4}$$

From (6.4) we immediately see an interesting feature, which is that for $\gamma = 0$, D is singular. The classical approach to studying escape problems involves associating a Hamiltonian

$$H(\mathbf{x}, \mathbf{p}) = \langle A(\mathbf{x}), \mathbf{p} \rangle + \frac{1}{2} \langle \mathbf{p}, D\mathbf{p} \rangle, \tag{6.5}$$

where $\langle \cdot, \cdot \rangle$ denotes the standard inner product. For this Hamiltonian, there is an associated Lagrangian

$$L(\mathbf{x}, \mathbf{y}) = \sup_{\mathbf{p}} \{ \langle \mathbf{y}, \mathbf{p} \rangle - H(\mathbf{x}, \mathbf{p}) \} = \left\langle \mathbf{y} - A(\mathbf{x}), D^{-1}(\mathbf{y} - A(\mathbf{x})) \right\rangle. \tag{6.6}$$

From (6.6) and (6.4), we see an immediate issue when D is noninvertible. This raises the question: Does metastable switching even occur at all? Geometrically, the singularity of D comes from the noise being one dimensional. To investigate this, we perform simulations of the switching problem, which can be seen in **Figure 6.1**.

From these simulations, we see that when $\varepsilon \neq 0$, the behavior around the metastable points is ellipsoidal as we expect. However, in the singular case, even though noise pushes the particle in the diagonal direction (and all the fixed points lie on a horizontal line), we still get metastable switching.

In the future, we hope to develop a framework for understanding this type of metastable escape problems. While it may be possible to transform this into a classical formulation, intuitive transformations such as rotations [19] do not alleviate the singular behavior. We plan to pursue extending both analytical frameworks such as [23] as well as numerical techniques such as the geometric minimum action method [18, 36]. The latter seems to depend on a Hamiltonian formulation, which may still exist, but appears distinct from the classical formulation. In doing this, new mathematical theory would enable the further study of the biological system posed in **Chapter 2**.

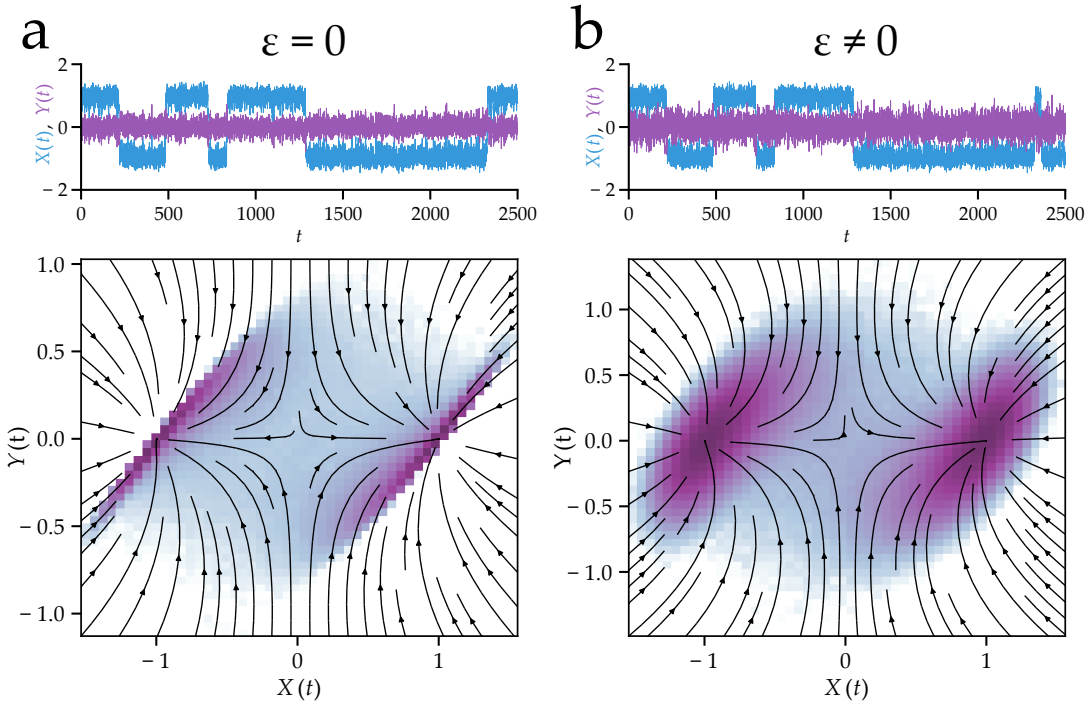

Figure 6.1. Metastable switching for the Maier-Stein problem for different values of ε and $\alpha = 1$ fixed. **a**: Singular D case with$\varepsilon = 0$, example trajectory and histogram in trajectory space are shown. **b**: Same parameters as previous but in this case, $\varepsilon = 1$ producing a nonsingular D.

6.2 Bayesian methods for motor-mediated transport data

The premise of **Chapter 4** was to understand motor-mediated transport data by constructing a toy model that agrees with distinct features of the data (summary statistics). More explicitly, the primary tool to characterize the spatio-temporal data in this context was mean-squared displacement (MSD) analysis [30]. While this tool has widespread success in categorizing data as diffusive, subdiffusive, or superdiffusive, further insight is limited or nonexistent. In **Chapter 4**, we do ultimately find that more information can be extracted from MSD analysis, but this issue is inherently caused by the fact that linear (diffusive) MSD curves are known to be driven by a variety of causes in this context [31, 8, 38].

For these reasons, it seems apparent that more sophisticated statistical analyses (specifically, Bayesian) may prove fruitful in this context. In some sense, MSD analysis is a maximum-likelihood-estimator (MLE) oriented analysis, as it is a "best fit" to the mo-

ments describing the data. However, there are two immediate limiting features of this. For one, the only models that can be compared against are subdiffusive, diffusive, and super-diffusive behaviors. While a number of systems can produce these statistics, using this as the statistical model to compare against limits the zoology of behaviors. Moreover, MLE-based tests do not provide model assessment. That is, Bayesian techniques have the feature of providing information (via the posterior distribution) about ranges of parameters. For instance, one could write a model of intracellular transport and use Bayesian techniques to infer parameters, and if a parameter is able to vary over several orders of magnitude with little impact, this reveals critical insight about agreement between the model and data. For this reason, Bayesian-based techniques are a natural tool for the study of these systems.

Application of Bayesian techniques toward spatio-temporal data already has a rich literature [21, 20]. While others have considered Bayesian techniques for motor-transport data (e.g. [22]), this body of literature seems underutilized in this context. The primary context that seems to be advancing this literature is tracking of subdiffusive particles [24]. In this literature, advancing the classification beyond subdiffusive is critical in order to understand the underlying mechanisms. Whether it be diffusive or ballistic motion, the same need exists in motor-mediated transport data. Other valuable features can be extracted from these techniques. For instance, in [2], a simple Ornstein–Uhlenbeck model is used to infer information about the environment, a hugely important component of transport by motors [15, 1].

As it seems as though Bayesian-based single particle tracking techniques are a natural and likely fruitful tool for connecting motor-mediated transport data and models, we hope to port the previously successful methods used in other contexts. Although powerful, one limitation is that these techniques are often model-specific, meaning that in doing so, new mathematical insight will likely be necessary, meaning this pursuit has both biological and mathematical benefits.

6.3 Cytoskeletal manipulation by nonprocessive motors

Chapter 5 investigates *how* nonprocessive motors (such as those in the kinesin-14 family) act cooperatively to produce transport, based on the experiments in [13]. In some

sense, this level of cooperativity is surprising, given the residence time of a single nonprocessive motor. However, from an evolutiontuned design perspective: *Why do cells have nonprocessive motors at all*? These motors are known to be used for transport in plants [37], but why use nonprocessive motors when processive seem superior (in the sense of efficiency) for this application? One might intuit that perhaps nonprocessive motors somehow are able to use their fast binding and unbinding to somehow "fine tune" a cellular process. We would like to find and model a context that reveals exactly this behavior.

In **Figure 6.2**, two applications of motors in the kinesin-14 family are shown. Aside from transport in plants, kinesin-14 motors are heavily utilized in mechanically manipulating cytoskeletal filaments [4, 5, 3, 6, 7, 12, 17] including during mitotic spindle assembly [14, 16, 32]. Aside from binding and unbinding rapidly, motors within this family are also reported to be particularly bidirectional [28, 29] perhaps enabling them to serve as a force-induced switch.

However, from all of these reports, it is not clear which features (if any) makes nonprocessive motors particularly suited for the job of cytoskeletal manipulation. We hypothesize that the *long* attachment times of processive motors would cause these processes to "get

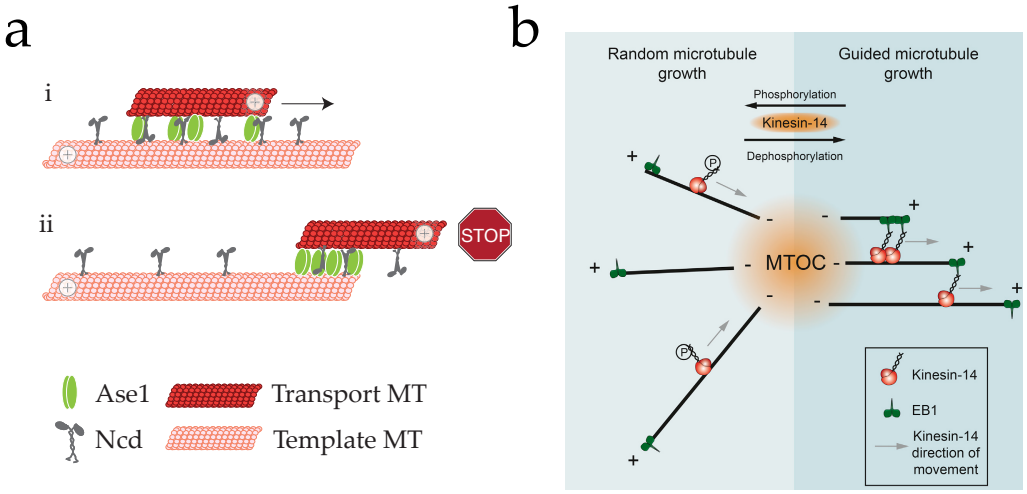

Figure 6.2. Cartoons depicting the utilization of nonprocessive motors in cytoskeletal regulation. **a**: Redrawn from [5], kinesin-14 motors are utilized in microtubule sliding. **b**: Redrawn from [28], kinesin-14 motors guide microtubules to form parallel bundles.

stuck," whereas rapid binding and unbinding allows for the process to achieve increased temporal resolution. The importance of the force-induced switch also remains elusive, especially considering the short periods of time the motor is exposed to force. We intend to construct a mathematical model of teams of nonprocessive motors manipulating cytoskeletal filaments with both of these features, parameterized in such a way that could also describe processive motors. From this model, we hope to discern whether it is ever "beneficial" to be a nonprocessive motor, a key insight in understanding the role that these motors play in the ecosystem of motor function within the cell.

6.4 Geometric effects in motor transport

In both **Chapter 4** and **Chapter 5**, the binding and unbinding kinetics of nonprocessive motors greatly influenced the net motion of the cargo. In the latter project, the conclusion was that the only way nonprocessive motors are able to achieve cooperativity is to utilize geometric effects (tethering) to increase the rebinding rate of a teammate motor. This effect has indeed been observed experimentally [11] and thought to be critical for nonprocessive motor driven microtubule sliding [7]. We raise the question: *What geometric influences dictate these tethering effects*? In the first scenario, the cargo is spherical (or linear, DNA origami), whereas in the second a microtubule serves as a long, cylindrical cargo, yet this geometric tethering effect appears to be apparent in both. For this reason, we hope to develop a quantitative understanding of how geometry influences motor binding kinetics. For this, we plan to use a binding site model [35], or perhaps a mean-first-passage formulation [10] to model the binding time with different motor configurations and cargo geometries.

Geometric influences can also influence intracellular transport in other ways. In [23], the authors find that a diffusible membrane surface to the cargo affects transport velocity, relating to the fact that motors often transport lipids [33, 22] with diffusible membranes. This membrane diffusion allows for the motor geometric configuration to be adjusted dynamically, and therefore closely relates to the theme of this proposed work. We hypothesize that diffusing along the membrane surface allows unattached motors to rebind faster and enhance net motion. However, it is also feasible that this diffusion allows for the motors to alleviate some force and stay attached for longer. We hope to construct a

model including diffusion along the cargo surface to explore where these geometric effects influence transport ability most significantly.

6.5 References

[1] J. P. Bergman, M. J. Bovyn, F. F. Doval, A. Sharma, M. V. Gudheti, S. P. Gross, J. F. Allard, and M. D. Vershinin, *Cargo navigation across 3D microtubule intersections*, Proc. Natl. Acad. Sci., (2018), p. 201707936.

[2] J. Bernstein and J. Fricks, *Analysis of single particle diffusion with transient binding using particle filtering*, J. Theor. Biol., 401 (2016), pp. 109–121.

[3] M. Braun, S. Diez, and Z. Lansky, *Cell biology: Kinesin-14 backsteps to organize polymerizing microtubules*, Curr. Biol., 26 (2016), pp. R1292–R1294.

[4] M. Braun, D. R. Drummond, R. A. Cross, and A. D. McAinsh, *The kinesin-14 Klp2 organizes microtubules into parallel bundles by an ATP-dependent sorting mechanism*, Nat. Cell Biol., 11 (2009), pp. 724–730.

[5] M. Braun, Z. Lansky, G. Fink, F. Ruhnow, S. Diez, and M. E. Janson, *Adaptive braking by Ase1 prevents overlapping microtubules from sliding completely apart*, Nat. Cell Biol., 13 (2011), pp. 1259–1264.

[6] M. Braun, Z. Lansky, F. Hilitski, Z. Dogic, and S. Diez, *Entropic forces drive contraction of cytoskeletal networks*, BioEssays, 38 (2016), pp. 474–481.

[7] M. Braun, Z. Lansky, A. Szuba, F. W. Schwarz, A. Mitra, M. Gao, A. Lüdecke, P. R. ten Wolde, and S. Diez, *Changes in microtubule overlap length regulate kinesin-14-driven microtubule sliding*, Nat. Chem. Biol., (2017), pp. 1245–1252.

[8] A. V. Chechkin, F. Seno, R. Metzler, and I. M. Sokolov, *Brownian yet non-Gaussian diffusion: From superstatistics to subordination of diffusing diffusivities*, Phys. Rev. X, 7 (2017), pp. 1–20.

[9] N. D. Derr, B. S. Goodman, R. Jungmann, A. E. Leschziner, W. M. Shih, and S. L. Reck-Peterson, *Tug-of-war in motor protein ensembles*, Science, 338 (2012), pp. 662–666.

[10] R. P. Erickson, Z. Jia, S. P. Gross, and C. C. Yu, *How molecular motors are arranged on a cargo is important for vesicular transport*, PLoS Comp. Biol., 7 (2011), p. e1002032.

[11] Q. Feng, K. J. Mickolajczyk, G.-Y. Chen, and W. O. Hancock, *Motor reattachment kinetics play a dominant role in multimotor-driven cargo transport*, Biophys. J., 114 (2017), pp. 1–12.

[12] G. Fink, L. Hajdo, K. J. Skowronek, C. Reuther, A. A. Kasprzak, and S. Diez, *The mitotic kinesin-14 Ncd drives directional microtubule-microtubule sliding*, Nat. Cell Biol., 11 (2009), pp. 717–23.

[13] K. Furuta, A. Furuta, Y. Y. Toyoshima, M. Amino, K. Oiwa, and H. Kojima, *Measuring collective transport by defined numbers of processive and nonprocessive kinesin motors*, Proc. Natl. Acad. Sci., 110 (2013), pp. 501–506.

[14] G. Goshima and J. M. Scholey, *Control of mitotic spindle length*, Annu. Rev. Cell Dev. Biol., 26 (2010), pp. 21–57.

[15] I. Goychuk, V. O. Kharchenko, and R. Metzler, *How molecular motors work in the crowded environment of living cells: Coexistence and efficiency of normal and anomalous transport*, PLoS ONE, 9 (2014), pp. 1–7.

[16] M. A. Hallen, Z.-Y. Liang, and S. A. Endow, *Ncd motor binding and transport in the spindle.*, J. Cell Sci., 121 (2008), pp. 3834–41.

[17] C. Hentrich and T. Surrey, *Microtubule organization by the antagonistic mitotic motors kinesin-5 and kinesin-14*, J. Cell. Biol., 189 (2010), pp. 465–480.

[18] M. Heymann and E. Vanden-Eijnden, *The geometric minimum action method: A least action principle on the space of curves*, Comm. Pure Appl. Math., 61 (2008), pp. 1052–1117.

[19] P. B. Kingsley, *Introduction to diffusion tensor imaging mathematics: Part I. Tensors, rotations, and eigenvectors*, Concept. Magn. Reson. A, 28A (2006), pp. 101–122.

[20] C. D. Kinz-Thompson and R. L. Gonzalez, *Increasing the time resolution of single-molecule experiments with Bayesian inference*, Biophys. J., 114 (2017), pp. 289–300.

[21] S. Kou, X. S. Xie, and J. S. Liu, *Bayesian analysis of single-molecule experimental data (with discussion)*, J. Roy. Soc. Stat. Sci. Ser. C, 54 (2005), p. 469.

[22] A. Kunwar, S. K. Tripathy, J. Xu, M. K. Mattson, P. Anand, R. Sigua, M. Vershinin, R. J. McKenney, C. C. Yu, A. Mogilner, and S. P. Gross, *Mechanical stochastic tug-of-war models cannot explain bidirectional lipid-droplet transport*, Proc. Natl. Acad. Sci., 108 (2011), pp. 18960–18965.

[23] Q. Li, K. F. Tseng, S. J. King, W. Qiu, and J. Xu, *A fluid membrane enhances the velocity of cargo transport by small teams of kinesin-1*, J. Chem. Phys., 148 (2018).

[24] M. Lysy, N. S. Pillai, D. B. Hill, M. G. Forest, J. W. R. Mellnik, P. A. Vasquez, and S. A. McKinley, *Model comparison and assessment for single particle tracking in biological fluids*, J. Amer. Stat. Assoc., 1459 (2016), pp. 1413–1426.

[25] R. S. Maier and D. L. Stein, *A scaling theory of bifurcations in the symmetric weak-noise escape problem*, J. Stat. Phys., 83 (1996), pp. 291–357.

[26] ——, *Limiting exit location distributions in the stochastic exit problem*, SIAM J. Appl. Math., 57 (1997), pp. 752–790.

[27] ——, *Noise-activated escape from a sloshing potential well*, Phys. Rev. Lett., 86 (2001), pp. 3942–3945.

[28] M. I. Molodtsov, C. Mieck, J. Dobbelaere, A. Dammermann, S. Westermann, and A. Vaziri, *A force-induced directional switch of a molecular motor enables parallel microtubule bundle formation*, Cell, 167 (2016), pp. 539–552.e14.

[29] A. R. Popchock, K.-F. Tseng, P. Wang, P. A. Karplus, X. Xiang, and W. Qiu, *The mitotic kinesin-14 KlpA contains a context-dependent directionality switch*, Nat. Comm., 8 (2017), p. 13999.

[30] M. J. Saxton, *Single-particle tracking: The distribution of diffusion coefficients*, Biophys. J., 72 (1997), pp. 1744–53.

[31] M. Scholz, S. Burov, K. L. Weirich, B. J. Scholz, S. M. Tabei, M. L. Gardel, and A. R. Dinner, *Cycling state that can lead to glassy dynamics in intracellular transport*, Phys. Rev. X, 6 (2016), pp. 1–9.

[32] Z.-Y. She and W.-X. Yang, *Molecular mechanisms of kinesin-14 motors in spindle assembly and chromosome segregation*, J. Cell. Sci., 130 (2017), pp. 2097–2110.

[33] G. T. Shubeita, S. L. Tran, J. Xu, M. Vershinin, S. Cermelli, S. L. Cotton, M. A. Welte, and S. P. Gross, *Consequences of motor copy number on the intracellular transport of kinesin-1-driven lipid droplets*, Cell, 135 (2008), pp. 1098–1107.

[34] V. Soppina, A. K. Rai, A. J. Ramaiya, P. Barak, and R. Mallik, *Tug-of-war between dissimilar teams of microtubule motors regulates transport and fission of endosomes*, Proc. Natl. Acad. Sci., 106 (2009), pp. 19381–6.

[35] M. Srinivasan and S. Walcott, *Binding site models of friction due to the formation and rupture of bonds: State-function formalism, force-velocity relations, response to slip velocity transients, and slip stability*, Phys. Rev. E, 80 (2009), pp. 1–15.

[36] E. Vanden-Eijnden and M. Heymann, *The geometric minimum action method for computing minimum energy paths*, The J. Chem. Phys., 128 (2008), p. 061103.

[37] W. J. Walter, I. Machens, F. Rafieian, and S. Diez, *The non-processive rice kinesin-14 OsKCH1 transports actin filaments along microtubules with two distinct velocities*, Nat. Plants, 1 (2015), p. 15111.

[38] B. Wang, S. M. Anthony, S. C. Bae, and S. Granick, *Anomalous yet Brownian*, Proc. Natl. Acad. Sci., 106 (2009), pp. 15160–4.

APPENDIX A

SUPPLEMENTAL INFORMATION FOR CHAPTER 2

In this appendix, we include the supplemental information that accompanied the published work detailed in Chapter 2, originally published in *Journal of Theoretical Biology*, **424** (2017) 37–48.

A.1 Steady-State Force Density

In this section, we construct an analytical solution to the steady-state mean field equation (4) with the particular choice of functional forms described in the chapter. Thus, we are looking at equations of the form

$$\partial_x \{(w(x) - v)m\} + k_{\text{off}} e^{k|x|/F_D} m = \left\{ M - \int_{-\infty}^{\infty} m(x)\,\mathrm{d}x \right\} k_{\text{on}} \delta(x).$$

The first observation that can be made is: due to the linearity of this equation, we can reduce it to the study of the simpler equation

$$\partial_x \{(w(x) - v)u\} + k_{\text{off}} e^{k|x|/F_D} u = k_{\text{on}} \delta(x), \tag{A.1}$$

where $m(x)$, the original solution can be recovered via the relationship

$$m(x) = \frac{M}{1 + U} u(x), \qquad U \coloneqq \int_{-\infty}^{\infty} u(x)\,\mathrm{d}x. \tag{A.2}$$

We now divide everything through by k_{off} in (A.1) and recall $w(x) = -ax + b$. Denote the rescaled variables $\cdot / k_{\text{off}}$ by $\tilde{\cdot}$ and also abbreviate $k/FD = \alpha$, yielding

$$\partial_x \left\{(-\tilde{a}x + \tilde{b} - \tilde{v})u\right\} + \exp\{\alpha|x|\}u = \tilde{k}\delta(x). \tag{A.3}$$

We can now split this into two scenarios: to the left of $x = 0$ and to the right:

$$\begin{cases} \partial_x \left\{(-\tilde{a}x + \tilde{b} - \tilde{v})u_L\right\} + \exp\{-\alpha x\}u_L = 0 & \text{for } x < 0, \\ \partial_x \left\{(-\tilde{a}x + \tilde{b} - \tilde{v})u_R\right\} + \exp\{\alpha x\}u_R = 0 & \text{for } x > 0. \end{cases} \tag{A.4}$$

These two equations must satisfy a matching condition at $x = 0$, so consider integrating (A.3) a tiny window around $x = 0$ from $-\varepsilon$ to ε, yielding

$$\int_{-\varepsilon}^{\varepsilon} \partial_x \left\{(-\tilde{a}x + \tilde{b} - \tilde{v})u\right\} + \exp\{\alpha|x|\}u = (b - v)\left[u_R(0) - u_L(0)\right] \quad = \quad \int_{-\varepsilon}^{\varepsilon} \tilde{k}\delta(x)\,\mathrm{d}x = \tilde{k}.$$

In other words, we have the matching condition

$$(b - v)\left[u_R(0) - u_L(0)\right] = \tilde{k}.$$

Integrating (A.4), we find

$$u_L(x) = \frac{\alpha_L}{\tilde{a}x - \tilde{b} + \tilde{v}} \exp\left\{\frac{1}{\tilde{a}} \exp\left(\frac{(-\tilde{b} + \tilde{v})\alpha}{a}\right) \mathrm{Ei}\left(-\frac{(-\tilde{b} + \tilde{v} + \tilde{a}x)}{\tilde{a}}\right)\right\} \tag{A.5a}$$

$$u_R(x) = \frac{\alpha_R}{\tilde{a}x - \tilde{b} + \tilde{v}} \exp\left\{\frac{1}{\tilde{a}} \exp\left(\frac{(\tilde{b} - \tilde{v})\alpha}{a}\right) \mathrm{Ei}\left(\frac{(-\tilde{b} + \tilde{v} + \tilde{a}x)}{\tilde{a}}\right)\right\}, \tag{A.5b}$$

where α_R, α_L are unknown constants and Ei is the exponential integral. The matching of these two can be simplified by the realization: only one of u_L, u_R is nonzero.

That is, if $-\tilde{a}x + \tilde{b} - v > 0$, then the advection is rightward (only starting from $x = 0$) and therefore $u_L = 0$. Similarly, if the advection is leftward then $u_R = 0$ necessarily. It should also be noted that (A.5) demonstrate the integrable singularity at $x^\star = \frac{-\tilde{v}+\tilde{b}}{\tilde{a}}$, beyond this point, the solution is also necessarily zero. Thus, the solution reduces to either the interval $[0, x^\star]$ or $[x^\star, 0]$ depending on the sign of $x^\star$, or really, if $b > v$.

Thus, if $b > v$, then $x^\star > 0$ and $u_L < 0$ and if $b < v$ then $x^\star < 0$ and $u_R = 0$. Thus, if $b > v$, then our matching condition provides us α_R:

$$\alpha_R = -\tilde{k} \exp\left\{\frac{1}{\tilde{a}} \exp\left(\frac{(\tilde{b} - \tilde{v})\alpha}{\tilde{a}}\right) \mathrm{Ei}\left(\frac{(-\tilde{b} + \tilde{v})\alpha}{\tilde{a}}\right)\right\}.$$

Similarly, in the case that $b < v$, we have

$$\alpha_L = \tilde{k} \exp\left\{\frac{1}{\tilde{a}} \exp\left(\frac{(-\tilde{b} + \tilde{v})\alpha}{\tilde{a}}\right) \mathrm{Ei}\left(\frac{(\tilde{b} - \tilde{v})\alpha}{\tilde{a}}\right)\right\}.$$

Thus, we have constructed all components of the analytical solution to the original steady state equation.

A.2 Force-Velocity Curves

In this section, we plot the steady state force-velocity curves described by (5). In the plots seen in **Figure A.1**, the parameter values are taken to be those described by **Table 2.1** except for one parameter (shown in the legend), which is adjusted over a range of values.

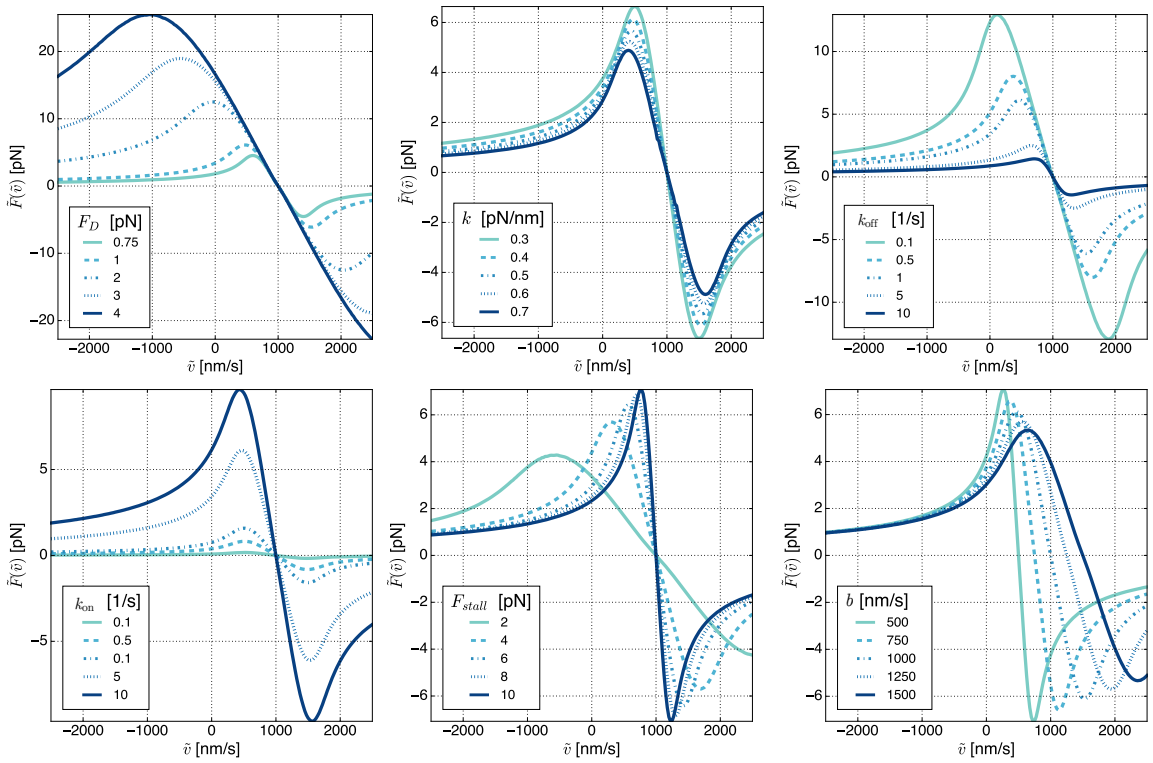

Figure A.1. Plots of the steady state force distribution $\tilde{F}$ parameterized by the velocity of the cargo for different parameter values.

A.3 Adiabatic Reduction Details

In this section, we perform an adiabatic reduction of (10), which, recalling the form of $w(x)$ and using $F(x) = kx$ for the sake of illustration, yields

$$\mathcal{M}\dot{v} + \gamma v = kx + \sqrt{2\gamma k_B T}\xi(t), \qquad \dot{x} = ax + b - v,$$

which is equivalent to the Fokker-Planck equation

$$\frac{\partial p}{\partial t} = -\frac{\partial}{\partial x}\{(ax + b - v)p\} - \frac{1}{\mathcal{M}}\frac{\partial}{\partial v}\{(kx - \gamma v)p\} + \frac{k_B T\gamma}{\mathcal{M}^2}\frac{\partial^2 p}{\partial v^2}. \tag{A.6}$$

We first perform a nondimensionalization. Let $y = x/x_0, \tau = t/t_0$, which provides a scaling on the velocity $u = vt_0/x_0$, all of which are dimensionless, where we particularly take $t_0 = \gamma/k$, and set $\gamma t_0/\mathcal{M} = 1/\varepsilon$, which gives us that $\gamma^2/k\mathcal{M} = 1/\varepsilon$. We can then also set the last term $\gamma k_B T t_0^2/\mathcal{M}^2 x_0^2 = 1/\varepsilon$, which gives us that $x_0 = \sqrt{k_B T\gamma^2/\mathcal{M}k^2}$. Then, (A.6) becomes

$$\frac{\partial p}{\partial \tau} = -\frac{\partial}{\partial y}\{(\alpha y + \beta - u)\, p\} + \frac{1}{\varepsilon}\frac{\partial}{\partial u}\left\{(u - y)p + \frac{\partial p}{\partial u}\right\}, \tag{A.7}$$

which we denote

$$\frac{\partial p}{\partial \tau} = \frac{1}{\varepsilon}\mathbb{L}_1 p + \mathbb{L}_2 p.$$

Note, the null-space of the fast operator, $\mathbb{L}_1$ is *not* the same as the classical Brownian due to a different choice of ε.

Now, if $\phi \in \text{null}(\mathbb{L}_1)$, then it satisfies the following differential equation:

$$\frac{\partial \phi}{\partial u} + (u - y)\phi = 0,$$

which has a solution

$$\phi(u) = \frac{1}{\sqrt{2\pi}} \exp\{-(u-y)^2/2\}. \tag{A.8}$$

Define the projection operator $\mathbb{P}$ as

$$\mathbb{P}f := \phi(u,y) \int_{-\infty}^{\infty} f(u,y)\, \mathrm{d}u, \qquad \mathbb{Q} := 1 - \mathbb{P}.$$

We then split our solution p into the part in the null-space of the fast operator and otherwise. That is,

$$p = \mathbb{P}p + \mathbb{Q}p = v + w,$$

where we take v to be of the form $v = f(y,t)\phi(u,y)$, as it is in the null space of $\mathbb{L}_1$, and f is some unknown amplitude.

We first consider applying $\mathbb{L}_2$ to v for later calculations

$$\mathbb{L}_2 v = \mathbb{L}_2 \mathbb{P} p = -\frac{\partial}{\partial y}\left\{(\alpha y + \beta - u)\, f(y)\phi(u,y)\right\}.$$

Now, applying $\mathbb{P}$ to this result yields

$$\mathbb{P}\mathbb{L}_2\mathbb{P}p = -\frac{\partial}{\partial y}\left\{(\alpha y + \beta - y) f\right\}\phi(u,y).$$

Next, we consider applying $\mathbb{P}$ and $\mathbb{Q}$ to the Fokker-Planck equation to yield the differential equation

$$\mathbb{P}\left(\frac{\partial p}{\partial \tau}\right) = \frac{\partial v}{\partial \tau} = \mathbb{P}\left(\frac{1}{\varepsilon}\mathbb{L}_1 + \mathbb{L}_2\right)(v+w) = \mathbb{P}\mathbb{L}_2 v + \mathbb{P}\mathbb{L}_2 w = -\frac{\partial}{\partial y}\left\{(\alpha y + \beta - y) f\right\}\phi + \mathbb{P}\mathbb{L}_2 w,$$

based on the first calculation and the fact that $\mathbb{P}\mathbb{L}_1 = 0$ by construction. Next, we have

$$\begin{aligned}
\mathbb{Q}\left(\frac{\partial p}{\partial \tau}\right) = \frac{\partial w}{\partial \tau} &= \mathbb{Q}\left(\frac{1}{\varepsilon}\mathbb{L}_1 + \mathbb{L}_2\right)(v+w) \\
&= \frac{1}{\varepsilon}\mathbb{L}_1 w + \mathbb{Q}\mathbb{L}_2(v+w) \\
&= \frac{1}{\varepsilon}\mathbb{L}_1 w + \mathbb{L}_2 v + \mathbb{L}_2 w - \mathbb{P}\mathbb{L}_2 v - \mathbb{P}\mathbb{L}_2 w.
\end{aligned}$$

Noting that, again $\mathbb{P}\mathbb{L}_1 = 0$ and $\mathbb{L}_1 v = 0$ by construction. We now take w to be in quasi-steady state, meaning it must satisfy

$$\frac{1}{\varepsilon}\mathbb{L}_1 w = -\mathbb{L}_2 v + \mathbb{P}\mathbb{L}_2 v,$$

which, when using the definitions of these operators yields

$$\frac{1}{\varepsilon}\frac{\partial}{\partial u}\left\{(u-y)w + \frac{\partial w}{\partial u}\right\} = \frac{\partial}{\partial y}\left\{(\alpha y + \beta - u)\, f(y)\phi(u,y)\right\} - \frac{\partial}{\partial y}\left\{(\alpha y + \beta - y)f\right\}\phi(u,y).$$

We integrate once with respect to u to get rid of a derivative on the left hand side, finding that

$$\frac{1}{\varepsilon}\left\{(u-y)w + \frac{\partial w}{\partial u}\right\} = \phi\left\{f(y)(u - \alpha y - \beta) + f'\right\}.$$

and therefore, using an integrating factor

$$w = \frac{\varepsilon}{2}\phi u\left\{f(y)(u - 2\alpha y - 2\beta) + 2f'(y)\right\}.$$

Now, using this form of w, we must compute $\mathbb{P}\mathbb{L}_2 w$, since that is the term in the $\partial v/\partial t$ equation. First, applying $\mathbb{L}_2$, by definition:

$$\mathbb{L}_2 w = -\frac{\partial}{\partial y}\left\{(\alpha y + \beta - u)\, w(u,y)\right\}.$$

and now projecting yields

$$\mathbb{P}\mathbb{L}_2 w = \varepsilon\left[f(y) + yf'(y) + f''(y)\right]\phi(u).$$

Thus, our differential equation for v is

$$\frac{\partial v}{\partial \tau} = -\varepsilon\frac{\partial}{\partial y}\left\{(\alpha y + \beta)f\right\} + \mathbb{P}\mathbb{L}_2 w = -\varepsilon\frac{\partial}{\partial y}\left\{(\alpha y + \beta)f\right\} + \varepsilon\left[f(y) + yf'(y) + f''(y)\right]\phi(u),$$

from which, we can conclude

$$\frac{\partial f}{\partial \tau} = -\varepsilon\frac{\partial}{\partial y}\left\{(\alpha y + \beta)f\right\} + \varepsilon\frac{\partial}{\partial y}\left\{yf(y)\right\} + \varepsilon\frac{\partial^2 f}{\partial y^2},$$

in the original variables,

$$\frac{\partial f}{\partial t} = -\frac{\partial}{\partial x}\left\{\left(ax + b - \frac{k}{\gamma}x\right)f(x)\right\} + \frac{k_B T}{\gamma}\frac{\partial^2 f}{\partial x^2}.$$

APPENDIX B

SUPPLEMENTAL INFORMATION FOR CHAPTER 5

In this appendix, we provide proofs for lemmas and propositions found in Chapter 5.

B.1 Proofs of Lemmas 5.2-5.5

Proof of Lemma 5.2. Between time τ_{off}^{k-1} and τ_{on}^{k}, the cargo is freely diffusing. Therefore, to control Y_{off}^{k}, we need to control the supremum of a Brownian motion. Now, for any fixed $T > 0$ and $C > 0$, it follows from Doob's martingale inequality (Theorem 3.8(i) in [3]) and symmetry of Brownian motion that

$$\mathbb{P}(\sup_{t\in[0,T]} |W(t)| \geq C) \leq 2\exp\Big(\frac{-C^2}{2T}\Big).$$

Hence, it follows that

$$\mathbb{P}(Y_{\text{off}}^{k} \geq C | T_{\text{off}}^{k}) \leq 2\exp\Big(\frac{-C^2}{2\sigma^2 T_{\text{off}}^{k}}\Big), \quad \text{almost surely.} \tag{B.1}$$

Note that (B.1) is an average over realizations of the diffusion W for fixed realizations of the time T_{off}^{k}. That is, the inequality holds for almost all realizations of T_{off}^{k}.

Now, T_{off}^{k} is exponentially distributed with rate $M\lambda_{\text{on}}(0)$. Hence, the tower property of conditional expectation (see Theorem 5.1.6 in [2]) yields

$$\mathbb{P}(Y_{\text{off}}^{k} \geq C) = \mathbb{E}[\mathbb{P}(Y_{\text{off}}^{k} \geq C | T_{\text{off}}^{k})] \leq 2M\lambda_{\text{on}}(0)\int_0^\infty \exp\Big(\frac{-C^2}{2\sigma^2 t} - M\lambda_{\text{on}}(0)t\Big)\,\mathrm{d}t. \tag{B.2}$$

Now, we have that

$$\int_0^\infty \lambda e^{\lambda t} e^{-a/t}\,\mathrm{d}t = 2\sqrt{a\lambda}K_1(2\sqrt{a\lambda}), \quad \text{if } a > 0,\ \lambda > 0, \tag{B.3}$$

where $K_1(x)$ denotes the modified Bessel function of the second kind. Hence, the proof is complete after combining (B.2) and (B.3) and the following bound,

$$K_1(x) \leq \sqrt{\pi/x}(1 + 1/(2x))e^{-x}, \quad x > 0,$$

which was proven in [6]. □

Proof of Lemma 5.3. To control Y^k_{on}, we note that each bound motor takes steps of unit length at a Poisson rate that is bounded above by $\Lambda := \max_{m\in\{1,\dots,M\}} \lambda_{\text{step}}(m)$. Since the number of bound motors is bounded above by M, and since the cargo is an OU process centered at the average bound motor position, it follows that

$$\mathbb{P}(Y^k_{\text{on}} \geq C | T^k_{\text{on}}) \leq \mathbb{P}\Big(P(T^k_{\text{on}}) + \sigma \sup_{t\in[0,T^k_{\text{on}}]} |W(t)| > C \Big| T^k_{\text{on}}\Big), \quad \text{almost surely,}$$

where $P(T^k_{\text{on}}) \geq 0$ is a Poisson random variable with mean $M\Lambda T^k_{\text{on}}$. Hence,

$$\mathbb{P}(Y^k_{\text{on}} \geq C | T^k_{\text{on}}) \leq \mathbb{P}\big(P(T^k_{\text{on}}) \geq C/2 \big| T^k_{\text{on}}\big) + \mathbb{P}\big(\sup_{t\in[0,T^k_{\text{on}}]} |W(t)| \geq C/(2\sigma) \big| T^k_{\text{on}}\big). \tag{B.4}$$

We thus need to control the distribution of T^k_{on}. Now, T^k_{on} is the first passage time of the Markov chain (5.6) to state $m = 0$ starting from state $m = 1$. This Markov chain is a finite state space birth-death process, and thus there exists [1] a unique quasi-stationary distribution $\nu \in \mathbb{R}^M$, which is a probability measure on $\{1,\dots,M\}$ so that if $\mathbb{P}(m(0) = m) = \nu_m$ for $m \in \{1,\dots,M\}$, then

$$\mathbb{P}\big(m(t) = m \big| m(s) \neq 0 \text{ for all } s \in [0,t]\big) = \nu_m, \quad m \in \{1,\dots,M\}.$$

Furthermore, it is known that the first passage time of $m(t)$ to state 0 is exponentially distributed with some rate $\lambda > 0$ if $\mathbb{P}(m(0) = m) = \nu_m$ for $m \in \{1,\dots,M\}$ [4]. If S is this first passage time, then

$$\mathbb{P}(T_{\text{on}} > T) \leq \mathbb{P}(S > T) = 1 - e^{-\lambda T}, \quad T > 0,$$

since S is the first passage time assuming $m(0) \geq 1$ and T_{on} is this first passage time assuming $m(0) = 1$. Thus, since both terms in the upper bound in (B.4) are increasing functions of the realization $T^k_{\text{on}} > 0$, the tower property yields

$$\begin{aligned}\mathbb{P}(Y^k_{\text{on}} \geq C) &= \mathbb{E}\big[\mathbb{P}(Y^k_{\text{on}} \geq C | T^k_{\text{on}})\big] \\ &\leq \mathbb{E}\big[\mathbb{P}(P(S) \geq C/2 | S)\big] + \mathbb{E}\big[\mathbb{P}(\sup_{t\in[0,S]} |W(t)| \geq C/(2\sigma) | S)\big].\end{aligned} \tag{B.5}$$

Next, if P is Poisson distributed with mean μ, then Corollary 6 from [5] yields

$$\mathbb{P}(P \geq C) \leq e^{C-\mu}\Big(\frac{\mu}{C}\Big)^C, \quad \text{if } C \geq \mu.$$

Hence, we have the following almost sure inequality,

$$\mathbb{P}(P(S) \geq C/2|S) \leq e^{\frac{C}{2}-M\Lambda S}\Big(\frac{M\Lambda S}{C/2}\Big)^{\frac{C}{2}} 1_{\frac{C}{2}\geq M\Lambda S} + 1_{\frac{C}{2}<M\Lambda S}. \tag{B.6}$$

Since $S \sim \text{Exponential}(\lambda)$, we have that

$$\begin{aligned}\mathbb{E}\Big[e^{\frac{C}{2}-M\Lambda S}\Big(\frac{M\Lambda S}{C/2}\Big)^{\frac{C}{2}} 1_{\frac{C}{2}\geq M\Lambda S}\Big] &\leq \int_0^\infty e^{\frac{C}{2}-M\Lambda s}\Big(\frac{M\Lambda s}{C/2}\Big)^{\frac{C}{2}} \lambda e^{-\lambda s}\, ds \\ &= \Big(\frac{C}{2}\Big)^{-\frac{C}{2}} e^{\frac{C}{2}} \frac{\lambda}{M\Lambda+\lambda}\left(\frac{M\Lambda}{M\Lambda+\lambda}\right)^{\frac{C}{2}} \Gamma(C/2+1),\end{aligned} \tag{B.7}$$

where $\Gamma(\cdot)$ denotes the Gamma function. Further,

$$\mathbb{P}(C/2 < M\Lambda S) = e^{-\lambda C/(2M\Lambda)}. \tag{B.8}$$

Also, as in Lemma 5.2, we have that

$$\mathbb{E}[\mathbb{P}(\sup_{t\in[0,S]} |W(t)| \geq C/(2\sigma)|S)] \leq (2x+1)\sqrt{\pi/(2x)}e^{-x}, \quad x = \tfrac{C}{\sigma}\sqrt{\lambda/2} > 0. \tag{B.9}$$

Therefore, taking the expectation of (B.6) and using (B.5), (B.7), (B.8), and (B.9) completes the proof. □

Proof of Lemma 5.4. Since $Y_k \leq Y_{\text{off}}^k + Y_{\text{on}}^k$ for $k \geq 1$, we have that if $C > 0$, then

$$\mathbb{P}(Y_k > C) \leq \mathbb{P}(Y_{\text{off}}^k + Y_{\text{on}}^k > C) \leq \mathbb{P}(Y_{\text{off}}^k \geq C/2) + \mathbb{P}(Y_{\text{on}}^k > C/2).$$

Hence, using the upper bounds established in Lemmas 5.2 and 5.3, we have

$$\begin{aligned}\sum_{k=1}^\infty \mathbb{P}(Y_k > \sqrt{k}) < \sum_{k=1}^\infty &\Big[\sqrt{\frac{\pi}{x_k}}(2x_k+1)e^{-x_k} + e^{-\lambda\sqrt{k}/(4M\Lambda)} + \sqrt{\frac{\pi}{y_k}}(2y_k+1)e^{-y_k}\Big] \\ &+ \frac{\lambda}{M\Lambda+\lambda}\sum_{k=1}^\infty \Big(\frac{\sqrt{k}}{4}\Big)^{-\frac{\sqrt{k}}{4}} e^{\frac{\sqrt{k}}{4}}\left(\frac{M\Lambda}{M\Lambda+\lambda}\right)^{\frac{\sqrt{k}}{4}} \Gamma\Big(\frac{\sqrt{k}}{4}+1\Big),\end{aligned} \tag{B.10}$$

where $x_k = \frac{\sqrt{k}}{2\sigma}\sqrt{2M\lambda_{\text{on}}(0)}$ and $y_k = \frac{\sqrt{k}}{2\sigma}\sqrt{\lambda/2}$. A straightforward application of the integral test confirms that the first series on the righthand side of (B.10) converges.

To check the convergence of the last series in (B.10), we recall Stirling's formula,

$$\lim_{z\to\infty} \frac{\Gamma(z+1)}{\sqrt{2\pi z}\left(\frac{z}{e}\right)^z} = 1,$$

and thus the limit comparison test implies that the last series converges if and only if

$$\sum_{k=1}^\infty k^{1/4}\left(\frac{M\Lambda}{M\Lambda+\lambda}\right)^{\frac{\sqrt{k}}{4}} < \infty. \tag{B.11}$$

The integral test confirms that (B.11) holds. Therefore, (B.10) converges, and thus the Borel-Cantelli lemma (Theorem 2.3.1 in [2]) completes the proof. □

Proof of Lemma 5.5. Since $Y_k \geq 0$ almost surely, we have that $\mathbb{E}[Y_k] = \int_0^\infty \mathbb{P}(Y_k > C)\,\mathrm{d}C$. Using the bounds in Lemmas 5.2 and 5.3 as in the proof of Lemma 5.4 shows that this integral is finite. □

B.2 Proof of Proposition 5.7

Proof. Fix a realization $\mathbf{J}$. Let $K \geq 0$ denote the almost surely finite number of jump times of $\mathbf{J}$ before time T, where t is said to be a jump time if $\mathbf{J}(t+) \neq \mathbf{J}(t-)$. Denote these K jump times by $0 < \tau_1 < \cdots < \tau_K < T$ and let $\tau_0 = 0$ and $\tau_{K+1} = T$.

For ease of notation, define the sequences

$$x_k := x(\tau_k), \quad \overline{x}_k := \overline{x}(\tau_k), \quad z_k^i := z_i(\tau_k), \quad \overline{z}_k^i := \overline{z}_i(\tau_k), \quad m_k := m(\tau_k),$$

for $k \in \{0, 1, \ldots, K\}$. Further, define the time between jumps, $s_k := \tau_k - \tau_{k-1}$, for $k \in \{1, \ldots, K\}$. It follows immediately from Proposition 5.6 that

$$x_{k+1} = x_k e^{-s_{k+1}/\varepsilon} + \mu_{k+1}(1 - e^{-s_{k+1}/\varepsilon}), \quad k \in \{0, 1, \ldots, K\}, \tag{B.12}$$

where for $k \in \{0, 1, \ldots, K+1\}$ we define

$$\mu_{k+1} := \begin{cases} \frac{1}{m_k} \sum_{i \in I(\tau_k)} z_k^i & \text{if } m_k > 0, \\ x_k & \text{if } m_k = 0. \end{cases} \tag{B.13}$$

Furthermore, it follows from the definition of $\overline{x}(t)$ that for $k \in \{0, 1, \ldots, K\}$,

$$\overline{x}_{k+1} := \begin{cases} \frac{1}{m_k} \sum_{i \in I(\tau_k)} \overline{z}_k^i & \text{if } m_k > 0, \\ \overline{x}_k & \text{if } m_k = 0. \end{cases} \tag{B.14}$$

Now, since motors take steps of size one, it follows that if $k \in \{0, \ldots, K\}$ and $i \in \{1, \ldots, M\}$, then $0 \leq z_k^i \leq K+1$ and $0 \leq x_k \leq K+1$. Hence, if $k \in \{0, \ldots, K\}$, then (B.13) implies

$$|x_k - \mu_{k+1}| < K + 1. \tag{B.15}$$

Next, we claim that if $k \in \{0, \ldots, K\}$ and

$$\max_{j \in \{0,\ldots,k\}} \left\{ |x_j - \overline{x}_j|, \max_{i \in \{1,\ldots,M\}} |z_j^i - \overline{z}_j^i| \right\} < \eta, \tag{B.16}$$

then

$$\max \left\{ |x_{k+1} - \overline{x}_{k+1}|, \max_{i \in \{1,\ldots,M\}} |z_{k+1}^i - \overline{z}_{k+1}^i| \right\} < (K+1)e^{-s_{k+1}/\varepsilon} + \eta. \tag{B.17}$$

To see this, we use (B.12) and (B.15) to obtain

$$\begin{aligned}|x_{k+1} - \overline{x}_{k+1}| &= |x_k e^{-s_{k+1}/\varepsilon} + \mu_{k+1}(1 - e^{-s_{k+1}/\varepsilon}) - \overline{x}_{k+1}| \\ &\leq (K+1)e^{-s_{k+1}/\varepsilon} + |\mu_{k+1} - \overline{x}_{k+1}|.\end{aligned}$$

Using (B.13) and (B.14), we have that

$$|\mu_{k+1} - \overline{x}_{k+1}| \leq \begin{cases} \frac{1}{m_k}\sum_{i\in I(\tau_k)} |z_k^i - \overline{z}_k^i| & \text{if } m_k > 0, \\ |x_k - \overline{x}_k| & \text{if } m_k = 0. \end{cases}$$

Furthermore, it follows from (5.7) and (5.27) that

$$|z_{k+1}^i - \overline{z}_{k+1}^i| \leq \max_{j\in\{0,\ldots,K+1\}} |x_j - \overline{x}_j|, \quad i \in \{1,\ldots,M\}.$$

Hence, the claim (B.17) is verified.

Define the largest time between jumps, $s := \max_{k\in\{1,\ldots,K\}} s_k$. Since $x_0 = \overline{x}_0 = z_0^i = \overline{z}_0^i$ for $i \in \{1,\ldots,M\}$, we apply (B.16) and (B.17) iteratively to obtain

$$|x_{K+1} - \overline{x}_{K+1}| \leq (K+1)^2 e^{-s/\varepsilon}.$$

Taking $\varepsilon \to 0$ completes the proof. □

B.3 References

[1] J. A. Cavender, *Quasi-stationary distributions of birth-and-death processes*, Adv. Appl. Probab., 10 (1978), pp. 570–586.

[2] R. Durrett, *Probability: Theory and Examples*, Cambridge University Press, 2010.

[3] I. Karatzas and S. Shreve, *Brownian Motion and Stochastic Calculus*, vol. 113, Springer Science & Business Media, 2012.

[4] S. Méléard, D. Villemonais, et al., *Quasi-stationary distributions and population processes*, Probab. Surv., 9 (2012), pp. 340–410.

[5] M. Short, *Improved inequalities for the poisson and binomial distribution and upper tail quantile functions*, ISRN Probab. Stat., 2013 (2013).

[6] Z.-H. Yang and Y.-M. Chu, *On approximating the modified bessel function of the second kind*, J. Inequal. Appl., 2017 (2017), p. 41.